

Functional surface microstructures inspired by nature – From adhesion and wetting principles to sustainable new devices

Eduard Arzt^{a,b,*}, Haocheng Quan^a, Robert M. McMeeking^{a,c}, René Hensel^a

^a INM – Leibniz Institute for New Materials, 66123 Saarbrücken, Germany

^b Saarland University, Department of Materials Science and Engineering, 66123 Saarbrücken, Germany

^c Departments of Materials and Mechanical Engineering, University of California, Santa Barbara, United States

ARTICLE INFO

Keywords:

Microstructure
Bioinspiration
Wetting
Adhesion
Micropatterning
Skin adhesive

ABSTRACT

In the course of evolution nature has arrived at startling materials solutions to ensure survival. Investigations into biological surfaces, ranging from plants, insects and geckos to aquatic animals, have inspired the design of intricate surface patterns to create useful functionalities. This paper reviews the fundamental interaction mechanisms of such micropatterns with liquids, solids, and soft matter such as skin for control of wetting, self-cleaning, anti-fouling, adhesion, skin adherence, and sensing. Compared to conventional chemical strategies, the paradigm of micropatterning enables solutions with superior resource efficiency and sustainability. Associated applications range from water management and robotics to future health monitoring devices. We finally provide an overview of the relevant patterning methods as an appendix.

1. Introduction to the patterning paradigm

One time there was a picket fence
with space to gaze from hence to thence.

An architect who saw this sight
approached it suddenly one night,
removed the spaces from the fence,
and built of them a residence.

The picket fence stood there dumbfounded
with pickets wholly unsurrounded,
a view so loathsome and obscene,
the Senate had to intervene.

The architect, however, flew
to Afri- or Americoo.

Christian Morgenstern (German poet, 1871–1914, translation¹ by Max Knight)

* Corresponding author.

E-mail address: eduard.arzt@leibniz-inm.de (E. Arzt).

¹ Original German version of this famous "nonsense poem", which alludes to the importance of space and structure: *Es war einmal ein Lattenzaun, mit Zwischenraum, hindurchzuschauen. Ein Architekt, der dieses sah, stand eines Abends plötzlich da - und nahm den Zwischenraum heraus und baute draus ein großes Haus. Der Zaun indessen stand ganz dumm, mit Latten ohne was herum, ein Anblick grässlich und gemein. Drum zog in der Senat auch ein. Der Architekt jedoch entfloh nach Afri- od- Ameriko.* (Translation published in: The Gallows Songs, Christian Morgenstern's Galgenlieder - A Selection, translated, with an Introduction, by Max Knight, University of California Press 1964. © 1963 by Max E. Knight)

<https://doi.org/10.1016/j.pmatsci.2021.100823>

Received 13 October 2020; Received in revised form 12 January 2021; Accepted 23 January 2021

Available online 26 May 2021

0079-6425/© 2021 The Author(s). Published by Elsevier Ltd. This is an open access article under the CC BY license

(<http://creativecommons.org/licenses/by/4.0/>).

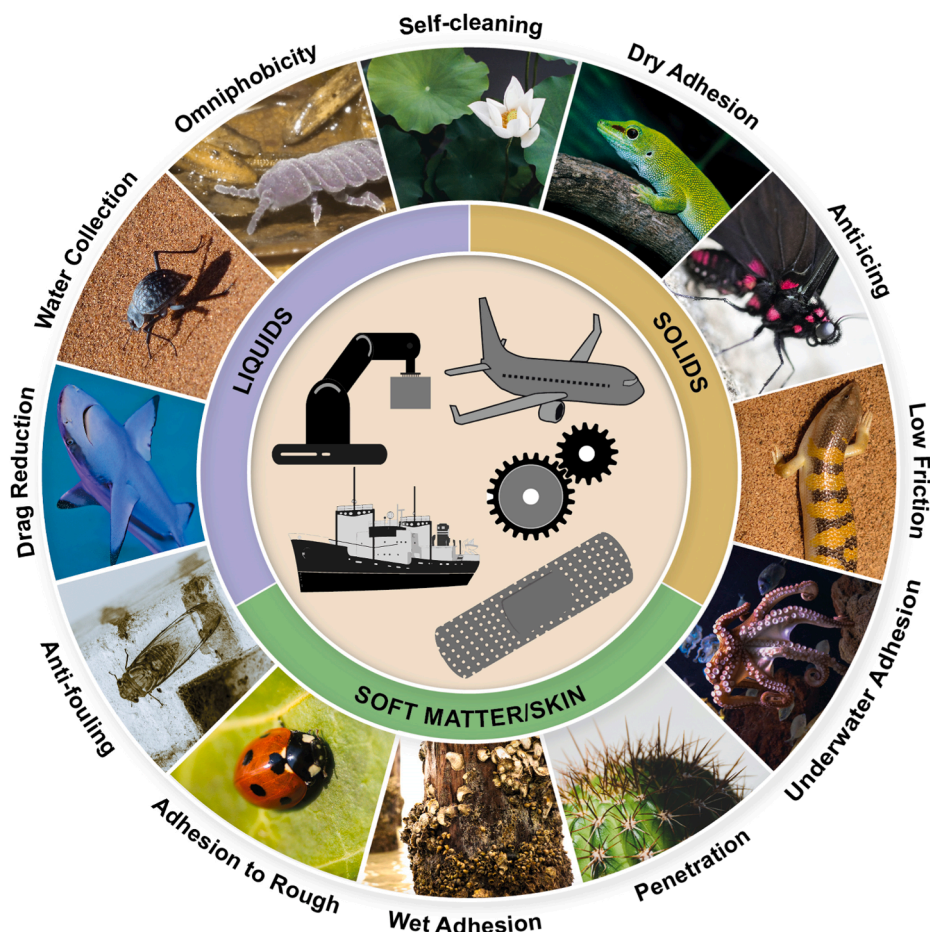


Fig. 1.1. The paradigm of surface micropatterning. A wealth of surface functions created by micropatterning: controlled interaction with other solids (adhesion, friction, and icing), with liquids (wetting, self-cleaning, and drag reduction), and with soft matter such as skin and tissue (adhesion, wound management, and tissue penetration). Surface structure modification pervades the biological world and is, through its inspiration, spurring technological innovations, e.g. in transportation, robotics, and health care. Not included in this review are tunable optical effects such as structural coloration or transparency [4,5]. Images and Illustrations from Unsplash (www.unsplash.com) and Pixabay (www.pixabay.com) under Creative Commons Zero License.

Imagine surfaces that, by design, repel water, ice and dust, that separate water from oil, that attract or release other objects on demand, or that cling to human organs and skin while recording vital body signals. All of these functions have been demonstrated, at least on the laboratory scale, as a result of tailoring the *surface microstructure*. Such micropatterning has paved the way to microscopic “picket fences”, in which the gaps are as important as the material in between.

Much of the fascination with materials derives from the functional impact – coupled with intrinsic beauty – of architectural patterns on a scale significantly larger than atoms and molecules. Materials science is hence preoccupied with *microstructure*: the spatial arrangement of the building blocks in the form of phases and defects (for a modern account see e.g. Mittemeijer [1]). Very fine structures can give rise to dramatically new properties, e.g. [2,3]: ultra-high strength of otherwise deformable metals, superior damage tolerance of otherwise brittle materials, higher energy density of batteries, efficient charge separation in solar cells, etc. Surfaces, which are a material’s site of interaction with the “outer world” [6], can also inherit exciting new functions through patterning (Fig. 1.1).

The living world has, by trial and error, exploited the principle of growing surfaces with “gaps” of various dimensions in countless instances. Biological surfaces in the plant and the animal kingdoms exhibit protrusions with sometimes remarkable complexity: fibrils, papillae, ridges, hairs, bristles, gratings, spikes or cups have been described with dimensions ranging from millimeters down to several nanometers. Why has nature gone to great lengths to form such complicated and mechanically sensitive architectures?

The apparent evolutionary advantage serves as an *ex post* explanation: surface microstructures open up a space with many design parameters, which may make up for the relative scarcity of compositions of biological materials [7]. Following Nachtigall [8], the

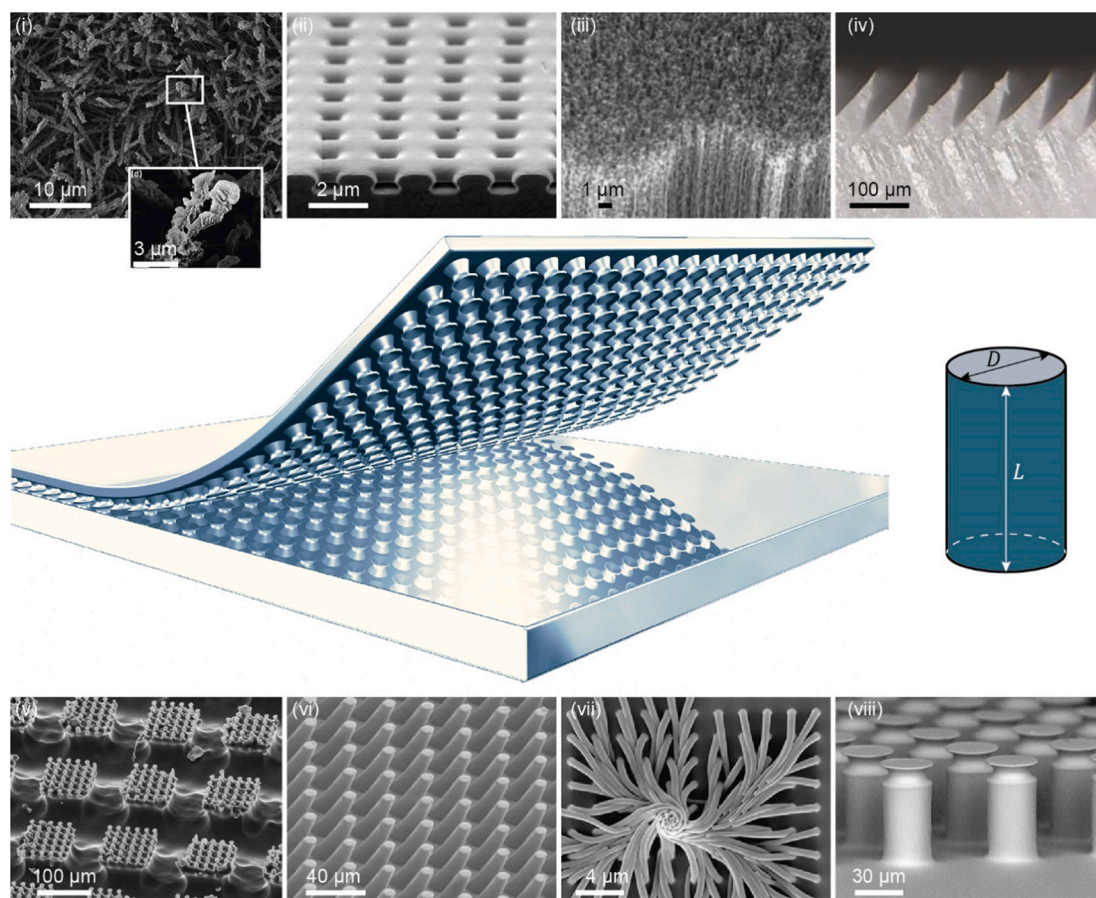


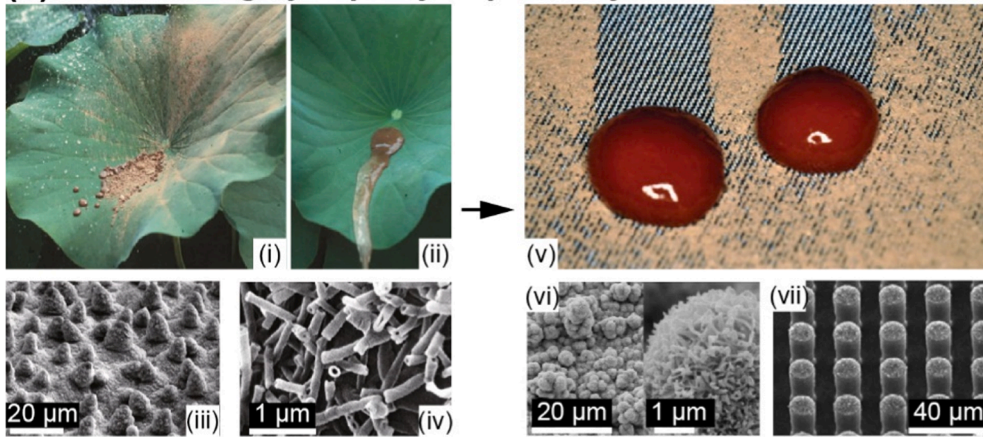
Fig. 1.2. Generic surface microstructures. Geometric protrusions create “gaps” that impart the surface with dramatically enhanced functionalities - ranging from control of wetting, through handling of objects to biocompatible adhesion to skin. Structures reported in the literature take many different shapes. Important design parameters are the length L , ranging typically from submicron to sub-millimeter, diameter D , and aspect ratio L/D (from 1 to >10). Fibril shape sensitively affects the functionality, and hierarchical structures with different size levels have been reported. Methods for fabrication of microstructured polymers, metals and ceramics are reviewed in the Appendix. Electron micrographs reproduced with permission from (i) [9], copyright (2014) American Chemical Society. (ii) [10], copyright (2014) American Chemical Society. (iii) [11], copyright (2008) American Chemical Society. (iv) [12], copyright (2019) Wiley. (v) [13], copyright (2010) IOP Publishing. (vi) [14], copyright (2019) American Chemical Society. (vii) [15], copyright (2009) AAAS. (viii) [16], copyright (2018) Wiley.

challenge for the rapidly growing community of “bioinspiration” (“biomimetics” or “biomimicry” are frequent synonyms) is to, first, understand the biological function and governing principle of these natural surfaces; this is by no means a simple task as all natural surfaces are multi-functional and do not respect the man-made separation between material and structure. Second, based on this “inspiration”, an abstraction process leads to a design that can be implemented in the laboratory. Finally, translation of this abstraction creates artificial microstructures for targeted applications, with functionalities that match or even surpass those in nature (Fig. 1.2).

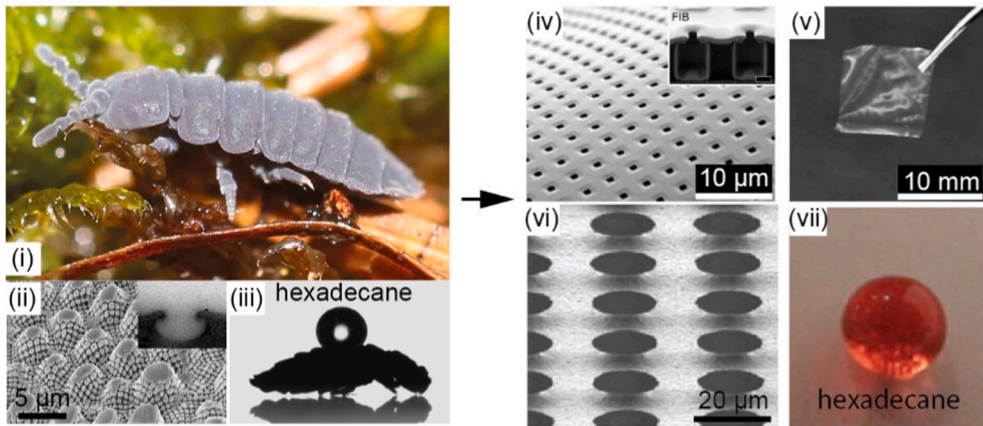
Biological evolution has always favored efficient and energy-saving solutions. A bioinspired micropatterning strategy has therefore an intrinsic benefit over chemical modification of surfaces to achieve the same functions: due to the use of fewer substances and less reliance on chemicals that may be toxic or polluting, micropatterned devices will exhibit superior resource efficiency and environmental sustainability. Functional surface microstructures are set to innovate or disrupt such diverse technologies as water management, surface protection, robotic handling, and digital health monitoring, where the need for eco-friendly solutions will dramatically increase in the future.

This paper will briefly review the lessons learnt from nature about surface design. We will then apply the resulting paradigm of micropatterning to the design rules of artificial microstructures. Structure, size and function will be recurring overarching topics. In Section 2, we review micropatterns in contact with liquids and the associated phenomena of wetting and self-cleaning. The

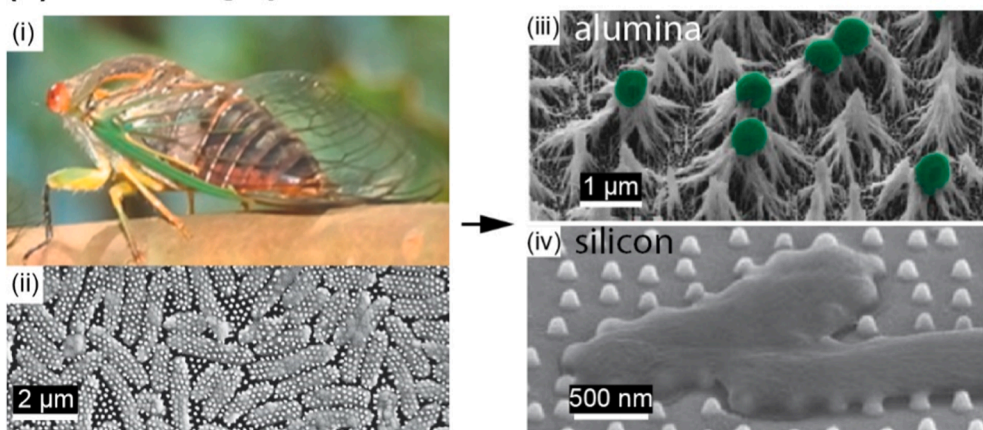
(a) Self-cleaning by superhydrophobicity



(b) Omniphobicity by microstructures with overhangs



(c) Anti-fouling by surface nano- and microstructures



(caption on next page)

Fig. 2.1. Examples of bioinspired microstructures designed for interactions with liquids. (a) Self-cleaning inspired by sacred lotus: (i,ii) Dirt is easily removed by rinsing water; (iii) the leaves are covered with papillous microstructures and with (iv) nanoscopic wax crystals; (v) Lotus-inspired synthetic superhydrophobic surface cleaned by ketchup droplets; (vi) superhydrophobic copper surface; (vii) artificial microfibrils covered by wax crystals. (b) Omniphobicity inspired by springtails: (i) The springtail (*Collembola*, *T. bielensis*) with (ii) papillous microstructures and overhanging nanostructures (inset) repels (iii) a hexadecane droplet on its non-wetting surface; (iv,v) Bioinspired omniphobic membrane with overhangs repelling (vi,vii) water and low-surface tension liquids. (c) Anti-fouling inspired by cicadas: (i) The cicada (*P. claripennis*) with (ii) nanofibrils (dots) on the wing surface with attached and killed bacteria (*P. aeruginosa*). (iii) Reduced colonization of a nanopatterned alumina surface by bacteria (green, *S. aureus*). (iv) *E. coli* bacteria killed by a nanopatterned silicon surface. (a:i-iv) Reproduced with permission from [54] under CC BY 4.0 license. (a:v,vii) Reproduced with permission from [37], copyright (2016) Royal Society. (a:vi) Reproduced with permission from [55], copyright (2005) American Chemical Society. (b:iv,v) Reproduced with permission from [56], copyright (2013) Wiley. (b:vi,vii) Reproduced with permission from [47], copyright (2007) AAAS. (c:i,ii) Reproduced with permission from [57], copyright (2013) Elsevier. (c:iii) Reproduced with permission from [58], copyright (2017) American Chemical Society. (c:iv) Reproduced with permission from [59], copyright (2019) IOP Publishing.

functionality of temporary and controllable adhesion to microfibrillar surfaces is reviewed in Section 3. Finally, we discuss the recent developments of artificially patterned surfaces designed for contact with the human body, which are currently paving the way to novel digital devices for medical and other purposes (Section 4). The Appendix will briefly review methods for creating microstructures on polymeric surfaces. Our intention is to bridge fundamental mechanisms, as elucidated by observation, experiment and theoretical modeling, with experimental laboratory designs and emerging real-world applications.

As in any vibrant field of research, progress is happening at breath-taking speed. A review can only capture a snapshot of the current state of the art. Discriminating choices had to be made out of more than a thousand literature references covering the research work of numerous research groups worldwide. Emphasis will be placed on progress over the past decade. Some extensive previous monographs and reviews are available in the literature. The reader is directed, e.g., to [17] for bioinspiration, to Meyers and Chen [18] and Bhushan [19,20] for biological and biomimetic materials, and to del Campo and Arzt [21] on fabrication.

2. Microstructures for interaction with liquids: Wetting, self-cleaning and anti-fouling

Wetting of surfaces is the spreading of liquids deposited on solids in a gaseous surrounding. It is an important phenomenon which is of interest for the biological world, for our daily life and for many industrial applications. Technically, wetting can be influenced by surface chemistry, e.g. by applying fluorinated coatings, which can be harmful to the environment. A more sustainable strategy, showcased in the biological environment, is the microstructural modification of surfaces.

Surface roughness is well known to affect wetting phenomena; the insight that designed surface micropatterns on several size levels can control wetting through capillarity is a more recent development. The controlled spreading of a liquid on a surface can lead to intriguing surface properties, such as liquid repellency, anti-fogging, self-cleaning, delayed icing, and anti-fouling. Such functions are attractive for numerous applications, e.g. in water management, construction industry, packaging of liquids, optical systems, solar cells, heat exchangers, rotors for wind power stations, airplane wings and ship hulls etc.

Superhydrophobicity is the function of a surface to completely repel water. Originated by a desire to understand this function in the leaves of sacred lotus plants, it has now become a driver for the discovery and exploration of new wetting properties, such as omniphobicity (i.e. the ability to repel ‘everything’ including oil and other low surface tension liquids). By contrast, superhydrophilicity is the ability of a surface to spread water evenly and to reduce droplet formation. Numerous studies exist on the manufacture of synthetic surfaces with specific wetting characteristics, including all disciplines of lithography, dip- and spray-coating, sol-gel processes, chemical and physical vapor deposition, electrochemical methods, and self-assembly (see Appendix and e.g. [22–24]).

In this section of the review, we restrict ourselves to wetting with three phases, namely a liquid in contact with a solid surrounded by vapor. We will not consider lubricated surfaces, where a liquid wets a liquid film [25]; for a recent review on that topic, see [26]. Further emerging topics related to wetting of surfaces not covered by this review are water harvesting [27], water oil separation [28–30], and anti-icing [31–36].

2.1. Biological inspiration - keeping surfaces dry and clean

The interaction of liquids with natural surfaces was a decisive element in biological evolution [37]. For example, water repellency is common and has an immense variety of biological functions (Fig. 2.1): For leaves and wings, the prevention of weight increase by wetting is a crucial measure for surviving rain, mist or temporary flooding without mechanical collapse. Aquatic and semi-aquatic plants and animals trap air underwater to maintain buoyancy, respiration, and locomotion. Seeds, spores and insect eggs are dispersed by passive floating on the water surface. Aquatic springtails and fire ants take advantage of capillary forces to assemble into colonies, enhancing buoyancy and reducing the risk of sinking [38]. Fisher spiders and backswimmers use entrapped air reservoirs (referred to as *plastrons*) to respire underwater, as the gas transfer rate in air is much higher than in water [39,40]. In plants, a *plastron*

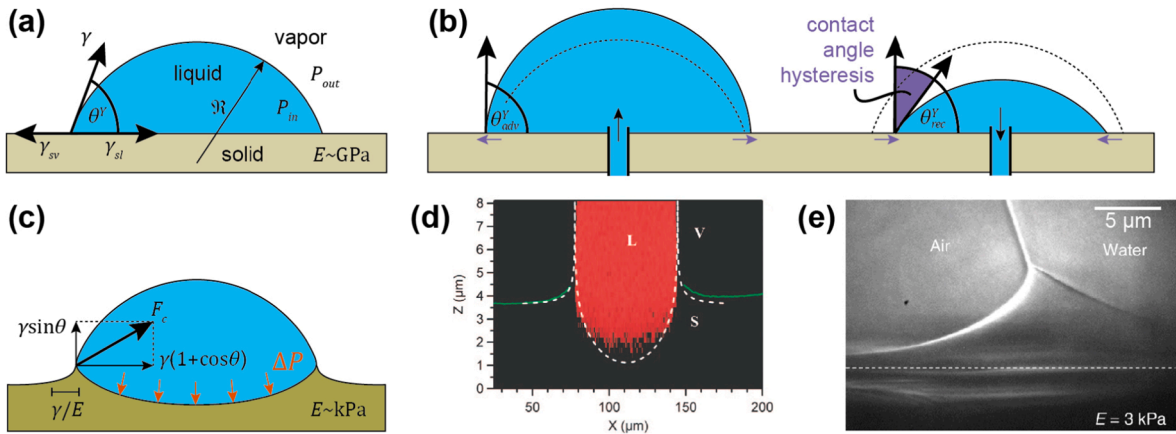


Fig. 2.2. Droplet on a smooth (a,b) rigid and (c–e) soft solid. (a) The static contact angle θ^Y results from the force balance in relation to the interfacial energies γ , γ_{sv} , and γ_{sl} at the three-phase contact line. The droplet radius is \mathcal{R} and pressures outside and inside the droplet are P_{out} and P_{in} . (b) Dynamic contact angle of advancing (left) and receding (right) three-phase contact lines with θ_{adv}^Y and θ_{rec}^Y , respectively. The difference between the two contact angles determines the contact angle hysteresis (purple shaded area). Dotted lines correspond to the static droplet illustrated in (a) with $\theta_{rec}^Y < \theta^Y < \theta_{adv}^Y$. (c) The Laplace pressure ΔP deforms the liquid–solid interface and a net force pulls on the substrate near the three-phase contact line. The force has a vertical and tangential component, which results in an inward-directed force. (d) Laser scanning confocal micrograph of an ionic liquid doped with Nile red on a soft silicone substrate. Reproduced with permission from [61], copyright (2008) American Chemical Society. (e) X-ray image of a wetting ridge. Reproduced with permission from [62] under CC-BY 4.0 license.

similarly supports photosynthetic metabolism by faster CO_2 diffusion [41]. In addition to gaining buoyancy from an entrapped air layer, the locomotion of water striders and backswimmers benefits from an associated drag reduction [42]. This seems counterintuitive, as entrapped air will simultaneously reduce propulsion efficiency [43]. However, tilted hairs covering the legs of such creatures show anisotropic wetting behavior, which water striders utilize for propulsion by using their legs as rowing paddles and the meniscus as a blade [44]. Moreover, entrapped layers of air underwater can act as thermal insulation, provide sensory function via bristles connected to mechanosensors, or induce camouflage through total reflection [37].

Self-cleaning is a mechanism by which highly mobile droplets remove dust from a surface. It was first discussed in the context of water repelling plant leaves (Fig. 2.1a) [45,46]. However, the wetting characteristic is often not the primary function of natural surfaces. In fact, a rough wax coating, which reduces adhesion, acts primarily as a defense mechanism against fungal spores, bacteria and other microorganisms. Superhydrophobicity is moreover a consequence of surface roughness in combination with a non-wettable material such as wax or other hydrocarbon coatings. The implementation of several structural levels at various length scales, for example by papillose cells or hairs and bristles, further increases roughness and enhances robustness.

Superhydrophobicity of plants is limited to water (as indicated by its name) and fails with low surface tension liquids such as oils, solvents, and water with surfactants. However, there exists a design strategy for enhancing wetting resistance against such liquids. This concept of omniphobicity (see Section 2.3 below) enables a non-wetting regime for liquids that intrinsically spread over a surface (Fig. 2.1b) [47]. Springtails exhibit an omniphobic skin (cuticle), as these soil-dwelling arthropods have to sustain respiration through the entire skin in temporarily flooded habitats with contaminated water [48]. The characteristic skin patterns of springtails consist of proteins that are mechanically more robust than wax crystals found on plant surfaces [49,50].

Anti-fouling of surfaces is their ability to repel or destroy microbes, e.g. bacteria and fungi, and, hence, prevent the formation of usually undesirable biofilms. In nature it contributes to evolutionary adaptation by ensuring survival in diverse habitats where microorganisms are omnipresent. In marine environments, the surfaces of whales, sharks, and invertebrates such as sea stars, sea urchins, and sea cucumbers exhibit excellent anti-fouling properties, and remain largely free from epibiont growth [51]. The leaves of mangrove trees have recently attracted much attention, as they show excellent anti-fouling properties due to a combination of low wettability, the presence of oleanolic acids and low adhesion of foulers such as barnacles [52]. Even bactericidal activity in nano-fibrillar outgrowths covering cicada wings has been observed [53]. The mechanism is based mainly on membrane rupture during bacterial attachment to the surface (Fig. 2.1c).

2.2. Contact angle and wetting hysteresis

To provide an understanding of wetting phenomena, we introduce here the basic driving forces. The spreading of a liquid on a solid surface depends on interactions along three different interfaces: the solid–liquid, the liquid–vapor, and the solid–vapor interface will attempt to attain equilibrium (Fig. 2.2a). The resulting force balance at the three-phase contact line is expressed by the well-known Young’s equation for the intrinsic contact angle θ^Y :

$$\cos\theta^Y = \frac{\gamma_{sv} - \gamma_{sl}}{\gamma}. \quad (2.1)$$

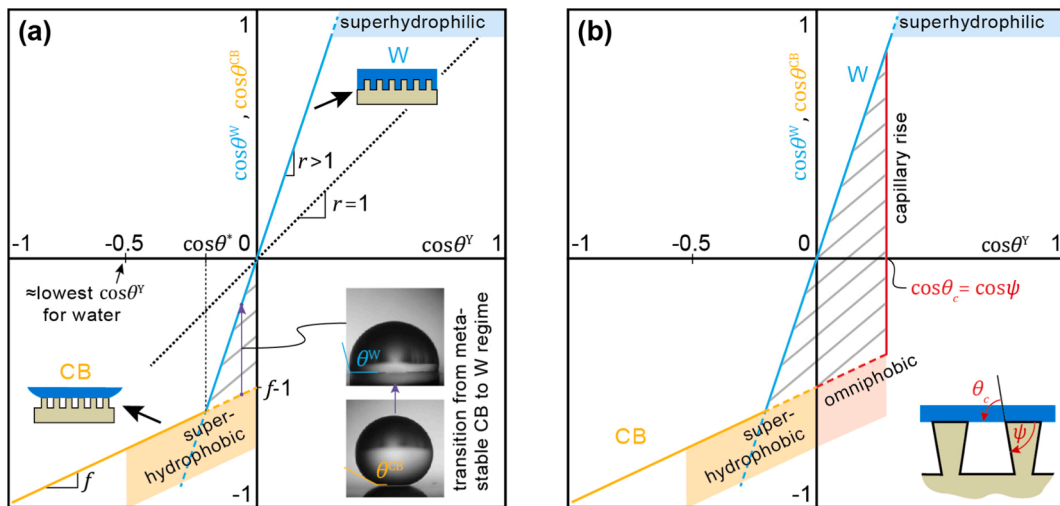


Fig. 2.3. Models for wetting on micropatterned surfaces. (a) The micropattern consists of microfibrils with straight sidewalls. Apparent contact angles, $\cos\theta^W$ and $\cos\theta^{CB}$, as linear functions of the intrinsic contact angle, $\cos\theta^Y$. The Wenzel (W) model corresponds to complete wetting of the surface (blue line, see Eq. (2.2)). The Cassie-Baxter (CB) model corresponds to incomplete wetting, where air is trapped below the droplet (orange line, see Eq. (2.3)). The black dotted line represents a perfectly smooth surface ($r = 1$) as a control. The marked areas highlight superhydrophilic (blue) and superhydrophobic (orange) wetting regimes. The gray hatching marks the metastable CB wetting state, at which the droplet can undergo a transition from CB to W by rapid reduction of the apparent contact angle, as shown in the insets. Reproduced with permission from [89], copyright (2005) Royal Society of Chemistry. (b) The micropattern consists of micropillars with overhangs described by the edge angle $\psi < -90^\circ$ (ψ is negative as anti-clockwise is defined positive). The transition from CB to W occurs at a critical intrinsic contact angle, θ_c that is equal to ψ . The red area highlights the omniphobic regime.

Here the solid–liquid specific interfacial energy is denoted as γ_{sl} , the surface tension of the liquid as γ , and the surface free energy as γ_{sv} . Complete wetting corresponds to the case in which the force balance cannot be achieved, i.e. $\gamma_{sv} > \gamma_{sl} + \gamma$. Partial wetting occurs for $0 < \cos\theta^Y < 1$ and non-wetting for $-1 < \cos\theta^Y < 0$. Young's equation is used extensively to classify these wetting regimes. However, theoretical prediction of the contact angle for various combinations of liquids and solids remains difficult, since γ_{sv} and γ_{sl} cannot be measured directly. Strictly speaking, Eq. (2.1) does not describe a thermodynamic equilibrium, as the volume and pressure of the liquid are not specified [60].

In dynamic measurements, the difference between advancing and receding contact angles is referred to as contact angle hysteresis, which is attributed to the pinning of the three-phase contact line by roughness or chemical heterogeneities of the solid surface [63,64] (Fig. 2.2b). However, there exists convincing evidence that the hysteresis can even evolve on smooth homogeneous surfaces without pinning centers due to attractive molecular interactions [65]. A comprehensive review is given by Brutin and Starov [66], for reliable measurements of the contact angle hysteresis see Korhonen et al. [67].

A relatively recent insight is that soft surfaces deform elastically under the action of capillarity [68,69]. Young's equation (Eq. (2.1)) ignores the vertical force component of the liquid surface tension, $\gamma \sin\theta^Y$, acting in the direction normal to the surface at the three-phase contact line. Furthermore, the Laplace pressure inside the droplet (given by the radius of curvature and the surface tension) deforms the liquid–solid interface (Fig. 2.2c). Both lead to the formation of a dimple below the liquid and a wetting ridge at the three-phase contact line, with dimensions comparable to γ/E , where E is the elastic modulus of the solid. Practically, the ridge is of molecular scale for $E \geq 1$ GPa, but is of the order of several microns for much softer materials such as polymer gels ($E \sim$ kPa). Their existence was confirmed experimentally by Butt and co-workers [61] using laser scanning confocal microscopy (Fig. 2.2d) and by Park et al. [62] using X-ray microscopy (Fig. 2.2e).

To determine the substrate deformation by theoretical methods, tractions between the liquid and the solid have to be considered in addition to the balance of the interfacial energies (Eq. (2.1)) [70]. Surface tension of solids, $Y = \gamma_{sv} + d\gamma_{sv}/d\varepsilon$, can differ from the surface energy, γ_{sv} , as it contains an additional term accounting for the strain, ε , of the solid surface [71]. For soft substrates, it has been demonstrated that $d\gamma_{sv}/d\varepsilon$ can be of the order of γ and, thus, should not be neglected [72]. Snoeijer and co-worker [73,74] further suggested that the capillary force acts into the droplet at the three-phase contact line giving a tangential force component, $\gamma(1 + \cos\theta^Y)$, superimposed on the vertical component of the surface tension.

The deformation of the substrate affects the spreading of the droplet and therefore the contact angle and related phenomena such as condensation [75], evaporation [76], and ice formation [77]. This effect is also important for the stability of fine fibrils on a surface, which have a propensity for clumping in the presence of liquids (see Section 3.2.3.1).

2.3. Models for wetting on rough and micropatterned surfaces

Surface roughness can drastically change the spreading of a liquid and therefore the macroscopic contact angle [78]. As far back as

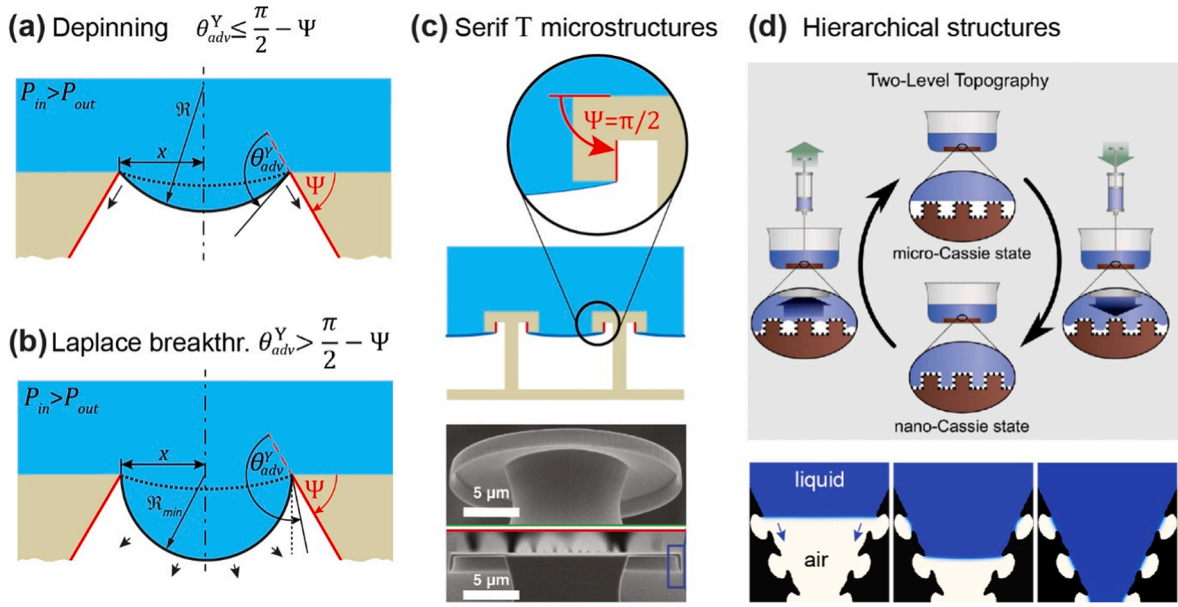


Fig. 2.4. Pressure-induced plastron collapse. Liquid phase pinned at the edge of two surface feature with distance $2x$. The liquid sags into the surface (dotted line), as liquid pressure, P_{in} is larger than the air pressure, P_{out} . The edge angle is ψ , negative as anti-clockwise is defined positive. (a) Increasing P_{in} results in depinning of the three-phase contact line when the local contact angle (related to the sidewall (red)) reaches θ_{adv}^Y . (b) Increasing P_{in} results in a breakthrough when the curvature radius, $R = x$ before depinning occurs. (c) Model and electron micrographs of a “serif-T” microstructure. Note that ψ is now positive. Reproduced with permissions from [90], copyright (2013) American Chemical Society and [91], copyright (2014) AAAS. (d) Plastron collapses on hierarchical surfaces. First the macroscopic roughness features collapse while nanopores remain dry. Upper images illustrate wetting states on such surfaces. Reproduced with permission from [92]. Lower snapshots show numerical results of the wetting transition of a hierarchical surface with $\theta_{adv}^Y = 60^\circ$. Reproduced with permission from [49] under CC-BY-NC-ND 3.0 license.

1936, Wenzel developed a model to describe the apparent contact angle, θ^W , for the case of a fully wetted surface [79]:

$$\cos\theta^W = r\cos\theta^Y, \quad (2.2)$$

where r is a geometrical roughness parameter given by the ratio of the real to the apparent surface area. For a smooth surface, $r = 1$ and for a rough surface $r > 1$. Roughness acts as an amplifier of the intrinsic wetting behavior, i.e., a liquid spreads more on a partially wettable surface and spreads less on a non-wettable surface. The latter can induce the situation in which the retention of the drop shape is energetically more favorable than the penetration of the liquid into the grooves of the rough surface. As a consequence, the droplet then only partially contacts the surface. This so-called heterogeneous wetting state was first described by Cassie and Baxter in 1944. The apparent contact angle, θ^{CB} , is then given by [80]:

$$\cos\theta^{CB} = f\cos\theta^Y + f - 1, \quad (2.3)$$

where f is the fraction of the solid surface in contact with the liquid.

Fig. 2.3a displays the apparent wetting angles as a function of the intrinsic contact angle corresponding to the Wenzel and the Cassie-Baxter models (Eqs. (2.2) and (2.3)). The figure, adapted from [81], suggests that microstructuring of surfaces is a powerful strategy to modify their wetting behavior. The modification ranges from superhydrophilicity (with an apparent contact angle close to 0° , blue region) to superhydrophobicity (orange region). The intersection of the linear functions corresponds to the transition between the two models at a critical contact angle, i.e. $\cos\theta^* = (f-1)/(r-f)$. However, due to pinning of the three-phase contact line by roughness features, the heterogeneous wetting state can be maintained for smaller contact angles (orange dashed line) even though the homogeneous wetting state is energetically favored [81]. Therefore, both wetting states can coexist, but the Cassie-Baxter regime is metastable and can be transformed to the Wenzel regime (hatched area) while the apparent contact angle simultaneously decreases (inset in Fig. 2.3a). We note that, for water on a perfluorinated surface such as Teflon, the highest possible intrinsic contact angle is about 120° due to van der Waals interactions. For liquids with lower surface tension such as oils or alkanes, θ^Y is typically less than 90° , so that a Cassie-Baxter regime does not seem to be feasible. An intuitive explanation is the capillary rise of the liquid between the roughness features, which leads to homogeneous wetting of the surface.

A strategy to prevent complete wetting is the implementation of overhanging structures such as trapezoidal features, as illustrated in Fig. 2.3b. The resulting structural omniphobicity (red area) was first proposed by Herminghaus [82]. To a first approximation, the wetting limit is reached when the edge angle, ψ , is equal to the critical intrinsic contact angle, θ_c , at which the wetting transition by capillary rise occurs. Hence, a heterogeneous wetting state can be realized for low surface tension liquids and high surface free energy

solids.

These considerations demonstrate that microstructural design can dominate liquid repellency, while surface chemistry plays only a minor role. For microstructured surfaces, surface chemistry can therefore gain new degrees of freedom, e.g. by integrating entities that perform additional functions. This approach is in contrast to the commonly used fluorinated superhydrophobic surfaces. The stability of the omniphobic regime will be discussed in the next Section 2.4. Examples of omniphobic surfaces are diverse, ranging from porous metal [83] and polymer [84] surfaces over microfibril and hierarchical surfaces [85] to fabrics [86] and membranes [56]. Reviews for further reading on this topic are e.g. [84,87,88].

2.4. Structural liquid repellency - The concept of plastron stability

It is now established that microstructure design can effectively control liquid repellency. However, the metastable Cassie-Baxter regime can be forced into the Wenzel regime by surpassing an energy barrier whose level is defined by the “gap” between microstructures. The thermodynamic energy barrier can be obtained from Gibbs free energy calculations, which typically require numerical simulations for complex geometries. Alternatively, the critical pressure to reach the transition can be calculated. Higher pressures lead to sagging of the liquid into the surface (Fig. 2.4a,b), whereby the curvature radius decreases in relation to the Laplace pressure, $\Delta P = P_{out} - P_{in} = -2\gamma/R$. Simultaneously, the local contact angle increases due to pinning at the edge of surface features. When this angle exceeds θ_{adv}^Y , the three-phase contact line depins and propagates downwards, whereby the liquid fills the gap (Fig. 2.4a).

The critical pressure can be determined as follows:

$$\Delta P_{break} = \frac{2\gamma \sin(\theta_{adv}^Y + \psi)}{x}, \quad (2.4)$$

where x is the lateral distance between the meniscus and the symmetry line and ψ the edge angle; note that ψ is negative (as anti-clockwise is defined to be positive, see Fig. 2.4a,b). Inspection of Eq. (2.4) reveals the concept of overhanging structures for $\psi < -\frac{\pi}{2}$. It should be further noted that ψ may vary along the sidewall for complex-shaped surface features. The general expression of ψ is the arctangent of the slope (i.e., the first derivative) of the function describing the sidewall profile [10,90]. For intrinsic contact angles $\theta_{adv}^Y > \frac{\pi}{2} - \psi$ (Fig. 2.4b), Eq. (2.4) can be further reduced to [90]:

$$\Delta P_{break} = \frac{2\gamma}{x}. \quad (2.5)$$

Now, the critical pressure difference depends only on the surface tension and the distance between the surface features, but is insensitive to surface chemistry, as the contact angle is eliminated from Eq. (2.4). This result affords the design of robust omniphobic surfaces even from materials that are nearly completely wettable (Fig. 2.4c). This concept of so-called “serif-T” structures was first proposed on theoretical grounds by Hensel et al. [90]. It was later demonstrated experimentally by Liu and Kim [91], who identified omniphobicity for alkanes and perfluorocarbons with $\gamma = 10$ mN/m on non-treated silicon surfaces.

Following Eqs. (2.4) and (2.5), the stability of the plastron depends inversely on the distance, $2x$, between adjacent surface features; hence, a plastron supported by a hierarchically patterned surface breaks down in several steps. Verho et al. [92] and Hensel et al. [49] demonstrated experimentally and numerically that the meniscus adapts first to macroscopic surface features before the more robust micro and nano-features collapse (Fig. 2.4d). Interestingly, a first collapse on a macroscopic scale can even be reversible when the external pressure is released. Requirements for that are a low energy barrier for the transition and a low contact angle hysteresis of the Cassie-Baxter state supported by small surface features [93]. This fact may explain the frequent evolution of hierarchical structures as superhydrophobic surfaces in nature, including plant surfaces and arthropod cuticles.

In addition to the pressure-induced collapse of the plastron, several other mechanisms can lead to an unintended transition from the Cassie-Baxter to the Wenzel regime, i.e. the collapse of the plastron: condensation, diffusion of air into the liquid, fluid flow along the interface and even cavitation. Xue et al. [94] provide a comprehensive review of all these mechanisms. Briefly, when a superhydrophobic surface is completely exposed under water, the air entrapped between the liquid and the solid saturates, which can lead either to diffusion of air into the liquid or to condensation of the liquid on the surface structures [56,95,96]. Duan and co-workers [97] recently proposed a strategy to restore plastrons through a gas wicking effect inspired by salvinia leaves.

2.5. Self-cleaning surfaces

Self-cleaning is the most prominent field of application for liquid-repellent surfaces. The process of self-cleaning involves the rolling-off of water droplets from the surface, taking along contaminating particles. Besides superhydrophobicity, the presence of water is required for the self-cleaning action; this is in contrast to the alternative strategy of photocatalytic self-cleaning, where organic residues are decomposed by free radicals generated in semiconductors under the action of sunlight [98,99].

Since Barthlott and Neinhuis' first publication pointing out this striking feature [45], it has been frequently demonstrated and is now well known as the “lotus effect”. Such self-cleaning or, better, easy-to-clean surfaces require a weak interaction of the dirt with the substrate accompanied by mobile droplets that can take up and carry off the dirt. Surface roughness supports both of these features as it reduces adhesion between two solids (see Section 3.5.1) and is a prerequisite for the Cassie-Baxter regime with a small contact angle hysteresis. Although this qualitative description is intuitively persuasive, it took about two decades to develop a complete understanding of the self-cleaning mechanism, including propagation of droplets and uptake of particles by the liquid meniscus.

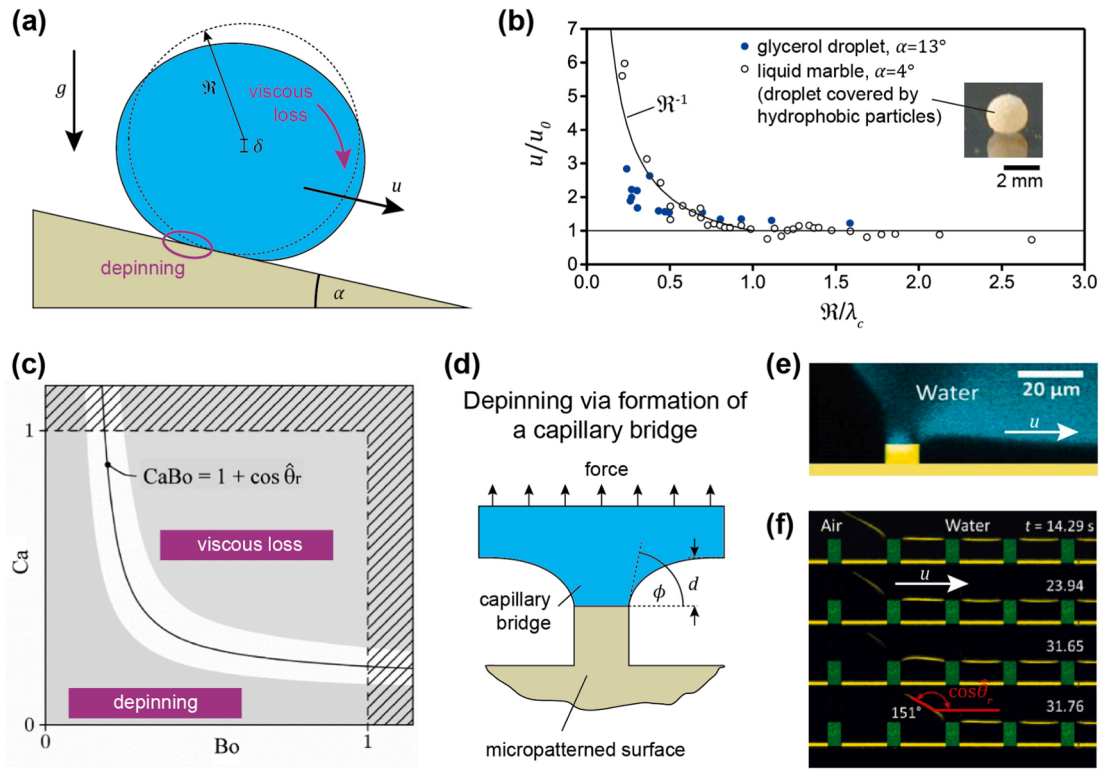


Fig. 2.5. Droplet motion on an inclined surface. (a) Schematic of a non-wetting droplet of radius R moving at velocity u on an inclined surface with angle α . The center of mass is displaced by δ due to the weight of the droplet. (b) Normalized droplet velocity u/u_0 versus normalized droplet radius R/λ_c of glycerol droplets (blue dots) and liquid marbles (empty circles), i.e. a droplet covered by particles (see inset). Graph replotted with data from [103] and [105]. (c) Two regimes of energy dissipation of moving droplets where Bo and Ca are between 0 and 1, where Bo is the Bond number and Ca the capillary number. Reproduced with permission from [107], copyright (2013) American Chemical Society. (d) Schematic of a capillary bridge formed due to pinning of the liquid at the post of a micropatterned surface, constraining the liquid. (e) Confocal microscopic image of a water droplet with a capillary bridge that has formed due to pinning to a micropillar. Reproduced with permission from [108], copyright (2017) American Chemical Society. (f) Sequence of confocal microscope images showing the rear three-phase contact line depinning from micropillars with $10\ \mu\text{m}$ diameter with the dynamic receding contact angle θ_r . Reproduced with permission from [101], copyright (2016) by the American Physical Society.

On inclined surfaces, gravitation is the driving force for droplet motion and is counteracted by the capillary force acting at the three-phase contact line (Fig. 2.5a). Balancing these forces gives a critical angle at which a droplet will start to roll off [100]:

$$\sin\alpha = \frac{s\gamma w}{mg} (\cos\theta_{rec}^{CB} - \cos\theta_{adv}^{CB}), \quad (2.6)$$

where m is the mass of the droplet, g the gravitational acceleration, w the width of the apparent contact area normal to the moving direction, s a shape factor, and the term in the bracket the contact angle hysteresis. The critical value of α depends on the size of the droplet, hence the classification of superhydrophobic surfaces by a critical roll-off angle below 10° is not suitable [101]. The force balance further implies that there exists a critical size (radius R of the droplet) above which droplets start to move, as the capillary force scales with R and the gravity force with R^3 .

It has further been shown that moving droplets on superhydrophobic surfaces tend to roll rather than slide [102,103]. However, initial slip of the droplet along the liquid–solid interface can initiate rolling [104]. Mahadevan et al. [102] and Richard et al. [103] found that the propagation velocity, u scales with $1/R$ for small droplets and tends to be constant, $u_0 \sim \gamma/\eta$, for large droplets, where η is the dynamic viscosity (Fig. 2.5b). The transition between small and large droplet size has been shown to be related to the capillary length, $\lambda_c = \sqrt{\gamma/(\rho g)}$, i.e. the critical length at which capillary and gravitational forces balance. Therefore, due to gravity, large droplets ($R > \lambda_c$) flatten and form a liquid film with the thickness $\approx \lambda_c$. Viscous forces that scale with R^4 dominate during propagation, which explains why smaller droplets move faster than larger ones [102,103,105]. Slight modifications of Quéré’s model were recently proposed by Abolghasemibizaki et al. [106], but made no difference to scaling. Interestingly, liquid marbles, i.e. spherical droplets completely covered with small hydrophobic particles, propagate similarly as droplets with contact angles close to 180° (Fig. 2.5b) [105]. This leads to the conclusion that droplets that pick up dirt from a surface move in a similar way as clean droplets, as long as dirt particles do not adhere strongly to the substrate and do not trap the droplet.

Viscous losses during droplet motion originate mainly from two sources, viscous flow inside the droplet and depinning events at the receding contact line (Fig. 2.5c) [107]. The latter becomes dominant for $CaBo \ll 1 + \cos\theta_r$, where $Ca = \eta u/\gamma$ is the capillary number,

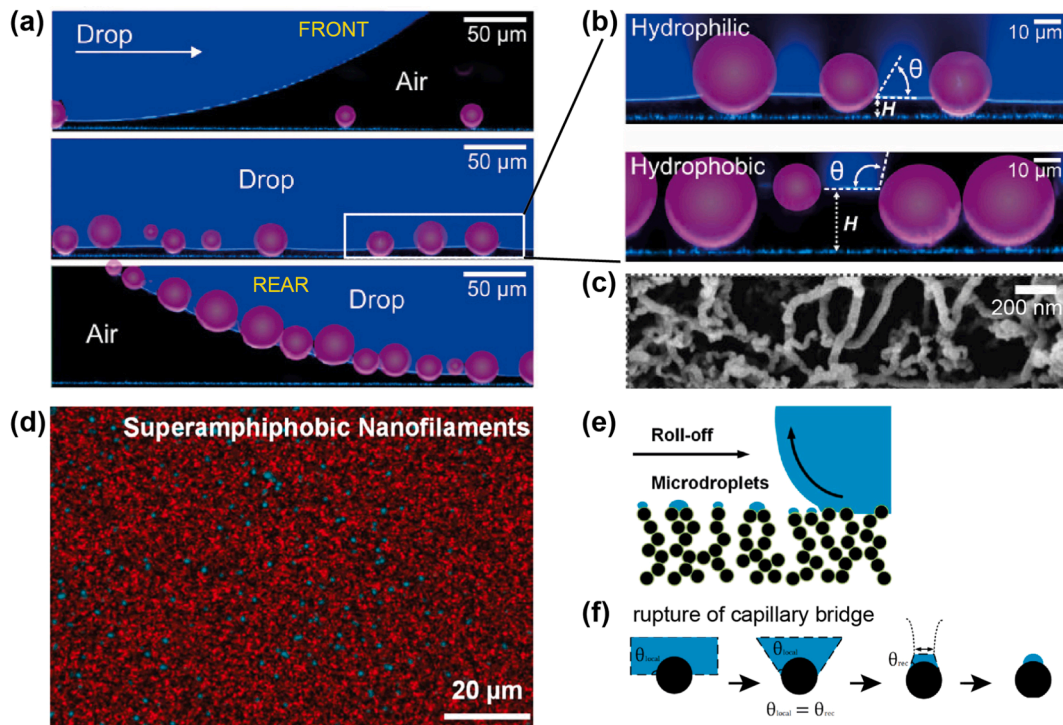


Fig. 2.6. Self-cleaning of a contaminated nanoporous superhydrophobic surface. (a) Laser scanning confocal micrographs (LSCM) of the uptake of micron-sized particles (purple) by a water droplet (blue) moving from left to right. (b) High resolution LSCM highlighting the local contact angle, θ of hydrophilic and hydrophobic particles and the distance of the meniscus from the surface, H . (c) Scanning electron micrograph of the nanoporous surface. (a–c) Reproduced with permission from [117] under CC-BY-NC 4.0 license. (d) LSCM of ethylene glycol droplets (blue) deposited on a superhydrophobic surface (red) after roll-off as illustrated in (e). (f) Rupture of a capillary bridge due to thinning causing Rayleigh instability. (d–f) Reproduced with permission from [118] under CC-BY license.

$Bo = (l/\lambda_c)^2$ the Bond number with l the characteristic length, and $\hat{\theta}_r$ the dynamic receding contact angle at the pinning site at the moment of depinning (Fig. 2.5f). Depinning of the receding contact line is decisive for all droplets that are accelerated from a rest position, as $Ca = 0$ for $u = 0$. With increasing droplet velocity, Ca increases and the viscous losses caused by liquid flow inside the droplet becomes dominant when $CaBo > 1 + \cos\hat{\theta}_r$.

Surface micropatterns influence the self-cleaning effect by interacting with the droplet motion. The energy dissipation during depinning of the contact line from surface features was studied in detail by Butt and co-workers [108]. They demonstrated that depinning of the three-phase contact line involves capillary bridges formed at the rear side of the droplet (Fig. 2.5d–f). The work to form n capillary bridges per unit area is:

$$nW = \gamma(\cos\theta_{rec}^{CB} - \cos\theta_{adv}^{CB}) \quad (2.7)$$

and corresponds to the energy dissipated upon their breakage [108]. This relation links microscopic events with the contact angle hysteresis measured macroscopically by contact angle goniometry. The relationship is valid under quasi-static conditions, $u \rightarrow 0$, further identified as the energy barrier that has to be overcome to initiate roll-off by depinning. The mechanical resistance of a capillary bridge against stretching and rupture depends on γ and on surface features including size, tip geometry and areal density. The latter can cause complex deformations of the three-phase contact line depending on the distance between the features in relation to the capillary length [104,109,110].

Recent studies using laser scanning confocal microscopy confirmed the presence of capillary bridges at the rear of the droplet (Fig. 2.5e,f) [101]. Microscopic contact angles in the vicinity of the three-phase contact line were found to vary (or oscillate during rolling of the droplet); this is in contrast to rather stable macroscopic contact angles. The formation of capillary bridges can be rather complex as it depends on the density of pinning sites, e.g. microfibrils per area, and the surface tension of the liquid. These studies also confirmed earlier assessments of the applicability of the Wenzel and the Cassie and Baxter models, both of which must take into account roughness near the contact line rather than global roughness [111–113]. Similarly, friction of a sliding droplet on a surface is dominated by contact line friction, whereas friction at the liquid–solid interface can often be neglected, especially when the droplet is

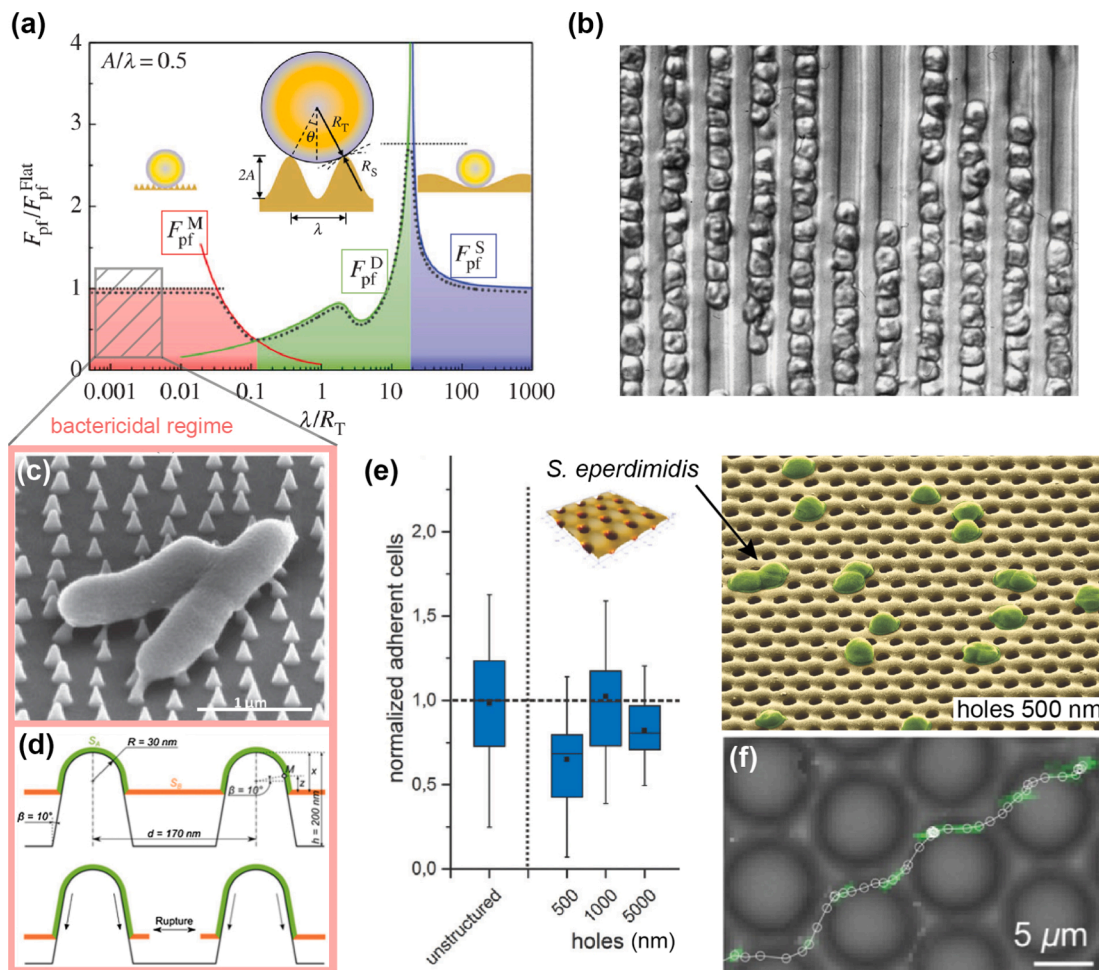


Fig. 2.7. Anti-fouling surfaces. (a) Normalized adhesion force in terms of the ratio of the surface wavelength, λ , to radius of the microbe, R_T , in three possible configurations. (b) Spores attached to 5 μm wide channels. (c) *E. coli* attached to nanopatterned silicon surface. (d) Model that describes the stretch and rupture of the cell membrane (orange). (e) *S. epidermidis* adhered to surfaces with holes of various diameters. The micrograph highlights the adhesion of bacteria to surfaces with holes of 500 nm. (f) Time-lapse of a bacterium traversing a micropatterned surface with 8 μm features. Images reproduced with permission from (a) [148], copyright (2018) Royal Society. (b) [144], copyright (2002) Taylor & Francis. (c) [59], copyright (2019) IOP Publishing. (d) [150], copyright (2013) Elsevier. (e) [140], copyright (2016) Royal Society of Chemistry. (f) [156], copyright (2018) American Chemical Society.

rolling instead of sliding. Therefore, static and dynamic friction forces can be obtained from expressions similar to Eqs. (2.6) and (2.7) [114]:

$$F_s = \gamma w_s (\cos\theta_{rec}^s - \cos\theta_{adv}^s) \quad \text{and} \quad F_{kin} = \gamma w_{kin} (\cos\theta_{rec}^{kin} - \cos\theta_{adv}^{kin}), \quad (2.8)$$

where “s” and “kin” denote the static and kinetic friction regimes, respectively.

The mechanism of how a rolling droplet picks up dirt particles from a surface is important for understanding self-cleaning. First, the front of the droplet encloses and partially wets the particles adhering to the substrate (Fig. 2.6a–c). When the receding contact line of the rolling droplet then pulls on particles of radius r , the capillary force rises linearly with increasing deflection of the meniscus, δ , according to $F_c = k\delta$, where $k = (2\pi\gamma)/\ln(2d/r)$ with d being the average interfacial distance between particles [115]. Hence, the capillary force together with Eq. (2.7) provides an upper bound for the applied work, W_c at which a capillary bridge ruptures while pulling on a particle. This gives $\delta_c = r(0.947 - \ln(r/r_c))$ and $W_c = \gamma(1.58 - \ln(r/\lambda_c))$ for $d \rightarrow \infty$ [108,115]. The particles will detach from the surface when W_c exceeds the work of adhesion, W_{ad} , which is typically of the order of 10 to 100 mJ/m^2 [116]. The effective adhesion of a particle to a rough surface can be even smaller due to a reduced contact area (see also Section 3.5.1 below). Furthermore, there exists a size limit below particles can penetrate into the gaps of the microstructured surface, where the meniscus cannot reach them [117].

A critical issue was recently brought up by Butt et al. [118] regarding liquid remnants upon detachment of a rolling droplet (Fig. 2.6d–f). They demonstrated that when capillary bridges rupture at the receding three-phase contact line, nano-droplets can remain on surface features. These residues do not affect the self-cleaning properties of the surface when the liquid is pure and volatile. However, droplets may carry particles or contain dissolved components such as salts, surfactants and other species. Then these contaminants will be deposited on the surface, which in turn will alter the wetting characteristics of the surface in repeated wettings or cleaning attempts [119]. The design of the microstructure has therefore to be optimized to suppress pinning of the receding contact line, e.g. by preventing sharp edges. Furthermore, the attraction of the liquid to the surface enhances with increasing surface energy, whereas the reduction of the surface tension of the liquid that is applied reduces the strength of the capillary bridge. Both phenomena are frequently discussed in relation to omniphobic surfaces, where self-cleaning must then be critically evaluated.

2.6. Anti-fouling

Fouling is the contamination of surfaces by microorganisms such as bacteria, fungi, algae, and small animals. Strictly speaking, the settlement of such organisms does not result from the interaction of a liquid with a solid, but the presence of water which mediates fouling. Therefore, all strategies to reduce wetting will help prevent fouling. Furthermore, the wetting state on a rough surface defines the solid–liquid interface, making it accessible to microbes. Fouling of surfaces has been discussed in three major fields, marine fouling, fouling in a biomedical context and in an industrial setting [120].

Marine fouling can involve more than 4000 microbial species, leading to highly diverse scenarios. A typical result of marine fouling is the enhanced surface roughness on the hull of a ship that in turn increases drag and, consequently, fuel consumption [121]. Biomedical fouling is the attachment of bacteria on catheters, implant surfaces and other medical devices in contact with the human body, raising the risk of infection [122]. Moreover, the adsorption of blood platelets on implant surfaces can cause blood clotting, inflammation, or an activation of the immune system [123]. Industrial fouling includes, as examples, the contamination of separation membranes and heat exchangers, which can lead to reduced flow and pipe corrosion.

Fouling commonly starts with the adsorption of proteins and attachment of microorganisms to the surface. The expression of extracellular material and the reproduction and colonization of microorganisms lead to continuous biofilm formation which can then attract macrofoulers [124]. Most biocide-free, anti-fouling concepts focus on inhibition at an earlier stage of fouling, i.e. preventing proteins from adsorbing and microbes from adhering to the bare surface. Among other approaches, protein adsorption can be reduced by immobilization of peptides and peptoids [125,126] and the surface hydration by hydrophilic or zwitterionic polymers to sterically hinder protein adsorption [127–130].

On superhydrophobic or omniphobic surfaces, proteins can only immobilize at the solid–liquid interface and possibly extend over the plastron for as long as it is intact. Hannig et al. [131] demonstrated that after short-term exposure (3 min) to the human oral cavity, a thin film of proteins, glycoproteins and lipids (i.e. the pellicle) adsorbed to the mushroom-shaped microstructures of springtails and spanned a 5 to 20 nm thick film in between them. With ongoing exposure to oral fluids, further protein adsorption and bacteria colonization was observed that finally led to a biofilm after 24 h. Reduced liquid–solid contact was also claimed by Zhao et al. [132] to reduce the amount of blood platelet adhesion.

In contrast to protein adsorption, bacterial adhesion is much more complex as it includes physical, chemical, and biological interactions between bacteria, the solid surface, and the surrounding medium. Bacteria are very efficient in colonizing surfaces and, in fact, can attach to virtually all material classes [133]. Detailed mechanisms of bacterial attachment including force sensing, quorum sensing, and activation of signaling pathways are comprehensively reviewed in [134–136]. Among diverse strategies recently proposed in the literature [137–139], we will focus below on effects related to surface topographies (Fig. 2.7).

2.6.1. Reduced fouling on microstructures

Micropatterning is a useful strategy to reduce fouling. Compared to smooth surfaces, patterns have been shown to reduce the amount of adhered microorganisms. Unfortunately, small changes of the pattern dimensions or geometry can enhance fouling as the same organisms then profit from microstructures (or surface defects in general) (Fig. 2.7b), which complicates the approach. Based on numerous studies, it is now accepted that the ratio of the microstructural feature size to the organism size has to be considered in the design of an anti-fouling surface (Fig. 2.7e) [58,140–143]. As the size of bacteria and other microbes vary between species, a general design to prevent overall fouling cannot exist. However, surface modifications to combat specific pathogens are feasible. Based on the literature on initial bacteria attachment to surfaces over the past two decades, an important issue is the evaluation of the versatility of surface microstructures in the context of anti-fouling.

Earlier models predicting initial adhesion of microorganisms are the attachment point theory [144,145], the engineered roughness index model [146], and their combination [147]. The attachment point theory is based on maximizing the contact area between the organism and the surface topography that, for example, can explain why organisms tend to align along grooves (Fig. 2.7b). The engineered roughness index model is based on Wenzel's roughness parameter, r (see Eq. (2.2)) and the areal fraction, f given in Eq. (2.3). Both models evolved empirically and lack a physical basis. A first attempt to provide a more predictive model was recently published by Fu et al. [148]. Based on contact mechanics, they provide a plane strain model of a cylinder adhering to a sinusoidal rough substrate, where the maximum adhesion force depends on the ratio of the wavelength, λ , to the radius of the cylinder, R_T (Fig. 2.7a). Fu et al. discovered three regimes in terms of λ/R_T , where only the second regime exhibits reduced adhesion. In this regime, there are two local minima for $\lambda/R_T = 0.1$ and $\lambda/R_T = 4$. A global maximum was found for $\lambda/R_T \approx 20$. It should be noted that these numbers correspond to $\lambda/A = 0.5$, where A is the surface amplitude. The authors found that higher amplitudes are more effective for reducing adhesion, but force minima and maxima can shift to other λ/R_T ratios. The model is a first attempt to theoretically predict

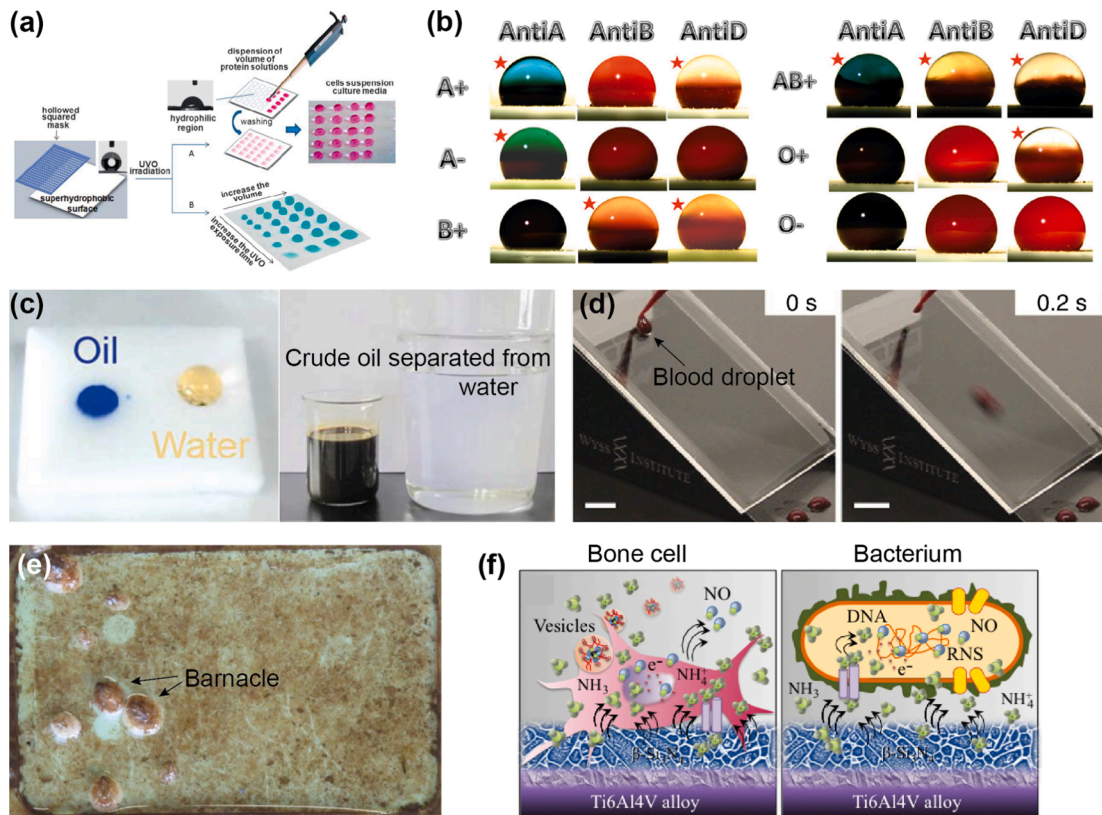


Fig. 2.8. Applications of superhydrophobic and omniphobic surfaces. (a) High-throughput protein-cell interaction tests and (b) blood type screening test, where residues at the surface have to be avoided. (c) Foam which absorbs crude oil from water for water–oil separation. (d) Omniphobic surface repelling blood droplet. (e) Reduced biofilm formation and attachment of barnacles to a micropatterned surface (5×8 cm) upon exposure for 16 weeks to Baltic sea. (f) Schematic of titanium implant with nanoscopic Si_3N_4 coating for improved bactericidal and osteogenic function. Images reproduced with permission from (a) [175], copyright (2011) Royal Society of Chemistry. (b) [176], copyright (2013) Elsevier. (c) [177], copyright (2017) Wiley. (d) [123], copyright (2014) Springer Nature. (e) [178] under CC-BY license. (f) [179], copyright (2020) Elsevier.

adhesion of tubular microorganisms to wavy surfaces, but would need to be extended to 3D spherical organisms adhering to holes or pillars to provide a clear guideline for preventing initial adhesion of microorganisms.

2.6.2. Bactericidal nanostructures

In addition to reduced bacteria adhesion discussed above, Ivanova et al. [53] discovered that bacteria (*P. aeruginosa*) attaching to cicada wings (*P. claripennis*) were killed within 3 min (Fig. 2.1c). The phenomenon has been associated with the presence of conical-shaped nanostructures (height ~ 200 nm, base diameter ~ 100 nm and tip diameter ~ 60 nm) densely packed on the cicada wing. Other Gram-negative bacteria were killed at those surfaces with similar efficiency, whereas Gram-positive bacteria were resistant [149]. Based on this observation, a physical–mechanical model was proposed that describes the rupture of the cell membrane when the bacterium sinks into the surface (Fig. 2.7d). The adsorption of the cell membrane to the surface is driven by minimizing surface free energy. Simultaneously, the free membrane in between the nanostructures stretches and ruptures at a critical strain, killing the bacterium [150]. This model further explains why Gram-positive bacteria are more resistant, as they exhibit stiffer membranes that counteract adsorption into the nanostructures. The nanotopography varies between cicada species [151]. Kelleher et al. [152] demonstrated that such structural variations can affect the efficiency of the bactericidal effect.

For synthetic surfaces made via nanoreplication, Wu et al. [153] found variations in the bactericidal efficiency related to topographical changes, such as areal density of nanofibrils and their height (Fig. 2.7c). They claim that the bactericidal efficiency is associated with the areal density of the nanostructures, as it controls the stretch of the cell membrane, whereas the size of the nanostructures, which may relate to the penetration of nanostructure into the membrane, has only minor effects. However, a systematic study with independent variations of each design parameter is still lacking [154]. Furthermore, other parameters controlling bacteria-surface interaction, such as cell rigidity, adhesion forces, and the role of surface chemistry have been neglected so far [155].

Overall, surface topography can control the initial bacteria attachment, whereby it can have both promoting and inhibiting effects. In addition, the bactericidal effect of nanostructures opens up a novel approach to prevent fouling with high efficiency.

2.7. Outlook – Microstructures for control of liquids

Surface wetting has been studied extensively over many years and is now reasonably well understood. Macroscopic contact angles, while easily determined, classify only the surface wettability but disregard details at the vicinity of the three-phase contact line. The theoretical prediction of contact angles remains difficult, as the interfacial energies of the solid–liquid and the solid–vapor interface cannot be measured directly. The situation is even more complex on deformable or rough surfaces, where the macroscopic apparent contact angle can strongly deviate from the actual microscopic angle in the vicinity of the three-phase contact line. Such differences can be caused by the deformation of the surface (wetting ridge) due to elastocapillary interactions or the deformation of the liquid (capillary bridge) due to pinning of the contact line. Nevertheless, the significant progress in understanding these phenomena now opens emerging fields such as capillarity-controlled shape-transforming soft materials [157]. Wetting and dewetting dynamics in contact with deformable solids is another topic of high interest, for example for underwater adhesion [158].

Superhydrophobicity is a very desirable property, e.g. for optical systems, glasses, and touch devices. In the past, superhydrophobic surfaces have been associated with sufficiently rough surfaces and intrinsically non-wettable materials with low surface free energy. This results in a Cassie-Baxter regime, in which air is trapped at the surface below the liquid. The invention of omniphobic surfaces based on surface features with overhangs contradicts this definition; it allows the usage of all wettable and non-wettable materials as long as other interactions with the liquid, such as dissolving, swelling, and so on are prevented. This finding has major advantages for the generation of future liquid-repellent surfaces: (i) Environmentally-friendly coatings can replace harmful perfluorinated alkyl chains that are commonly used to reach high contact angles [159]; (ii) additional entities can be added to omniphobic coatings to enhance their functionality for specific applications such as preventing thrombosis [160]; and (iii) the incorporation of hydrophilic patches enhances adhesion at the liquid–solid interface, making drag reduction more robust [121,161].

Superhydrophobic and self-cleaning functionalities are often loosely used as synonyms. But superhydrophobicity does not necessarily lead to self-cleaning. In fact, a moving droplet can worsen the situation by leaving residues due to rupture of capillary bridges pinned to the surface. Surface designs therefore have to be optimized to suppress pinning of the receding contact line, for example, by rounding sharp edges. Residues must be avoided especially if superhydrophobic or omniphobic surfaces are to be applied to biomedical diagnostic systems (Fig. 2.8a,b). Here droplets containing enzymes, cells, or other bioactive components are transported over superhydrophobic pathways, which then could be cross-contaminated by residues during repeated use [162,163].

Still challenging and a major concern for superhydrophobic surfaces is their mechanical durability, as fine structures are easily damaged by scratching or similar abrasive treatments. Hierarchical surfaces can enhance mechanical resistance. Large, often conical-shaped protrusions resist higher shear loads and can shield smaller features located in between these protrusions as only the tops are exposed to mechanical contact [164,165]. The latter was also discussed for springtails adapting to different habitats: conical-shaped protrusions are only present in soil-dwelling species, whereas species living on plants do not express these features [166]. Furthermore, holes, grids and membranes are typically more robust than fibrils or needles [167]. A major problem in comparing the robustness of different designs is that, to emulate friction and wear, abrasion tests vary greatly between groups [168]. From a materials perspective, robustness against wear could be improved by raising the hardness without increasing brittleness; consequently, tough composites could possibly be a better choice [169].

Anti-fouling strategies are of immense importance in biomedical, marine and industrial applications where liquids are in long-term contact with surfaces. Superhydrophobic and omniphobic surfaces can have both deterrent and attractive effects on attachment of microbes depending on their size relative to the feature spacing (Fig. 2.8d,e). Upon settlement, microstructures can further restrict the mobility of such organisms (Fig. 2.7f), which probably depresses colonization as a next step towards biofilm formation [156]. Although the amount of microbes can be reduced by suitable micropatterning, strategies to eliminate bacterial adhesion or even to prevent biofilm formation over weeks are not well developed [122]. The only known concept so far is to cover the surface with nanoscopic bactericidal patterns. Interestingly, such surfaces can otherwise promote stem cells to differentiate towards bone formation (Fig. 2.8f) [170,171]. Further research in this direction is therefore indicated as bone implants could benefit considerably [172–174].

3. Microstructures for interaction with solids: Adhesion and handling

Adhesion is a fundamental mechanical phenomenon occurring in the contact region of two finite-sized solids. It is omnipresent in our daily life: in the fixation of wallpaper a chemical glue mediates adhesion between two bodies and in chewing gum the softness - annoyingly - enhances the stickiness to delicate surfaces. In our bodies, the adhesion of blood platelets can lead to wound healing or thrombosis, e.g. [180], and the adhesion of bacteria to our teeth, e.g. [181] can ultimately destroy them. Adhesion is, with exceptions, an inescapable consequence of electronic interactions in the adjacent objects and it is frequently the absence of adhesion that would require an explanation (see *The Sticky Universe* [182]).

The literature on adhesion phenomena is vast. To set the focus for this section, we will cover only temporary or reversible adhesion by intermolecular interactions. This excludes glues and technical adhesives based on chemical reactions from our discussion. Also “velcro”-type adhesion, sometimes referred to as probabilistic fasteners, will be outside the scope of the review as it requires two

adequately structured surfaces. The surfaces discussed here derive their enhanced adhesiveness from microfibrils generated by established microstructuring techniques (see Appendix). Interestingly, this implies that the material which makes up the microstructure may be intrinsically non-adhesive - a prime example of the fascinating paradigm of micropatterning.

Adhesion by intermolecular interactions is modulated or enhanced by the presence of surface protrusions that in nature take on many shapes and forms². Van der Waals interactions, which are unspecific and relatively insensitive to surface chemistry, have been concluded to be dominant under most circumstances (for modern treatments see e.g. [116,183]). Such contacts can be separated, without damage, on demand and re-formed repeatedly.

We will focus on *normal* adhesion of microstructures and touch only briefly on related friction phenomena; interesting variants of fibrillar adhesives have been developed that engage strongly by shear, e.g. in the Cutkowski [184] and Sameoto groups [185]. The principle of manipulating adhesion by shear was identified in animals by Autumn et al. [186] and by Federle and Labonte [187] and was analyzed in depth in the Israelachvili group (“frictional adhesion”) [188].

The reader is cautioned that the usage of the terms adhesion and friction is not always unambiguous in the literature: by definition, adhesion between two objects is the resistance to their separation in the direction *perpendicular* to the two surfaces whereas friction is the resistance to shearing in the *tangential* direction. It is conceded that friction and adhesion forces can superimpose and that these definitions will be somewhat ambiguous when the surfaces exhibit finite roughness. To avoid confusion, the term “adhesion” should however not be used for the results of friction measurements as is sometimes encountered in the literature. Another limitation of numerous previous papers is the fact that only adhesion *forces* for a particular set-up are reported instead of the *stresses* transmitted through the contact; this often prohibits quantitative comparison of adhesion results among different literature sources.

The field of fibrillar adhesive microstructures has occupied many groups over the past two decades and the literature is therefore extensive. This interest is not only driven by scientific curiosity but also by the realization that tunable adhesion could eventually be used to advantage in numerous applications. Examples are pick-and-place handling of objects, e.g. [16,189–191], climbing robots [192], retrieval of space debris [193,194], and biomedical devices (to be discussed in Section 4).

Biological examples of adhesives microstructures are impressively described, e.g., by Nachtigall [195], Gorb [196,197], Federle [198], Dhinojwala [199] and Speck [200]. Insightful overviews focusing on certain aspects of artificial microstructures are available, e.g. from the following groups: Bartlett [201], Creton [202], Crosby [203–206], Cutkowski [184], Dhinojwala [207], del Campo [208], Gorb [209–211], Grunlan [212], Israelachvili [213], Kim [214], Kwak [215], O’Rorke [216], and Sameoto [217].

This section will review the current understanding of adhesion modulation by functional surface microstructures, with particular emphasis on advances in the last decade. Wherever possible, we will emphasize the micromechanistic understanding and identify gaps in previous investigations. This section will substantially expand on our earlier reviews [218,219] and a more recent feature article [16].

3.1. Biological inspiration of adhesion by microstructure

Nature has demonstrated in many instances that adhesion can be modulated over a wide range by geometric design of surface features: fibrillar outgrowths on insects, spiders, and lizards, for example, were discovered to control the animals’ locomotion and clinging ability and other functions ranging from drag or wear reduction to anti-friction, anti-reflection and coloration [196,197]. A most celebrated example is the outstanding ability of geckos to cling to rough rocks or branches and to smooth walls or ceilings.

3.1.1. The gecko inspiration

Since Aristotle, observers have marveled at this feat of nature but, for centuries, lacked an explanation. A most fundamental insight was provided by a military physician of the Austro-Hungarian empire: from experiments conducted with geckos, Dr. Franz Weitlaner [220–222] concluded as early as 1902 that the clinging ability could not be due to a suction effect as is often intuitively assumed. Following optical investigations in the 19th century, the first investigations of the gecko foot pads by scanning electron microscopy were reported by medical anatomists [223,224]; they revealed an unusual hairy structure with hierarchical architecture and extremely fine contact elements of submicron size. Adhesion was found to scale with the surface energy of the substrate but the exact mechanism remained obscure.

An important trigger for the field was provided by Autumn et al. [225,226] in 2000: they inferred from their experiments on gecko hairs in contact with hydrophobic (GaAs) surfaces that their adhesion had to be due to van der Waals interactions. Subsequently, Huber et al. demonstrated by AFM experiments on single attachment elements (*spatulae*) that, in the presence of humidity, capillarity can contribute about equally to adhesion [227]. The role of subsurface contributions was subsequently emphasized by Loskill et al. [223]. To complete the picture, observations of charge separation in artificial polymeric gecko structures have suggested a minor contribution from electrostatic forces [228]. It is emphasized that the current consensus on the predominance of van der Waals interactions, in dry conditions, is based on the exclusion of alternative mechanisms.

We note in passing that another counterintuitive consequence of surface patterns is that protrusions can help reduce friction as evidenced by the sandfish [229–231]. This effect has been utilized to develop low-friction surfaces for engineering components

² For consistency, we will refer to these protrusions predominantly as “fibrils” in this section. Alternative biological designations are, for example, ridges, spikes, hairs, setae, spatulae, papillae or bristles. As design elements, fibrils, pillars and posts are understood to be largely synonymous from a geometric point of view. We neglect that the designation “fibril” tends to be associated with a more flexible and bendable element whereas “pillar” invokes a stiffer response. The solid in contact with the fibrils will here be referred to as the “object”.

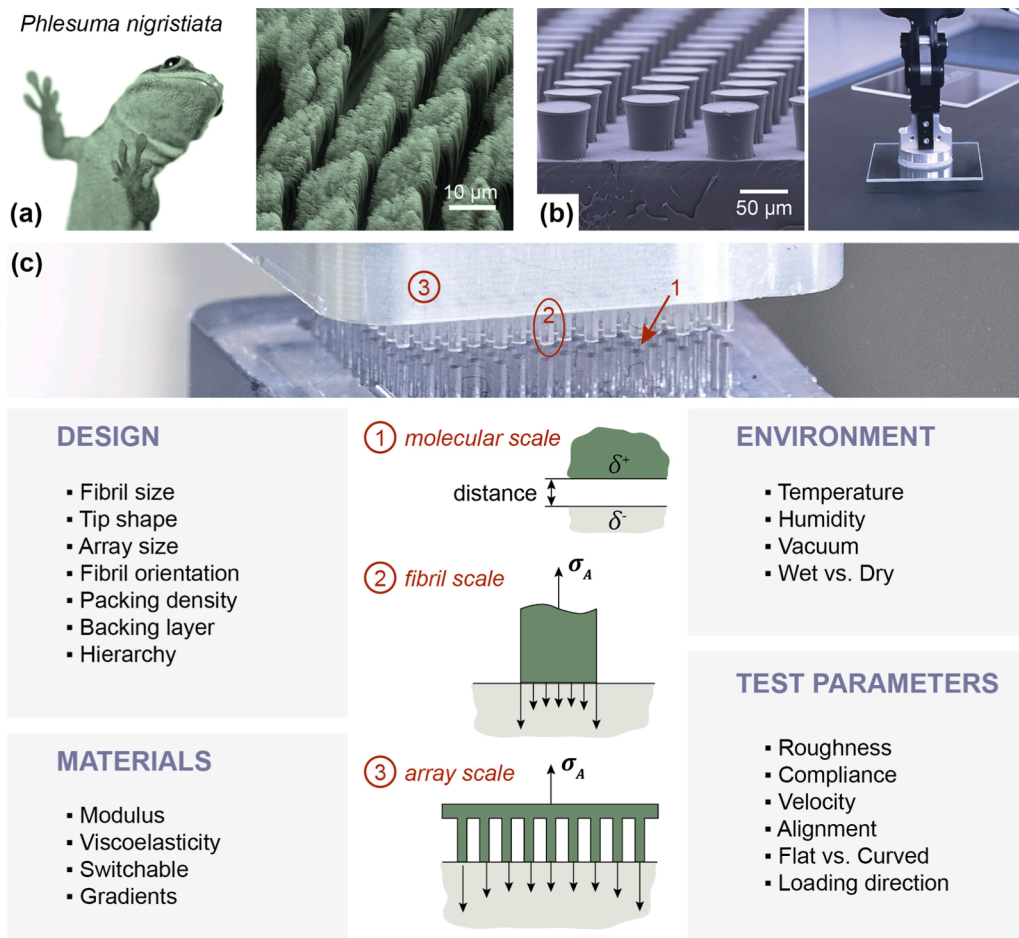


Fig. 3.1. Bioinspired adhesion and its path to handling applications. (a) Gecko adhesion as the natural example, mediated by a hierarchy of keratinous hairy structures with sub-micron thickness. (b) Laboratory samples of arrays with mushroom-shaped fibrils mimicking gecko adhesion [236] (reproduced under CC-BY license) and implementation in a pick-and-place device. (c) Parameter space for the design of artificial fibrillar microstructures. Important categories to be considered are geometric design, materials, environment, and testing parameters. Micropattern adhesion involves mechanisms at the molecular, the fibril and the array level; stress distributions govern the adhesive performance.

[232–235].

3.1.2. Towards artificial gecko structures

Intense research efforts were made in the 2000s to emulate gecko adhesion in the laboratory by designing artificial surface microstructures. The promise was that surface patterning could create sticky surfaces on intrinsically non-sticky materials. It was soon realized that the implementation of switchable adhesion could pave the way towards novel attachment concepts for robots and handling systems, among other applications (Fig. 3.1a,b).

The parameter space for designing synthetic adhesion microstructures was soon realized to be immense. Fig. 3.1c attempts to categorize these elements: for a given molecular interaction, adhesion can be tailored through (geometric) design of the fibrils and by choice of materials with various properties. Attention must be paid to the environment and the testing conditions typical for specific applications.

The research efforts of the two decades since 2000 can be grouped as follows:

- **Fibril level** (first decade): In the first decade, behavior, understanding and development of fibrillar elements in contact with model substrates were in the focus of attention. Fundamental effects included those of size, shape, elastic modulus, and humidity on the adhesion performance. They were explored mostly by model experiments and generic theoretical modeling.

- *Array level* (second decade): More recent is the realization that a microfibrillar array does not simply behave as the sum of its individual fibrils. Rather, the elastic communication of the fibrils through the backing layer of the array, the nature of the load distribution among the fibrils, and the statistics of individual fibril detachment play important roles. These advances prepared the way to increasingly reliable exploitation of the adhesive effect in emerging applications.

We will now give an overview of the current understanding of these elements.

3.2. Design of adhesive microfibrils

3.2.1. Size effect (scaling)

At first sight, the very nature of the “gecko effect” is counter-intuitive: Why should the removal of material from the contact region, to form a micropattern with less contact area than a bulk contact, improve adhesion? What is the role of the gaps between the fibrils? And why should a size reduction of the fibrils improve adhesion, as suggested by the much finer structures in geckos than in insects [237]?

3.2.1.1. The principle of contact splitting. Small things always stick - this size dependence is an essential result of the Johnson-Kendall-Roberts (JKR) theory of adhesion [238], which was originally developed for elastomeric materials. Assuming an – admittedly unlikely – spherical contact shape, this theory also provided an explanation for adhesion enhancement by splitting one large contact into finer elements [226,237]. Even with this oversimplification, JKR illustrates one of the main tenets of fibrillar adhesion: When an adhesive contact is created, elastic deformation enables surfaces to come together and allows the system to reduce surface area. In smaller contact elements, the “gain” in reduction of surface energy (a 2D effect) more easily offsets the elastic strain energy “penalty” (a 3D effect). This translates into higher adhesion strengths.

This “principle of contact splitting” provided a possible explanation for the inverse correlation between attachment fibril diameter and animal mass [237]: heavier animals, such as geckos, exhibit finer contact elements, which hence “amplify” the effect of the van der Waals interaction. More realistic contact shapes were analyzed theoretically by Hui et al. [239,240] and by Spolenak et al. [241]. For a critical discussion of dry versus wet adhesion in this size correlation see Federle [198].

Following categorization by [218,242], contact splitting can enhance adhesion in several ways:

- *Surface-to-volume effect:* Fibrils show a more favorable balance between elastic strain and surface energy [237,238].
- *Interfacial defect statistics:* Thin fibrils have a decreased likelihood of encountering a critical defect in the contact area [243,244].
- *Uniform stress distribution in the contact:* Below a critical diameter, fibrils are predicted to enter a defect-insensitive detachment regime and detrimental stress concentrations should disappear [239,245,246].
- *Crack trapping:* Detachment of discrete fibrils requires an interface crack to re-initiate at each subsequent fibril (extrinsic contribution to the work of adhesion) [247,248].
- *Adaptability to rough surfaces:* Fibrillar elements can conform to roughness with less strain energy penalty [249,250].
- *Contact redundancy:* The multiplicity of contacts reduces the sensitivity of the adhesive performance to local defects, delamination and contamination [251,252].

The scaling in JKR adhesion is most generally illustrated following Yao and Gao [253]. We divide their solution for the adhesion force F_p of axisymmetric contacts with a power-law profile by the characteristic area R^2 and arrive at the following generic dependences for the adhesion strength³:

$$\sigma_p \sim \frac{F_p}{R^2} \sim (E^*)^{\frac{n-2}{2n-1}} \left(\frac{W_{ad}}{R} \right)^{\frac{n+1}{2n-1}}. \quad (3.1)$$

Here E^* is the reduced elastic modulus, W_{ad} the thermodynamic work of adhesion, and n the exponent for the power-law profile. Eq. (3.1) clearly predicts higher adhesion for structures of smaller size R (for all admissible values of $n \geq 1$). It is instructive to consider some limiting cases: The equation reduces correctly to the modulus-independent solution for an approximately spherical shape ($n = 2$) [238]. The smooth flat punch ($n \rightarrow \infty$) exhibits a proportionality to the square root of the modulus, in agreement with the Kendall solution [254]. Interestingly, adhesion will be inversely related to modulus for a sharp cone ($n = 1$); this suggests that soft microstructures will be advantageous in situations of low contact area, as e.g. in the presence of asperities on rough surfaces (see also Section 3.5.1).

3.2.1.2. The fracture mechanics analogy. Contact formation is the opposite of crack advance and is therefore related to linear elastic fracture mechanics. The scaling law proposed by Crosby and collaborators [255] reflects the Griffith criterion for the instability of cracks with the fibril dimension substituting for the crack length. Expressed in terms of adhesion strength, it reads:

³ Throughout this review, the term *adhesion strength* will be used to denote the maximum tensile force, sometimes called critical or pull-off force, necessary to separate the two objects, when divided by the nominal contact area. In the literature, pull-off stress, maximum tensile stress or critical stress are used interchangeably.

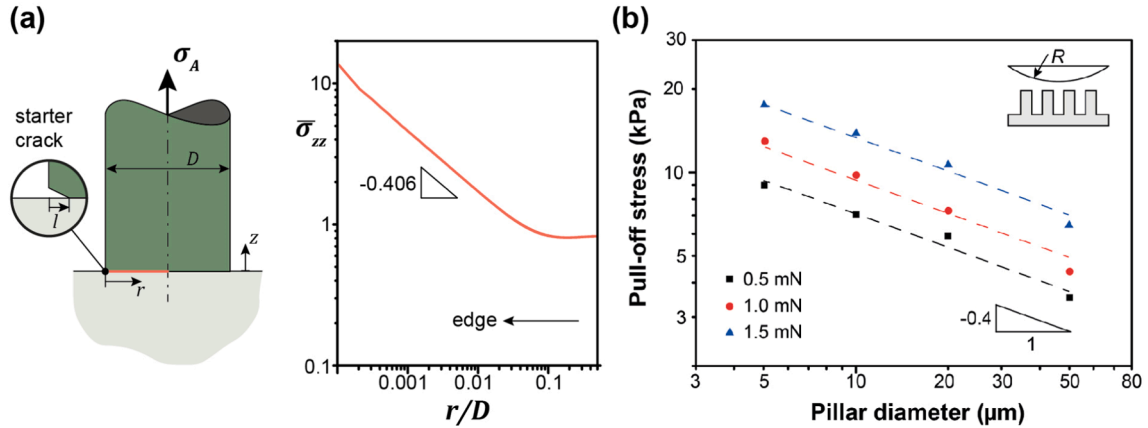


Fig. 3.2. Size effect in adhesion of cylindrically-shaped fibrils (defect-sensitive regime). (a) Detachment is considered by propagation of a starter crack from the fibril edge. The calculated distribution of the normal stress $\bar{\sigma}_{zz}$ normalized by the applied remote stress σ_A exhibits, under no-slip conditions, a singularity at the edge (red line). The model predicts a dependence of adhesion on the fibril diameter D as given in Eq. (3.3) [260]. (b) Experimental evidence for the size effect in fibrillar polydimethylsiloxane (PDMS) microstructures; experiments vs. a glass sphere, the colors correspond to different levels of compressive pre-stressing. Data replotted from Ref. [261].

$$\sigma_p \sim \sqrt{\frac{G_c}{AC}} \sim \sqrt{\frac{G_c E}{D}}. \quad (3.2)$$

Here, G_c is a “property set by the materials comprising the interface” - in fracture mechanics terms the work of fracture (or energy release rate), A the surface (contact) area, and C the contact compliance. The second expression was derived in terms of Young’s modulus E and contact diameter D . This scaling was successfully applied to gecko pads and to artificial fibrillar structures under different loading situations [255,256]. It can qualitatively guide the development of fibrillar adhesives but it lacks quantitative predictive power. Eq. (3.2) reduces to the classical equation for stiff fibrils in contact with a compliant half space [254].

A treatment based on conventional fracture mechanics by Carbone and Pierro [257] arrives at the following size dependence for the adhesion strength: for sticking friction of an incompressible compliant fibril on a rigid, flat surface, the exponent on fibril diameter is stated to be about -0.4 ; the frictionless rigid punch on a compliant half space results in an exponent equal to -0.5 , i.e. the Kendall size dependence. While these results provide an initial assessment of the adhesion strengths of punch-shaped fibrils, they do not explore the full implications of fracture mechanics for adhesion of such fibrils.

For the interface between dissimilar materials, fracture mechanics needs to be modified as demonstrated by Fleck and McMeeking for punch-shaped fibrils adhering to a flat surface [258,259]. The more accurate calculations confirm the presence of the stress singularity at the circumferential edge of the fibril identified by Carbone and Pierro, at least under conditions of finite interfacial friction (Fig. 3.2a). However, in realistic fibril structures, the edge will have a finite radius of curvature; this modifies the singularity but adds a small starter crack which then propagates at a rapidly decreasing stress (inset in Fig. 3.2a). For compliant fibrils on a stiff object, this situation was analyzed in the “flaw-sensitive” regime, i.e. for cohesive zones much smaller than the fibril diameter [259,260]. The resulting adhesion strength σ_p is given by:

$$\sigma_p = \frac{0.6\sqrt{EW_{ad}}}{D^{0.406}l^{0.094}\hat{a}}, \quad (3.3)$$

where E is Young’s modulus of the fibrils, l the size of an assumed starter crack, and \hat{a} a calibration factor of order 1, established by numerical simulation. It is noteworthy that the adhesion strength increases with the square root of the modulus as expected. Furthermore, it is insensitive to l , which suggests tolerance to imperfections unavoidable in microfabrication. Finally, a scaling effect is predicted with fibril diameter D , with a universal power-law exponent of -0.406 . This exact result differs from the previous fracture-mechanics treatments. Eq. (3.3) will apply until the cohesive strength of the interface is reached.

Experiments confirmed the improved adhesion of micropatterned surfaces over unpatterned controls [252,261]. However, due to the scarcity of systematic investigations, the literature does not contain widespread experimental evidence for such size effect. Still the most comprehensive study to date is by Greiner et al. [261]. Their results exhibit a power-law exponent of -0.4 for the size effect (Fig. 3.2b), in good agreement with the fracture mechanics prediction.

3.2.1.3. Flaw-insensitive regime. Very thin fibrils may profit from another effect: they will become insensitive to interfacial defects

[239,245,246,262], similar to natural materials such as nacre or bone [3]. Detachment will then proceed, at a theoretical cohesion stress, as a cohesive failure of the interface without crack propagation. This transition is predicted to occur at a critical fibril radius given by

$$R_{cr} = \frac{8 E^* W_{ad}}{\pi \sigma_{th}^2}. \quad (3.4)$$

Taking typical parameters for polydimethylsiloxane (PDMS, $E = 2$ MPa) and for van der Waals interactions ($W_{ad} = 50$ mJ/m² and $\sigma_{th} = 0.6$ MPa [263]) suggest a critical radius of about 700 nm. Hence, thin and stiff gecko *spatulae* may profit from this effect [262] but the flaw-insensitive regime cannot be reached with most soft artificial fibrils. This highlights the need to optimize the tip shape to maximize adhesion (see Section 3.2.2 below).

Gao and Yao [245] proposed a theoretically optimal shape in the form of a slightly concave contact face to offset the edge singularity. The deviation from flatness is slight (of similar magnitude as given by Eq. (3.4)); this may explain why the concept has so far not been followed up by experimentalists.

3.2.1.4. Aspect ratio effect. An effect that has been studied in passing is how the aspect ratio of the fibrils, i.e. the ratio of length to diameter, affects adhesion. In a numerical finite-element analysis, Aksak et al. [264] arrived at the conclusion that the detachment of high-aspect ratio fibrils will tend to be under load control, which will destabilize crack growth emanating from defects. As a result, adhesion strength values were found to increase with decreasing aspect ratio up to the theoretical strength. However, the concomitant increase in stiffness would impair the adaptability to surface roughness and tolerance against misalignment. This limitation may explain why low aspect ratios are generally not found in natural adhesion systems and are not a design target for most artificial systems. Higher aspect ratios will be advantageous when a large work of separation is required [16,265]. Likewise, any viscoelastic effects will augment adhesion energy as the higher losses will contribute to the work of separation. For a discussion of viscoelastic contributions to adhesion, the reader is referred to the literature [266–269].

3.2.2. Shape effects

Nature has “invented” a wealth of different shapes, as is discussed e.g. by Gorb and Federle [196,241,270]. Arguably the most influential observation is that of the copulatory attachment organs of the male colorado beetle [196], which display a gradual thickening of the fibrils towards the contact area. Because of their superior properties, such mushroom shapes have become the standard synthetic design for most groups. Extensive comparison with cylindrical fibrils and other shapes [271] has demonstrated an enhancement of adhesion for mushroom shapes by more than an order of magnitude. The developments up to 2014 have been reviewed by Heepe and Gorb [252].

3.2.2.1. Mushroom-shaped artificial designs. Several benefits of mushroom microstructures over cylindrical fibrils have been claimed:

- increase in adhesion strength ranging from a factor of 2 [272] to more than 30, reaching the static adhesion of real gecko feet [271].
- increase of peel strength (by a factor of about 3 for PVS), also in the presence of contamination [251].
- increase of work of adhesion (by a factor of about 2.7) [251,273].
- interfacial crack formation in the interior of the contact - initially argued to be attributable to a suction component [274,275].
- decreased sensitivity of adhesion to moderate roughness [257].
- improved tolerance to misalignment between fibril and object surface [273,276,277].
- large increases (more than 20-fold) in adhesion force under water [278].

3.2.2.2. Interfacial stress distribution for mushroom structures. Intuitively, the addition of thin material caps to the contact area is expected to “diffuse” the axial tensile stresses acting along the stalk away from the cap edge; this will protect the edge of the cap from stress concentrations. Spuskanyuk et al. [279] were the first to model this effect numerically; they discovered that a cap can alleviate the stress singularities and shift the stress to the center of the contact. This suggests that any interfacial defects near the contact edge would be less damaging to the adhesion strength. An adhesion enhancement by a factor of 14 (for infinite friction) and larger than 20 (for the friction-free case) was deduced; these values are in reasonable agreement with several experiments.

Carbone and Pierro [257,280,281] have extended their fracture mechanics treatment to a special design of mushroom-shaped fibrils. They concluded that a mushroom cap of optimal thickness can eliminate the edge stress singularity. Also, they suggested that mushroom-shaped fibrils will be more tolerant to the presence of interfacial defects. Their model also includes an analysis of the effects of entrapped air and of a non-uniform pillar height distribution. The authors estimated that fibrils with radius in the nanometer range should detach spontaneously by thermal activation - an eventual lower limit for the contact splitting effect [257,281]. The main

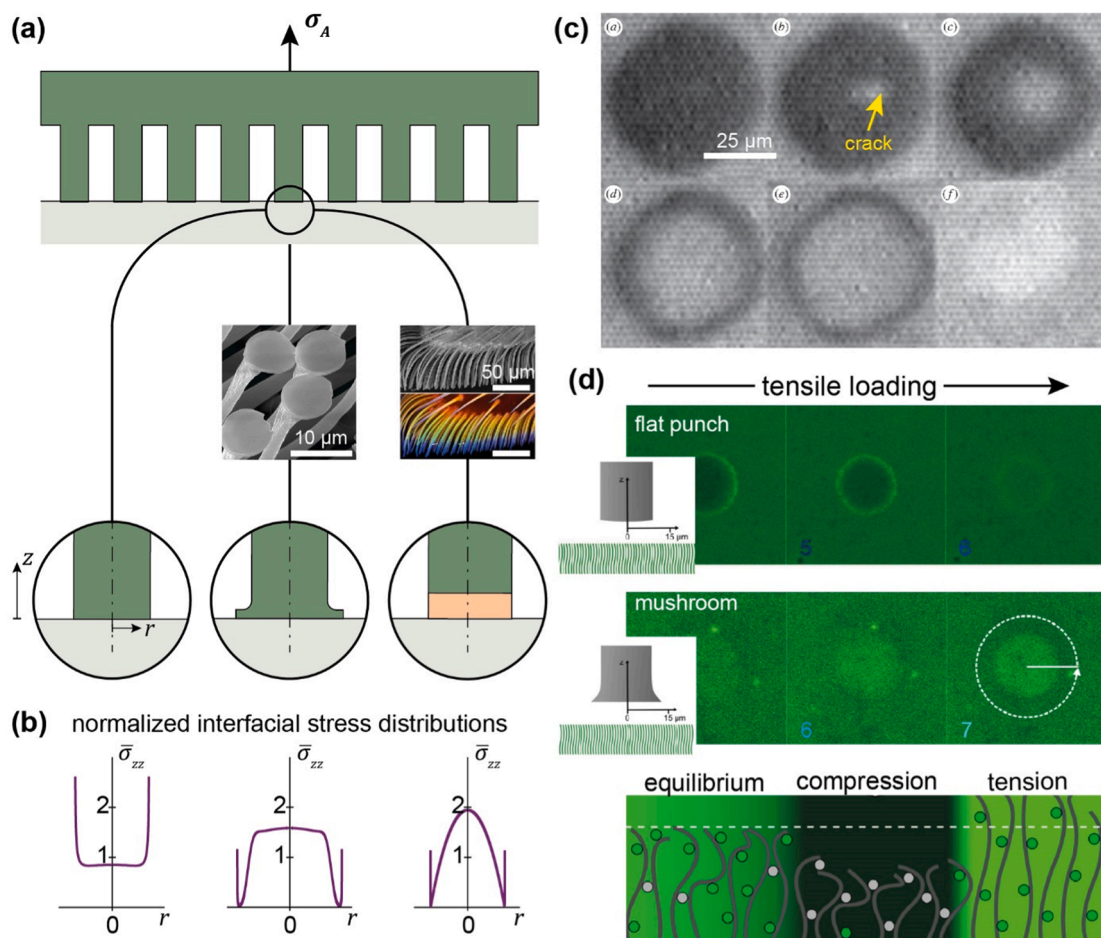


Fig. 3.3. Strategies to optimize adhesion by improving the interfacial stress distribution. (a) Schematic fibrillar microstructures with different cap designs: flat punch (left inset); mushroom-shape inspired by the colorado beetle [196] (center, copyright (2010) Springer); composite fibril inspired by the gradient structures in the ladybug [289] (right, copyright (2013) Springer Nature). (b) Exemplary normalized interfacial stress distributions for the different cap designs obtained by numerical simulations [260,290]. Both modifications attenuate the singularities at the edges, which prevents crack nucleation there and increases adhesion. (c) Still images demonstrating detachment of a mushroom-shaped fibril from the center of the contact, in agreement with the calculated stress distributions in (b). Reproduced with permission from [275], copyright (2011) Royal Society. (d) Direct detection of contact stresses with mechano-sensitive polyelectrolyte brushes: tensile stresses (bright) before detachment are concentrated at the edge for a flat punch (top) and at the center for a mushroom (center); schematic of the fluorescence response (bottom). Reproduced with permission from [288], copyright (2016) American Chemical Society.

limitation of this analysis lies in the unrealistic assumption of equal elastic properties in the fibrils and the object, leading to an inaccurate power-law for the size effect.

Balijepalli et al. [260] have modelled the more realistic situation of a compliant mushroom-shaped fibril in contact with a comparatively stiff object.⁴ By assuming a pre-existing detachment length at the edges of the cap, the adhesion strength was predicted for various cap geometries (flaw-sensitive regime). The calibration factors in Eq. (3.3), determined by finite element simulations, were found to be sensitive to cap shape. As a result, the singularity attenuation was predicted to increase for thinner caps which would create higher adhesion strength. The study suggests that adhesion is optimized for *thin* fibril stalks and *thin* caps. Such a strategy imparts the fibrils with extremely flexible contact elements that cannot build up high strain energy during detachment. The notion of arbitrarily thin mushroom caps is however limited by their fabricability [16].

⁴ Computer simulations of shaped fibrils generally rely on ideal modeling of geometry. During attachment to an object, variability of shape and slight distortions of fibril features such as mushroom flanges, when combined with the sticking friction that usually prevails, may lead to stress distributions at the fibril tip that are rather different from those that arise in the idealized state. As a result, the amplitude of singularities at crack-like adhesion defects and at corners may be wrongly estimated in such idealized computer simulations, leading to a poor approximation in predictions of adhesive strength. This issue may deserve some scrutiny in future steps of computer modeling.

More recent results by Zhang et al. point towards further optimization potential with regard to cap thickness [282]: too thin caps will eventually “feel” the presence of the stalk, leading to premature crack nucleation in the interior of the contact. Optimal adhesion is found at the cross-over between the formation of edge cracks and of interior cracks. Interestingly, an optimum cap diameter is also predicted, with an “overhang” of only about 12%. This agrees with a similar study on wedge-shaped mushroom tips conducted by Aksak et al. [283,284], who found a similar optimal shape for a wedge angle of 45°.

It can be concluded that the mushroom geometry is by now a classic, very powerful way of enhancing adhesion of fibrillar microstructures. This strategy is quite well understood from a micromechanical point of view. The concept of optimizing the interfacial stress distribution in order to maximize adhesion is now widely accepted and has led to other beneficial modifications (Fig. 3.3).

3.2.2.3. *In situ contact observation.* Direct observation of contact formation and of detachment processes has provided valuable insight into the workings of fibrillar adhesives, both on the fibril and the array level. Gorb and Varenberg [272] were the first to verify experimentally that in a mushroom cap interfacial crack formation is shifted from the contact edge to the interior. Their subsequent conclusion [285] that the growing void in the center of the contact was proof of a “passive suction” effect, was later reversed (see Section 3.4.2). Additional experimental studies have verified this center-crack detachment [286,287] (see also Fig. 3.3c,d).

In a particularly innovative approach, the contact stress distribution was recently imaged by applying mechano-sensitive surface coatings [288]. With a polyelectrolyte brush, labelled with a fluorescent dye, the local stress was converted into fluorescence intensities. Mapping of the stresses under the fibrils verified that the stress distribution had changed significantly by the addition of mushroom caps: a maximum of the tensile stress was clearly visible in the mushroom-shaped fibril prior to detachment (Fig. 3.3d). This constitutes the first direct evidence for a beneficial stress redistribution due to shape modification.

3.2.2.4. *Funnel or cup shaped designs.* As an alternative design, funnel or cup-shape elements, with an opening angle creating conically arranged flaps, were investigated [291]. Fabricated to an outer diameter of only 5 μm by two-photon lithography, single funnels exhibited an adhesion strength in excess of 5 MPa; this exceeds by an order of magnitude the values of previously reported structures. As the adhesion by far exceeded the atmospheric pressure and was insensitive to ambient air pressure, appreciable suction contributions were ruled out. The mechanisms behind this exceptional behavior are not fully understood and tests on whole arrays of funnel-shaped microstructures are still lacking. Similar structures in beetles [196] provided circumstantial evidence for a possible suction effect, which in view of the recent results may be questionable (we will return to the suction mechanism in Section 3.4.2).

We note in passing that various suction mechanisms have been verified for underwater adhesion. Because of the significantly reduced Hamaker constants in water [116], van der Waals interactions are considerably weakened in an aqueous environment. Therefore, designs other than fibrillar microstructures are required for such applications. Recent examples for microsuction devices with a deformable cup have been published by Wang et al. [292,293]: due to a self-sealing effect assisting the suction mechanism, the adhesion was found to be 20 times stronger than for comparable mushroom-shaped designs. We will return to the concept of micro suction cups in connection with biomedical applications in Section 4.4.

3.2.3. *Material effects, gradient and composite microstructures*

Besides the geometric design, the properties of the material will exert a strong influence on the adhesive performance of fibrillar arrays. Materials described predominantly in the literature are elastomers, with the vast majority using PDMS (Sylgard 184) as a model substance. Further polymers range from other types of silicones, such as polyvinyl siloxane, e.g. [294], to polyethylene, polypropylene [295], poly(meth)acrylates [296] and polyurethanes [264]. Thermoplastics and thermoplastic polyurethanes were investigated by Sameoto et al. [297]. The elastic modulus of these materials ranges roughly from 1 to 100 MPa. It is noted that these values are much lower than the moduli of many attachment materials found in nature: insects exhibit attachment pads made from chitin or keratin have a typical modulus of a few GPa.

3.2.3.1. *Influence of elastic modulus.* The elastic modulus will affect the adhesive behavior in various ways:

- All fracture mechanics approaches describing the separation of ideally flat interfaces predict a scaling of the adhesion strength with the square root of modulus (Eqs. (3.1) and (3.2)). The reason lies in the fact that the energy penalty in terms of elastic strain energy density is, in a stress-controlled situation, inversely proportional to modulus. Therefore, a high modulus will be favored. This explains the strong adhesion between ideally flat silicon wafers, a process exploited in wafer bonding, e.g. [298].
- A trade-off arises in the presence of fabrication tolerance, surface roughness, or misalignment, which cannot be accommodated by very stiff polymers (strain-controlled adaptation): hence under real-world conditions, a more moderate modulus will generally be preferred (see also discussion about Eq. (3.1)).

On the array level, the decisive quantity is the effective modulus or stiffness of the microstructure, which reflects the bending stiffness of the individual fibrils, e.g. [241,299]:

$$E_{\text{eff}} = CEf \left(\frac{R}{L} \right)^2. \quad (3.5)$$

Here f is the area fraction of fibrils, R their radius and L their length, C is a non-dimensional parameter of order 1. With high-aspect

ratio fibrils, the effective modulus can be orders of magnitude below that of the solid material. The resulting larger compliance will increase the area of contact with rough surfaces or curved objects and reduce the strain energy penalty [299–301]. In addition, high aspect ratio fibrils will be mechanically uncoupled and hence elastic strains in a given fibril interacting with an asperity will not influence adjacent fibrils. However, a lower limit on the fibril diameter is imposed by the onset of instability in the form fibril condensation, also called clustering or clumping, see e.g. [299,302–304].

To visualize the limitations on fibril design due to condensation, fibril fracture and theoretical contact strength, adhesion design maps were introduced by the Arzt group [302,305]. For certain simplifying assumptions, they allow the identification of the optimum design parameters for fibrillar adhesives under the different constraints. It is proposed that this worthwhile concept should be extended, possibly in numerical form, to incorporate the complex conditions under which fibrillar adhesives are expected to operate.

3.2.3.2. Material gradients and composite fibrils. Nature rarely uses materials with spatially homogeneous properties. Insects have evolved material gradients in their attachment systems [306]. For example, the ladybug has adhesive fibrils with an axial gradient of the elastic modulus. The tip (a composite of resilin and chitin) is about three orders of magnitude softer than the pure chitin base (1 MPa vs. 7 GPa) [289]. Other insects exhibit a softer transition zone which acts as a joint, thought to facilitate the adaptation to uneven and non-parallel surfaces [307]. Such a concept can combine two conflicting requirements: the soft tips ensure adhesion to rough surfaces while the stiff base raises the mechanical stability of the microstructure. The latter effect was modelled by Gorb and Filippov for high aspect ratio fibrils adhering to rough substrates (see Fig. 3.6b for the case of surface roughness [303]).

Gradients are difficult to implement in artificial structures. Synthetic adhesives were instead designed with a “composite” structure, i.e. an abrupt transition in properties [308]. The softer tips were reported to improve both the adhesion and the friction performance. With a similar design, Bae et al. demonstrated improved adhesion to skin [309] (see also Section 4.3.2). Minsky and Turner designed and analyzed composite posts with a stiff core and a soft shell [310,311] and concluded that adhesion was highest for very thin soft tip layers. Numerical simulations showed that the stress in the near-edge region of the composite was lowered compared to a homogeneous fibril and the adhesion force was found to be insensitive to edge crack length. In some cases, adhesion strengths in excess of 1 MPa were reported.

Gorumlu and Aksak [312] fabricated composite fibrils from polyurethane and pointed out an important optimization problem: while thinner layers showed superior adhesion to smooth objects, a certain thickness was required to accommodate roughness. Fischer et al. [313] also found for PDMS composite fibrils that crack formation shifted from the edge to the interior (sometimes finger-like crack growth was observed). Interestingly, the shape of the interface between the stalk and the tip layer had an effect: hemispherical interfaces resulted in better adhesion by concentrating the stress more in the center. In general, the composite fibrils responded better to roughness of the object. More recently, the addition of a thin layer of a pressure sensitive adhesive was shown to substantially increase the adhesion performance [314]. Thus, a composite structure exerts a similarly beneficial influence on the stress distribution as the mushroom structure; the advantage of composite fibrils is their higher stability and improved fabricability. The composite approach was also proposed for skin adhesion (see Section 4.3.2).

A full analysis of various designs of composite fibrils by interfacial fracture mechanics was carried out by Balijepalli et al. [290]. The simulation results demonstrated that a thinner layer more effectively decreased the magnitude of the edge stress singularity. Adhesion strength was predicted to increase for thinner layers and larger modulus ratios. Also the shape of the interface between the soft and the stiff region was found to modulate the stress distribution. The stress at the center was increased related to a “confinement effect” [315,316]. Model experiments were carried out by Fischer et al. [313], which showed the expected transition from edge crack to interior crack detachment. The results were in good agreement with the calculations. In particular, the composite microstructures exhibited excellent adhesion to rough surfaces (see also Section 3.5.1).

The “confinement effect” is the phenomenon that the equivalent modulus and the crack growth in a thin polymeric layer depend on the ratio of thickness to lateral extension (fibril diameter in this case) of the film. With decreasing film thickness, the detachment proceeds progressively by stable growth of finger-like or center cracks rather than by unstable growth of edge cracks. The confinement effect in the soft terminal layer depends strongly on material compressibility (i.e., Poisson’s ratio) [315]. The curvature of the interface was influential, particularly for very thin films: higher curvatures lead to enhanced tensile stresses at the center. This agrees with experiments in which a transition from edge to center crack detachment was observed [313]. In addition, composite structures exhibited similar adhesion in the presence of finite substrate roughness, whereas adhesion dropped by more than 50% for a flat punch. As almost all objects exhibit surface roughness on a scale relevant for attenuation of van der Waals interactions, this concept may be an important step toward practical applicability of micropatterned dry adhesives.

3.2.3.3. Hierarchical designs. Another strategy to avoid condensation of fibrils involves modifications on the array level: instead of a material gradient, as discussed above, a structural gradient can be implemented by reducing the size of the fibrils progressively over several hierarchical levels, as demonstrated by the four levels in the attachment pad of geckos. Yao and Gao [245,317,318] have demonstrated theoretically how a hierarchical structure can improve load sharing in an array and therefore resistance to defect propagation. They also calculated how many levels of hierarchy are required under specific conditions. Experiments with hierarchical artificial arrays have so far met with limited success, see review by Brodoceanu et al. [219,319]. The limitation is mostly due to fabrication issues: stacking several hierarchical levels is tedious and the resulting area coverage of fibrils is generally too low for the resulting structures to be competitive with single level structures. Still, the concept is enticing and may have to await more advanced direct writing methods to be successful.

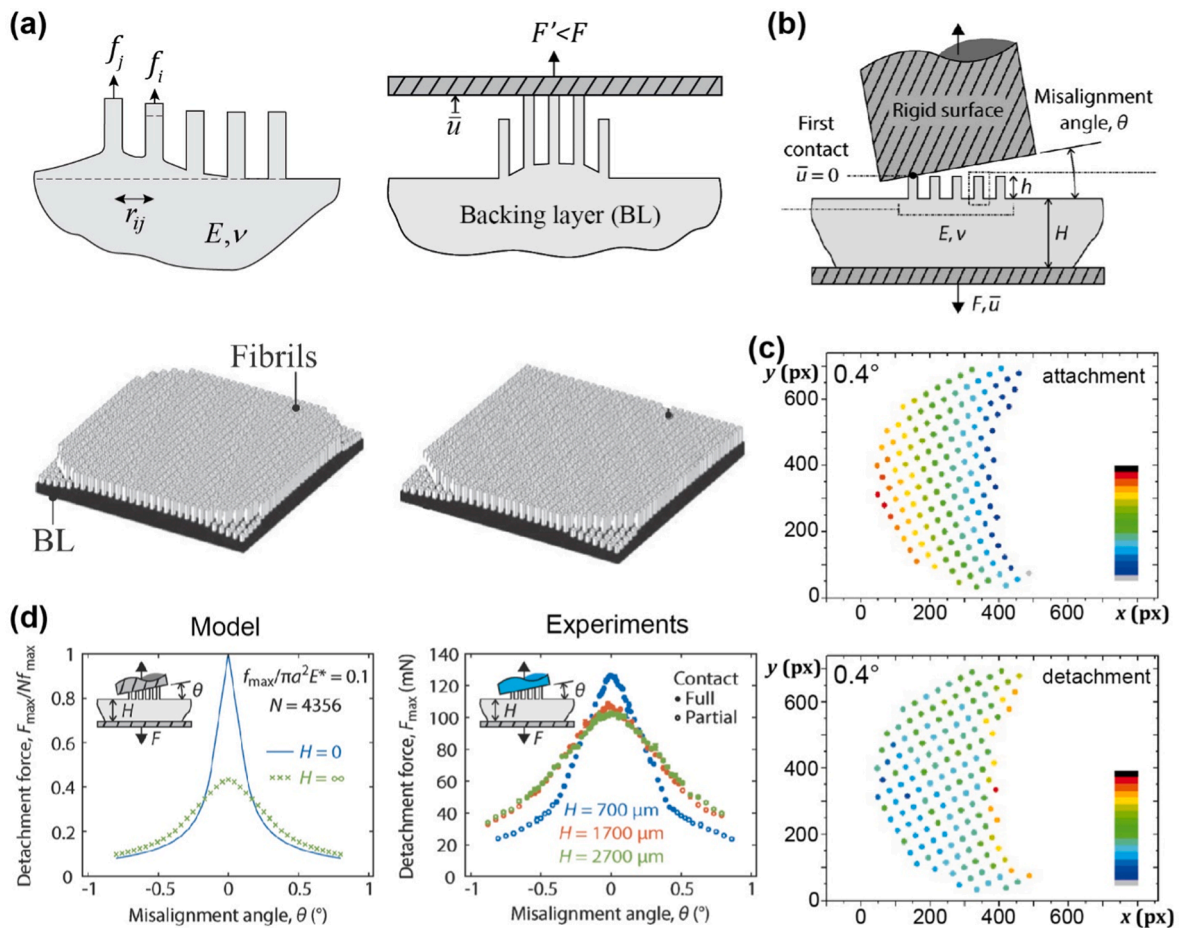


Fig. 3.4. Design of the backing layer for fibrillar arrays. (a) Due to elastic coupling, the backing layer induces an undesirable load concentration at the array edges (loss of equal load sharing). This results in premature detachment of fibrils along the periphery and a decay in load sharing with increasing array size. Reproduced with permission from [324], copyright (2016) Elsevier. (b) Schematic of the misalignment between array and object, as modeled by Booth et al. [325] shows unequal load sharing. (c) *In situ* frustrated total internal reflection visualizes the loss of load sharing by misalignment (above: large gradient during attachment, below: reduced gradient during detachment). Reproduced with permission from [326], copyright (2019) Wiley. (d) Model (left) and experiment (right) showing misalignment effect on detachment force for varying backing layer thickness H ; thicker compliant backing layers more efficiently accommodate misalignment. (b,d) Reproduced with permission from [325], copyright (2018) Wiley.

3.3. The array level - Backing layer and statistics of detachment

Strategies to increase adhesion of single fibrils, as discussed above, are useful only if the fibril strength can be efficiently distributed across an array, sometimes containing hundreds or thousands of fibrils. The maximum adhesive performance of a fibrillar array is realized only if all fibrils detach simultaneously at the identical deterministic local adhesion strength. This requirement has brought another element into the focus of research: the backing layer which elastically connects the individual fibrils. Most experimental and theoretical studies were conducted for single fibrils, under the assumption that the adhesive performance of an array would be the superposition of individual fibril effects. Several essential features were neglected in such an approach: the elastic coupling between the fibrils, the effects of unequal load sharing due to misalignment or surface irregularities, and the possibly statistical distribution of adhesive strengths in the different contacts. We now review the recent developments and their most important implications.

3.3.1. Backing layer effect - Design for improved load sharing

In most cases, fibrillar adhesion is the result of many fibrils interacting with an object surface at the same time although single fibrils can also be used to lift and place small objects. An array is most effective when all fibrils support the same stress, i.e. “equal load sharing” is ensured [239]. The backing layer connecting the individual fibrils plays at the very least a dual role: its compliance can reduce the adhesion performance of the array while providing tolerance to non-ideal alignment or surface roughness. The subject has recently been treated in more detail.

Under normal tensile loading, a load concentration exists along the edge of the array because the deformation behavior of the fibrils

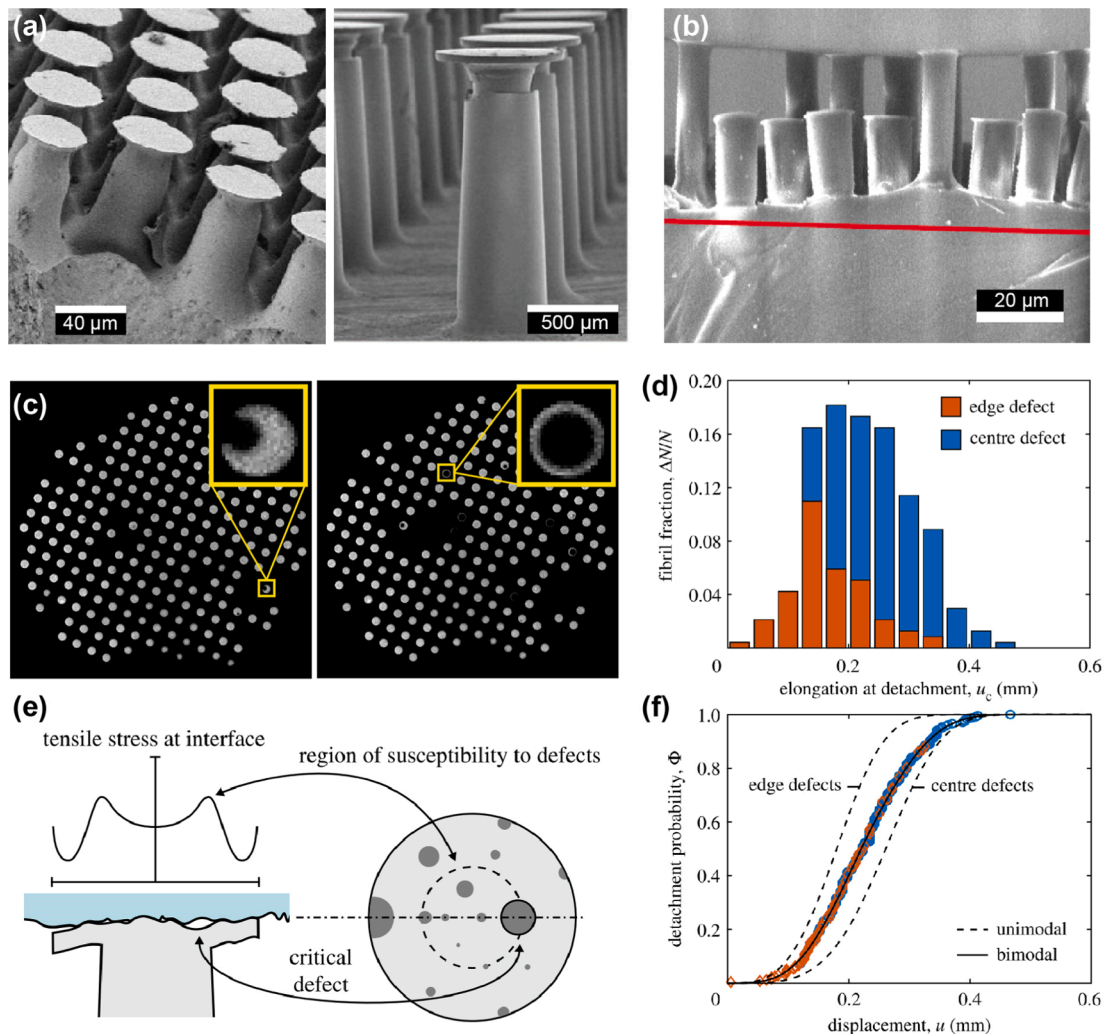


Fig. 3.5. Defects and statistical distribution of detachment events. (a) Microfibrils with various fabrication flaws, giving rise to defect-controlled detachment. Reproduced with permission from (left) [274], copyright (2008) Royal Society; (right) [326], copyright (2019) Wiley. (b) Distributed detachment events of microfibrils (PDMS, length 20 μm, diameter 10 μm, scale bar is 20 μm, red line denotes the location of the edge of the undeformed backing layer), side view inside an environmental scanning electron microscope [328], copyright (2011) Cambridge University Press. (c) Progressive detachment observed by frustrated total internal reflection, insets provide evidence for edge cracks (left) and interior cracks (right) (PDMS fibrils, length 1600 μm, cap diameter 710 μm, in contact with glass). Adapted from [326]. (d) Histogram of fibril fraction with a given elongation at detachment, revealing the strength distribution; these data are modeled with a bimodal statistical theory. (e) Schematic of defect-controlled detachment from a rough surface with a tensile stress distribution. (f) Calculated combined detachment probability using a bimodal statistical model for edge and center defects, with experimental data points. (d–f) Reproduced with permission from [244], copyright (2019) Royal Society.

along the perimeter is different from the fibrils in the center of the array [320–323]. This effect can be seen as analogous to the stress concentration at the edge of single fibrils with the resulting flaw sensitivity on the fibril level (Fig. 3.1c). As illustrated in Fig. 3.4a, the load concentration is caused by the compliance of the backing layer. Hence, it was concluded that, to optimize adhesion, the backing layer should be as thin as possible, the fibrils should be compliant and long, and the array dimension should be small. Alternatively, the elastic modulus of the backing layer could be chosen to lie substantially above that of the fibrils, though this is difficult to fabricate and may jeopardize the long-term durability of the array.

Bacca et al. [324] have developed a detailed model for the effect of a compliant backing layer. Their simulations demonstrate the premature detachment of fibrils at the edge of the array (Fig. 3.4a). As a countermeasure, it is proposed to grade the elastic modulus of the fibrils towards the array edges and to make the backing layer very compliant. In addition, they predict an important array size effect: As the array size increases, the efficiency of load sharing is predicted to decay monotonically, approximately as $1/N^{1/4}$ where N is the number of fibrils (or $1/S^{1/2}$ where S is the linear size of the array).

3.3.2. Effects of misalignment

Numerous early adhesion measurements for fibrillar microstructures were performed against spherical counter surfaces with a much larger radius of curvature than the fibril dimensions. This test method was favored initially because the relative orientation of the counter surface to the plane of the array is irrelevant. However, the contact stresses and adhesion strength values extracted from such experiments are inherently unreliable as the contact area must be inferred indirectly and changes during the test. Hence, a trend towards adhesion measurement in a flat–flat geometry has occurred, which substantially facilitates the interpretation and comparison of results [327]. On the downside, such tests require additional experimental effort to ensure an appropriate alignment of the object surface. Even for single fibrils, misalignment will sensitively affect adhesion [277]: tilt angles of the order of 1° were sufficient to halve the adhesion force of flat-ended PDMS fibrils.

For arrays, misalignment is even more critical. The decay of load sharing with array size found in [324] is exacerbated by interfacial misalignment. In a follow-up experimental paper, Booth et al. [325] found that misalignment angles on the order of 0.1° resulted in a peel-like detachment. Thicker, more compliant backing layers were shown to increase the adhesion, which was attributed to backing-layer deformation at the detachment front (Fig. 3.4d). Observation showed that differential stretching of fibrils was reduced, effectively lowering the angle of misalignment and the resulting load concentration. These results are of interest for applications of fibrillar microstructures under normal loading conditions without precise control of alignment, for example, in pick-and-place gripping systems.

Hence, the backing layer has a dual role with conflicting requirements for its optimization: in the aligned situation, its compliance should be small (small thickness, large modulus) to minimize edge load concentrations; in the presence of misalignment, thicker, more compliant backing layers will be beneficial. This points to the suggestion to tune the elastic properties of fibrils and backing layer independently to optimize the adhesion of fibrillar arrays. It is noted that Bacca's array size effect [324] is reminiscent of the fibrillar "contact splitting effect", now at the array level: One may conclude that a large array will be outperformed by a number of smaller arrays with the same total area (or number of fibrils). Experiments along this direction are urgently needed to validate the theoretical conclusions.

3.3.3. Adhesion strength distribution

Adhesive fibrils invariably exhibit fabrication or contact flaws or encounter contaminated objects (Fig. 3.5a). Experiments have provided circumstantial evidence that the adhesion strengths of individual fibrils is hence not deterministic, e.g. [328]. A large temporal spread in detachment was observed in an electron microscope image (Fig. 3.5b). The possibility that in a large array of fibrils statistical variations in contact strength will occur has largely escaped the attention of the research community.

A systematic *in situ* investigation of the detachment statistics was conducted by Tinnemann et al. [326]. They employed frustrated total internal reflection [326,329,330] to obtain high contrast between attached and detached regions within fibrillar contacts during adhesion experiment (Fig. 3.5c). Very detailed, previously inaccessible insight was obtained by this method. The adhesion strength values of the individual fibrils varied over about an order of magnitude, even though the microstructures exhibited a high degree of perfection. The reason for this variability lies in the presence of interfacial defects. Most fibrils detached via interior cracks, confirming Gorb's earlier observations and calculations, described above, of the distribution of stresses in the contact; a second detachment mode involved propagation of edge cracks from fabrication imperfections.

Interestingly, a large fraction of the fibrils, typically 30%, was already detached when the adhesion strength of the array was reached. This finding confirms earlier indications of premature detachment by Brörmann et al. [228]: during breakage of fibrillar contacts, light signals due to charge separation were recorded long before reaching the maximum tensile stress. Contrary to expectation, for the specimen design used by Tinnemann et al. [326], no evidence was found for elastic coupling through the backing layer, which would have led to cooperative behavior among the fibrils and preferential detachment of clusters of adjacent fibrils. The optical observation also allowed interior cracks to be distinguished from edge cracks (Fig. 3.5c), which dominated earlier in the detachment process; interior cracks would have been expected for the mushroom-shaped structures, but edge cracks dominated for rough surfaces.

Theoretical treatment of the statistical nature of fibrillar detachment has been performed (Fig. 3.5d–f). In an early study, Porwal and Hui [331] conducted Monte Carlo simulations using probability distributions for attachment strength and for fibril length. The strength of the array was found to decay as the strength variability increased, similar to brittle fiber bundles in composite materials; it was proposed that an increased compliance of the fibrils could compensate for the attachment strength variation. McMeeking et al. [243] assumed detachment to be controlled by weakest link defects, as described by Weibull statistics; this approach predicts an additional size effect as finer fibrils will encompass fewer and smaller interfacial defects. They arrived at a formalism for the expected strength distribution but lacked direct comparison with experiment.

Using the experimental platform of Tinnemann et al. [326], Booth et al. [244] performed a statistical analysis of defect-dependent detachment. The adhesive strength distribution was obtained in the experiments from the times at detachment for the individual fibrils, correlated to their stretch. The authors developed a bimodal statistical theory based on the Weibull distribution which agrees well with the experimental strength distribution associated with edge and interior defects (Fig. 3.5d,f). The authors proposed that such an analysis can be a valuable tool in judging potential improvements to the fabrication process. Another step that remains to be taken is to combine considerations of equal load sharing with statistical modeling. The design principles derived from this model have not yet been realized: the statistical nature of detachment can be advantageous in alleviating the effect of misalignment, which suggests that arrays with built-in randomness could be beneficial in realistic gripping situations.

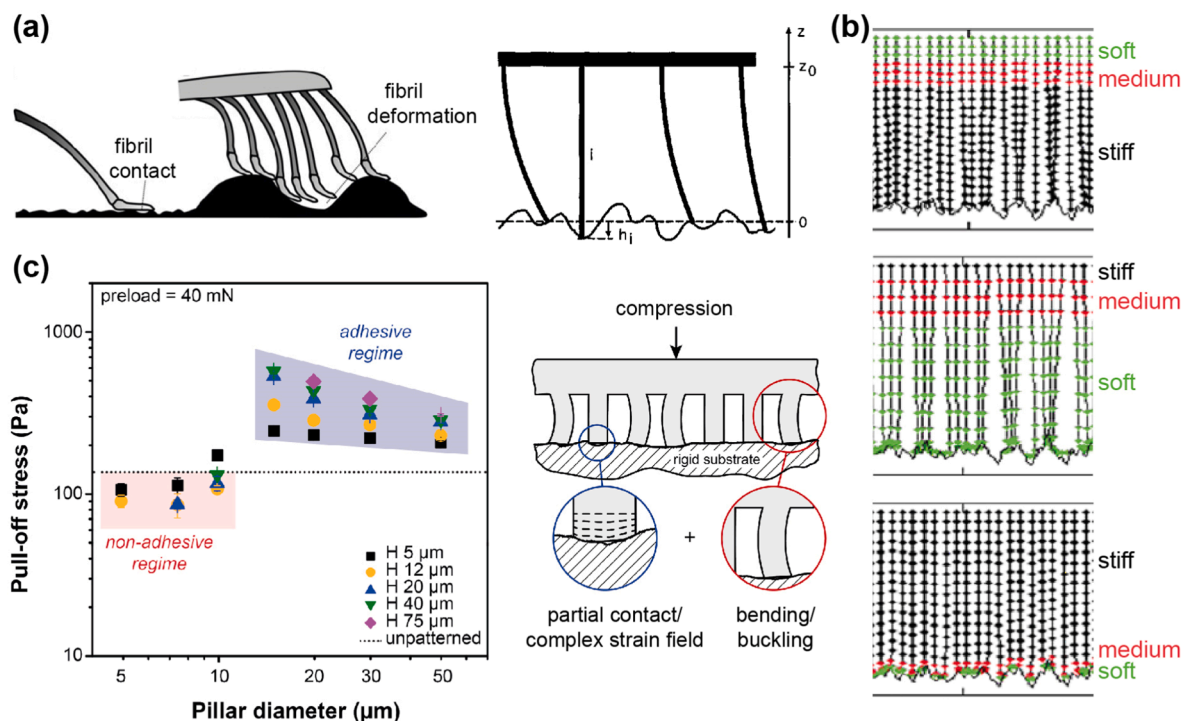


Fig. 3.6. Roughness effects in fibrillar adhesion. (a) A fibrillar array exhibits a much reduced effective modulus compared to a solid slab of the same material (Eq. (3.5)). This allows the array to accommodate surface roughness with little elastic energy penalty. Schematic left adapted from [360]; schematic right reproduced with permission from [299], copyright (2003) AIP Publishing. (b) Model by Gorb and Filippov for the competition between adhesion and clustering of individual fibrils in the presence of a numerically generated fractal surface. (adapted from [303] CC-BY 2.0 (2014)). (c) Experimental adhesion strength values for different fibril diameter and length (H) compared to an unpatterned sample (dashed line): a maximum in adhesion occurs when the fibril diameter matches the lateral roughness dimension (adapted from [300], copyright (2016) Wiley).

3.4. Environmental effects - Humidity, elevated temperatures, and vacuum

3.4.1. Humidity and temperature

Fibrillar microstructures have the potential to innovate robotic gripping systems and biomedical adhesives. They will thus be expected to operate under challenging conditions: For some applications, the temperature capability is an issue; elastomeric materials are limited to a temperature range from their material-specific glass transition temperature to the onset of thermal degradation (e.g. 200–250 °C). For temperature effects, the reader is referred, e.g., to [332]. Also humidity will affect fibrillar adhesion: it was demonstrated for a beetle, e.g. [333], and for gecko pads [227] that additional adhesion can be attributed to the effects of humidity; explanations ranged from capillary bridges that are reinforced by contact splitting [334–337] to water-induced changes in surface chemistry [338] or in stiffness [339]. The presence of water will strongly reduce van der Waals interactions [340] but suction effects can now become dominant [278]. For a review of humidity effects see also [341]. Designing for wet environments requires very different microstructures, e.g. as inspired by the tree frog [342].

3.4.2. The debate on suction

Vacuum or reduced air pressure is a potentially relevant environment for fibrillar adhesives, which have been evaluated for space applications, e.g. [193,343]. Also, for fundamental reasons, the role of suction has become the subject of considerable debate. Following the Weitlaner experiment with geckos [222], beetles with mushroom-shaped adhesive organs also failed to show an adhesion reduction under reduced air pressure [344]. Following theoretical analysis, it was speculated that suction would be inefficient in fibrillar adhesives as it does not scale inversely with fibril size, in contrast to intermolecular interaction for virtually all contact shapes [241]. Suction organs seem to be mostly confined to the aqueous environment where high stresses can be built up due to the incompressibility of water (see Section 4.4).

Close-up observation of the detachment process of mushroom-shaped fibrils led Varenberg and Gorb [274] to conclude that the fibrils acted as “passive suction devices”; later measurements under reduced pressure of 20 mbar quantified this effect as small, only about 10% of the total force and only prevailing at higher retraction velocities [275], presumably due to the loss of air sealing in slower retractions. Subsequent authors refuted a suction contribution for small fibrils altogether [193,274,345,346] or valued it at 25% [347]. Sameoto et al. [274,345,346] claimed suction to be negligible for tip diameters below 17 μm but speculated that larger caps could lead to non-negligible suction due to the propensity for interior interfacial cracks. The largest drop in adhesion was reported by Purto et al.

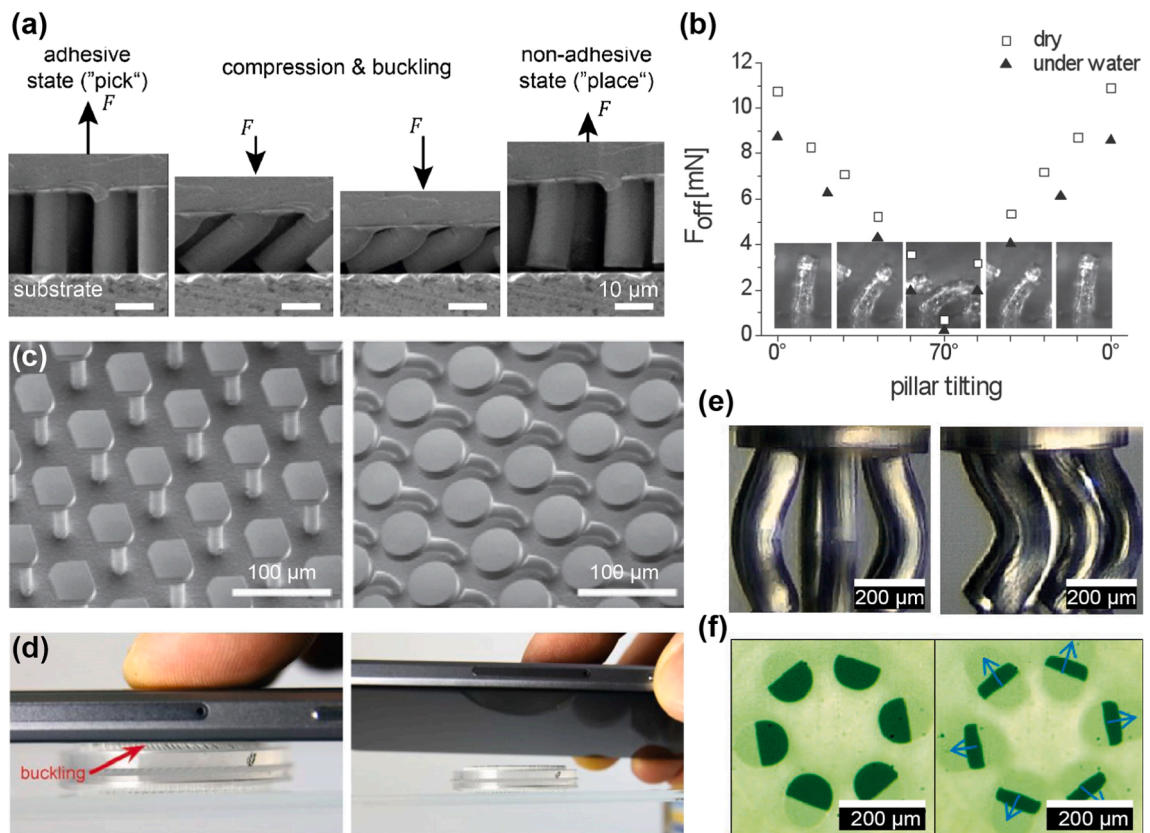


Fig. 3.7. Mechanical and magnetic switching from an adhesive to a non-adhesive state. (a) Microbuckling of fibrils under compressive overload leading to loss of contact. Adapted from [328]. (b) Tilting of modified polymeric fibrils by a magnetic field resulting in strongly reduced adhesion force, F_{off} . Reproduced with permission from [371], copyright (2013) Wiley. (c) Off-center caps promise easy directional switchability [376], copyright (2020) IOP Publishing. (d) Demonstration of buckling-induced release of a macro object through a double-sided micropatterned adhesive. Reproduced with permission from [191], copyright (2019) Elsevier. (e) New design for controlled symmetric buckling (left) vs. biased bending (right). (f) Controlled loss of contact area for reliable handling of micro objects. Reproduced with permission from [375], copyright (2020) INM.

[348] as 30% for relatively coarse model fibrils of diameter 0.4 mm. Interestingly, the authors found that the pressure for object release due to buckling was not affected by air pressure.

In their extensive *in situ* investigation, Tinnemann et al. [326] also quantified the contribution of suction, conducting tests at different ambient air pressures while observing individual contacts. The suction effect varied greatly across the array due to inhomogeneities of the cap surfaces, with a mean contribution between 6 and 20% depending on surface roughness. This behavior was interpreted in terms of the varying occurrence of interior cracks, necessary for a sustained suction contribution. However, the suction contribution could not be predicted from the number of observed interior cracks. The authors conclude that to benefit from suction in air, the interface must be as smooth as possible to avoid air leaking into the void created by an interior crack. It was concluded that leakage could be reduced by making the mushroom flaps thin enough to conform to the roughness (see Eq. (4.1)). For a theory of leakage effects in suction devices the reader is referred to Tiwari and Persson [349].

At the present state, the dominance of van der Waals interactions over suction in the adhesion of fibrillar microstructures seems to be confirmed for dry conditions. Even in cases where a difference was found, additional effects of remnant humidity or surface contaminations cannot fully be excluded. Overall, it can be concluded that, in a dry environment, the suction contribution is, depending on fibril diameter, small to negligible. This has important implications for realistic contact systems, e.g. in robotic pick-and-place systems, which exhibit a unique performance characteristic: unlike conventional suction devices, gecko-inspired systems will not be degraded by a vacuum environment.

3.5. Testing conditions - Roughness and switchability

Adhesion is generally affected by the testing conditions. For example, the shape of the object will make a difference: spherical glass objects, which were used in earlier adhesion tests, simplified the experiment but complicated the analysis. Strictly speaking, such a testing geometry turns a tack test into a peeling test. Moreover, the resulting dependence of adhesion on the level of compressive

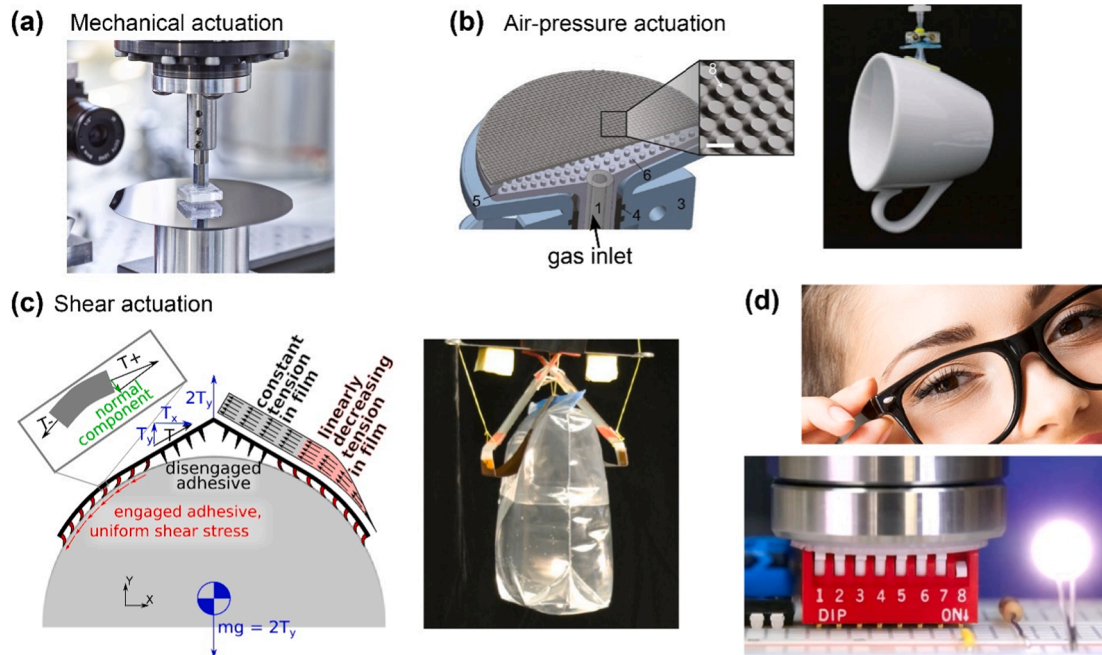


Fig. 3.8. Examples of applications for fibrillar microstructures. (a) Reversible handling of sensitive objects such as silicon wafers exploiting the buckling instability for release at INM. (b) Pick-and-place of curved objects with air-pressure actuation Reproduced with permission from [383]. (c) Gripper equipped with directional adhesive for frictional adhesion. Reproduced with permission from [384], Copyright (2015) IEEE. (d) Commercial developments of anti-slip nose pads (top, nanogriptechnology.com) and robotic pick-and-place (bottom, innocise.com).

preload obscures comparison of adhesion data obtained by different groups [261]. An early model assuming a rigid backing layer [350] was recently extended to include the discrete nature of the fibrillar structure, as well as the compliance of fibrils and backing layer [351]. They arrive at the recommendation that a numerical simulation should accompany each experimental test with spherical objects. By contrast, flat test set-ups suffer from the limitation that accurate alignment is required (e.g. [327]). Nevertheless, a trend towards adopting this test procedure, which renders more easily interpreted results, is noticeable in the literature. Other parameters include speed of retraction, system compliance, and the time in contact with the object [352]. We focus here on two testing-related aspects that are relevant for applications: roughness of the counter surface and release of objects.

3.5.1. Roughness of object surface

Surface roughness is a classic impediment to adhesion by short-range intermolecular interactions and has been extensively studied. It is well recognized that, depending on the degree of roughness, the contact area over which interactions contribute to adhesion is usually much smaller than the apparent area [353–355]. Any elastic strain energy at the contact will counteract adhesion [250]. Hence in order to ensure adhesion to a rough object, the elastic modulus of the fibrillar material or the object, or both, must be sufficiently small. Several contact mechanics models exist for computing the adhesive properties of rough interfaces from the roughness power spectrum of the surface [356,357].

Fibrillar surfaces can compensate for surface roughness by virtue of their enhanced compliance, as was calculated for spherical JKR contacts by Hui et al. [301]. The effective modulus of a fibrillar structure can be several orders of magnitude below the modulus of the material it is made of, minimizing elastic strain energy, see Eq. (3.5) above [299]. In contrast to unpatterned adhesives, micropatterned adhesives exhibit the potential to adhere better to rough objects (Fig. 3.6). Some roughness parameter correlations are discussed by Kasem and Varenberg [358]. For PDMS fibril diameters of 10 and 20 μm , a relative maximum in adhesion was identified when the fibril diameter and the lateral asperity size roughly coincided [359]. From a systematic study, Barreau et al. [300] deduced a strategy for dealing with surface roughness: the fibril diameter should be small to take advantage of the contact splitting effect, but not smaller than the mean spacing between local peaks on the object surface (Fig. 3.6c). Otherwise, local bending and buckling will reduce the contact area, whereas slightly thicker fibrils undergo only small elastic deformations during contact formation. To obtain the highest compliance, the fibrils should be as long as possible without jeopardizing stability of the structures. These intuitive concepts, which still need to be validated by theoretical modeling, suggest that fibrillar microstructures could be designed with architectures optimized for a given object roughness.

Additional progress is expected by combining the concepts of roughness with those of statistical detachment. Following Bacca et al. [324,325], a two-fold influence is expected: At length scales smaller than the characteristic dimension of fibrils, roughness is expected

to introduce defects in the fibril tip-object contact. The tip geometry will then control the interfacial stress distribution and hence the regions where defects are important. This will result in statistical variation of the local detachment force. For roughness with larger characteristic length scales the tip geometry is expected to be less dominant. A full analysis will have to include the roughness-induced non-uniform load distribution in conjunction with the statistical framework.

3.5.2. Switchability - from gripping to release

One of the key features of fibrillar microstructures is their switchability (Fig. 3.7): by applying a stimulus, the contact mechanics can be altered in a way that allows easy detachment. This function, which cannot be realized with unpatterned contacts, is central to gripping and releasing objects in innovative robotic systems. Switchable adhesives have recently been reviewed and categorized by Croll et al., including mechanical, electromagnetic, fluidic and thermal stimuli [201], and by Meiners and Tracht [361].

An elegant mechanical approach is to apply a compressive overload to the adhesive structures: the resulting elastic instability due to buckling of the fibrils leads to contact loss and creates a transition to a non-adhesive state (Fig. 3.7a) [274,328,362–365]. Such a load-controlled stimulus constitutes a reliable strategy and is straightforward to implement in industrial robotic systems [189]. Subsequently, multistep switchable adhesives were developed, in which fibrils of varying length enable tuning of the adhesion strength [366]. Other actuation mechanisms involve thermal stimuli, e.g. in combination with trained shape memory polymers [367,368] or with shape memory alloys as a backing layer [369]. Alternatively, magnetic fields or UV light can trigger the bending of fibrils and induce a loss of contact [370–372]. The different stimuli need to be evaluated for a given application in the light of time constants, reversibility and long-term behavior.

Controlled release of objects is a particular challenge in microfabrication, where the weight of the objects to be handled is insufficient for easy detachment. Here, adhesive microstructures need to be optimized no longer just for adhesion but also for transition to small release forces. Strategies include anisotropic fibrils [308,345,373,374] that are more easily detached in specific directions or with intentional “defects” in the form of overhangs or steps [373]. More recently, specially designed microstructures were developed in which the buckling direction is prescribed by a deliberate imperfection; they will enable detachment of micro objects at low forces and with high lateral precision (Fig. 3.7e–f) [375]. Also, double-sided fibrillar adhesives have been demonstrated that allow selective detachment at a pre-determined interface (Fig. 3.7d) [191].

3.6. Outlook – Adhesive fibrillar microstructures

Research on adhesive microstructures has come a long way since the turn of the century: motivated by numerous natural examples studied by biologists, groups all over the world have contributed to the development of adhesive microstructures. As a result, many of the fundamental questions are now reasonably clear. The molecular dimension, the fibril and the array level all interact and result in the adhesive performance of the microstructure. On the molecular scale, the dominant role of van der Waals interactions is commonly accepted although capillarity and suction contributions cannot be totally ruled out. Contact splitting, shape modification and gradient strategies on the fibril level are generally accepted as efficient means of enhancing adhesion and of making it switchable. The design concept of protecting the contact interface from deleterious stress concentrations has spurred the optimization strategy, especially by the modification of fibril shape and by tuning of materials properties. The array level has received detailed attention only in recent years; its optimization will however strongly determine the applicability and reliability of fibrillar microstructures in technical solutions.

The switchability of fibrillar microstructures has turned out to be one of their most useful properties: innovative pick-and-place processes have been demonstrated, e.g. in [16,189,190,311,377,378]. Examples of handling and micromanipulation applications are illustrated in Fig. 3.8. Strategies for large-area roll-to-roll patterning have been successfully developed, e.g. in [236,296,379]. Benefits over conventional vacuum suction grippers include compatibility with a vacuum environment, handling of microcomponents and delicate objects, ease of integration, and sustainability in terms of energy and resources. For an extensive comparison of different handling concepts the reader is referred to Shintake et al. [380].

In spite of considerable progress, there is still room for further improvements and extensions. Biological solutions will never cease to surprise the observer and will continue to inspire the researcher and the engineer. A recent example is the clingfish which seems to exploit a combination of adhesion mechanisms in its wet environment [381,382]. Also, the strategy of employing material gradients, as described e.g. in [307], has considerable, yet untapped potential for artificial microstructures. More sophisticated microstructures are only beginning to be reproduced in the laboratory. It is to be expected that numerous unknown natural solutions are still hidden in extreme environments, such as the rain forest or the deep sea.

Some of the fundamental concepts of fibrillar adhesion still require experimental verification. The size effect suggested by several micromechanical arguments has been proven only in some instances. The reason seems to be that, in the literature, preference is often given to one-shot experiments and a systematic variation of design parameters over larger ranges is rarely reported. The sub-micron size range has hardly been touched although gecko toe pads exhibit hairy structures of this size. Therefore, the prediction of a defect-insensitive regime governed by the ideal cohesive strength of the interface has so far not been validated. Experiments with carbon nanotubes [385,386] gave interesting initial results but do not seem to have been pursued further. The actuation by electrostatic effects [380,387–389] and by liquid crystal elastomers [390] could lead to new ways of gripping - albeit with a loss of the elegance inherent to simple mechanical manipulation. Obvious difficulties in the fabrication of polymeric high-aspect ratio fibrillar structures with nanoscale diameters will need to be overcome. Attempts to produce “gecko structures” by biological means would be a sustainable approach that should be pursued with vigor. To avoid condensation or clumping, nature prefers hierarchical architectures; this strategy has been investigated on a laboratory scale but has so far not led to demonstration of promising properties. This is in contrast

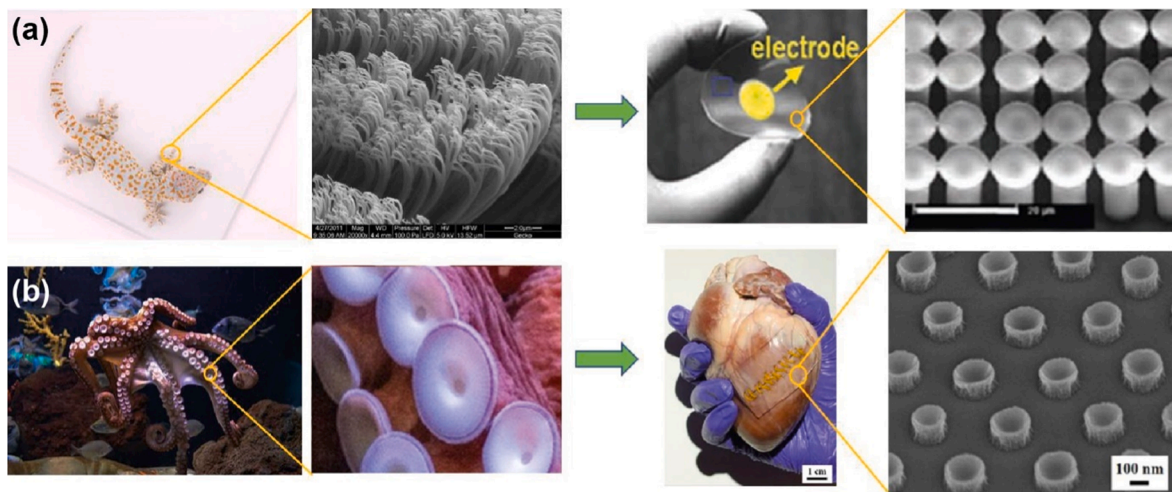


Fig. 4.1. Bioinspired surface microstructures with applications in medical devices. (a) The gecko foot with submicron attachments inspires novel skin adhesives with electrodes for health monitoring applications. Left two panels copyright INM. Right panels reproduced with permission from [399], copyright (2011) Wiley. (b) A micropatterned wet adhesive with micro suction cups, illustrated for a heart, inspired by octopus suction cups. Left two panels are from Unsplash (www.unsplash.com) under Creative Commons Zero License and the right two panels are reproduced with permission from [400], copyright (2017) American Chemical Society.

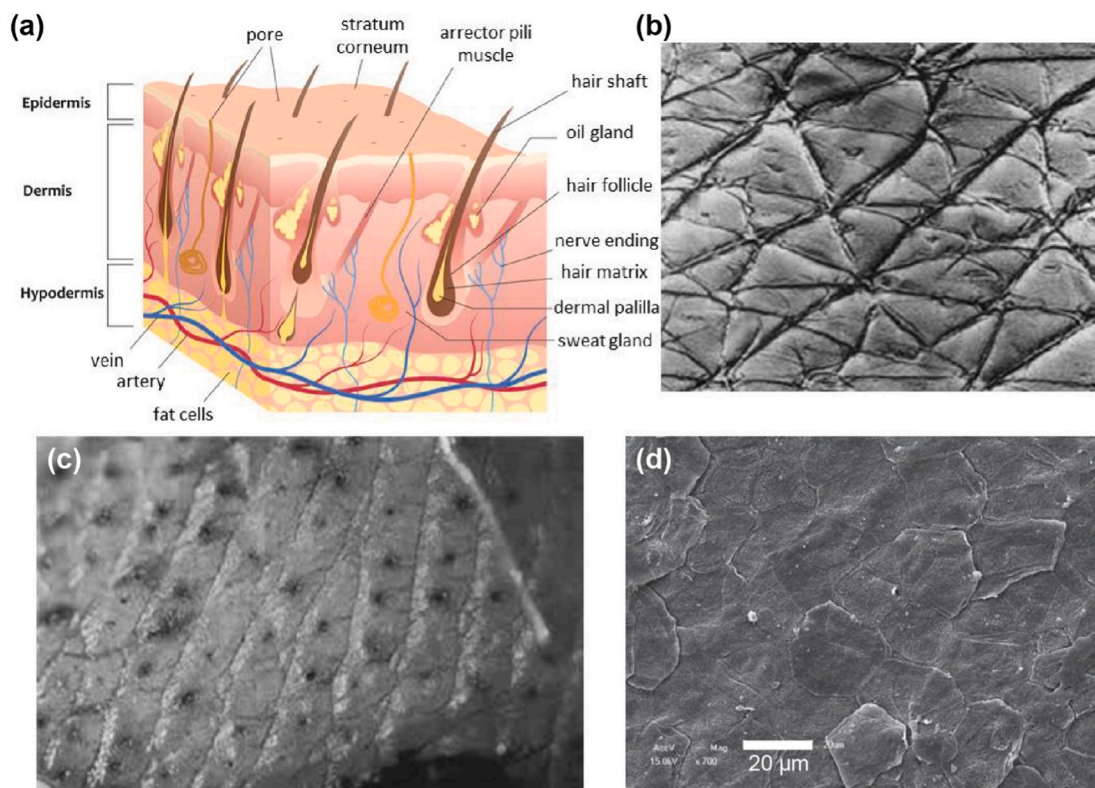


Fig. 4.2. Schematic cross-section of mammalian skin and its surface characteristics. (a) Skin is a layered composite with various vessels, glands and nerves embedded in it. Challenges for adhesive microstructures are skin roughness, glandular secretions, hair follicle and the constant renewal of the surface [412]. (b) Furrows on the inner side of the forearm conferring good isotropic extensibility. (c) Fingerprints on the finger pad; regular concentric ridges increase friction and turn our finger a sensitive gripping tool. (b,c) Reproduced with permission from [401], copyright (2004) Springer. (d) Corneocytes on the skin surface. Reproduced with permission from [413] under CC-BY-NC license.

to superhydrophobic surfaces that now routinely leverage the concept of hierarchy (see Section 2).

Where is the current state of the art for artificial micropatterned adhesives in comparison with their natural examples? While fibrillar micropatterns easily reach or even exceed the adhesion strength of gecko pads on smooth surfaces (typically 100 kPa), nature still holds the record in adhesion to arbitrarily rough surfaces. Roughness has turned out to be a deep and rich fundamental problem for physicists and controversies on some subtle points persist. Generating reliable adhesion of artificial systems on rough surfaces would be a worthwhile achievement that would probably open up a wealth of applications. First concepts for rationally designing microstructures for a given roughness power spectrum have been formulated but need to be refined and validated. Here again, the availability of stable microfibrils with submicron diameters may be a key issue in the future.

Overall, the concept of contact splitting and fibrillar adhesion is now sufficiently mature to be marketed by small businesses. Promising innovations will happen very likely in the areas of robotics, handling and automation, and consumer products. In the quest for success in these efforts, the main technical issues will lie in the design of reliable arrays, taking the recent findings about defect statistics and equal load sharing into account. Other vital issues will be robustness, the long-term durability of the materials and the associated repeatability of attachment-detachment switching cycles (see e.g. [391,392]). Finally, new processes will have to ensure efficient and cost-effective fabrication on large areas to turn an attractive design idea, derived from millennia of natural evolution, into an innovation enriching our daily lives.

4. Microstructures for interaction with the human body: Biocompatible adhesion and sensing

In the preceding sections, bioinspired micropatterned surfaces for contact with the non-living “outer world” were reviewed. A growing number of groups worldwide have dedicated their research to another promising frontier: the interaction of designed surfaces with human skin and other organs and tissues. The driving force for these developments is provided by the health care sector, where innovative materials and concepts based on bioinspiration can significantly accelerate progress.

4.1. Bioinspiration for biomaterials

The materials used to correct, repair, or supplement natural functions in human organs are often referred to as biomaterials [18]. The demand for and spending on biomaterials has been surging in recent years [393]. One of the challenges is that optimization for most biomaterials is based on tuning their compositions [394], requiring enormous research effort and repeated approval processes (e.g. by FDA). Also here, learning from nature with emphasis on structural optimization [395] may provide more promising solutions.

The human body as a contact “object” is of course far more complex than non-living materials. Skin is one of the most challenging surfaces to design an adhesive for. Besides its protective function, skin also transmits various physical and chemical biosignals which are vital health status indicators [396]. As will be discussed below, one of the main challenges for skin adhesives is conformation to its multi-level roughness. We will attempt to apply the basic principles of fibrillar adhesion, as discussed above, to the biomedical environment. In addition, other promising adhesion mechanisms, such as microsuction, will be discussed.

In this section, we will first review materials and concepts for the interaction with the first barrier of the human body, our skin. The concepts described in this section will inevitably be more descriptive and less quantitative than the earlier sections dealing with inanimate objects. As illustrated in Fig. 4.1, we will focus on two types of bioinspired microstructures that exhibit great potential for application in healthcare devices: gecko-inspired microfibrils (Fig. 4.1a) and octopus-inspired microsuckers (Fig. 4.1b). Such surfaces are essential for many medical purposes such as wound management, implant fixation, health monitoring and disease therapy [397,398].

4.2. Structure and surface characteristics of skin

Skin is the largest organ of the human body, covering typically an area of about 1.8 m² [401]. It protects homeostasis, i.e. steady internal physical and chemical conditions, against external agents such as heat, light, moisture, mechanical damage and microorganisms. The skin also hosts assorted nerves, glands, vessels and pores to enable the haptic perception of the environment and to regulate body temperature and hygrometry [402].

From a materials point of view, skin is a layered composite with a complex structure and surface (see Fig. 4.2a). It consists of profusely curved collagen fibers densely arranged in layers and embedded in a matrix consisting of transverse elastin fibers and grounding substances [403,404]. Among the three main constituents [401], the epidermis (with a thickness of about 0.1 mm and a Young’s modulus of about 1 MPa) is the external layer; the *stratum corneum* forms a hard tough keratin shelter on top [405,406], with a typical Young’s modulus of 1 GPa in dry and about 10 MPa in wet state. Being composed of dead tissue, the keratinized layer provides mechanical protection via its hardness and toughness; it also prevents the loss of body fluids as well as the penetration of external chemicals, infectious agents and electromagnetic radiation. The sublayers of the epidermis contain stem cells constantly differentiating and refreshing the protective barrier above. The dermis layer accounts for most of the skin’s mechanical properties (with a modulus from 100 to 300 kPa) and hosts various sensors, glands, and vessels. The subcutaneous layer, also called hypodermis, has a typical modulus of 30 kPa and provides thermal insulation, stores energy, and absorbs shocks [403,404].

When developing skin adhesives, the following complications must be considered:

- **Roughness:** Depending on body location, the skin surface exhibits different degrees of roughness on several scales, caused by association of furrows, hair follicles and sweat pores (Fig. 4.2b-d). The depth of furrows varies with gender, age and body site,

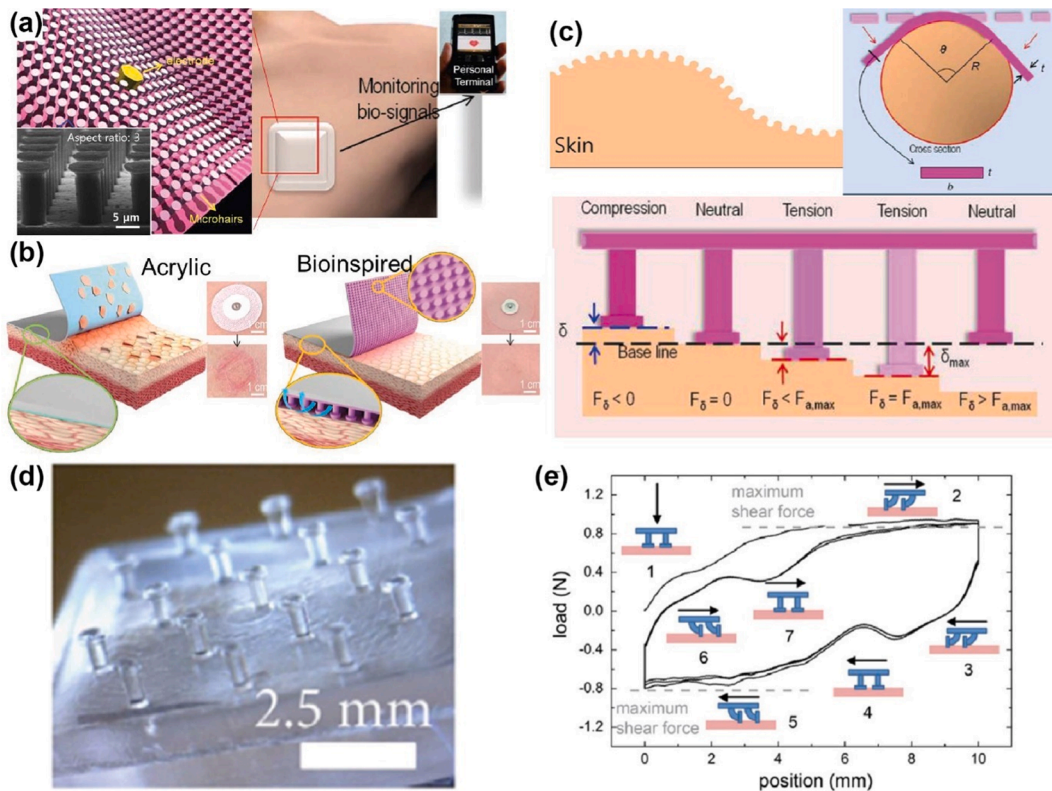


Fig. 4.3. Micropatterned skin adhesives fabricated with homogeneous microfibrils. (a) Schematic of a skin adhesive for use as a biomedical bandage in a diagnostic system. Insets show mushroom-shaped PDMS fibrils. (b) Schematics of the detachment of adhesive from skin: acrylic-based adhesive with skin damage (left) vs. a micropatterned adhesive (right). Insets show the skin condition after 48 h. (c) Mechanistic model of the patch conforming to skin at two levels of roughness. The upper right panel shows the adaptation to the macroscale roughness, while the lower illustrates the elastic deformation of microfibrils for adapting to the microscale roughness. (d) Microfibrils made of polyethylene-reinforced PDMS. (e) Shear resistance test of the fibrils on wet chicken thigh muscle. (a–c) Reproduced with permission from [399], copyright (2011) Wiley. (d,e) Reproduced with permission from [417], copyright (2016) Elsevier.

ranging from several microns to millimeters [401,407]. Their main function is mechanical, enabling the stretchability and friction of skin [408]. The hair follicles and sweat orifices constantly produce hairs and fluid, making the condition of the skin surface dynamically unpredictable. Kovalev et al. [409] determined the roughness power spectrum of human wrist skin and emphasized that both atomic force microscopy and white light interferometry were necessary to subsequently estimate real contact areas.

- **Viscoelasticity:** Whereas many of the materials used for microfibril fabrication have negligible viscoelastic losses, skin itself is highly viscoelastic [410]. This will create an additional energy contribution during detachment and may increase adhesion.
- **Regeneration:** The skin surface constantly regenerates [401]. Special cells (i.e. keratinocytes) migrate outwards and decay there to form the *stratum corneum*. Typically, every day one layer of this keratinized layer sloughs off as is shown in Fig. 4.2e [413]. This effect will put an upper limit on how long a microstructure can be expected to adhere.
- **Bacterial colonies:** The skin surface has various resident bacterial and mycotic flora on it, forming a stable ecosystem that plays a fundamental role in body health [411]. The density of these residents is normally stable over time. The colonies may also affect adhesion.

4.3. Gecko-inspired microfibrillar structures

Skin adhesives must create reliable conformal adhesion to the body to fulfill their function, e.g. in wound-healing, biosignal collection and controlled drug release [397,414]. Current pressure-sensitive adhesives (PSA) are mainly based on natural rubber latex or acrylate, which can cause skin irritation and allergy. Their strong adhesion may damage the outermost layers during removal, especially in baby or aged skin [415]. PSAs also leave behind sticky residues and lose grip after repeated use. Gecko-inspired adhesives could lead to several improvements here.

A comparatively new approach is to micropattern silicone elastomers for interaction with the human body. Silicone elastomers, as

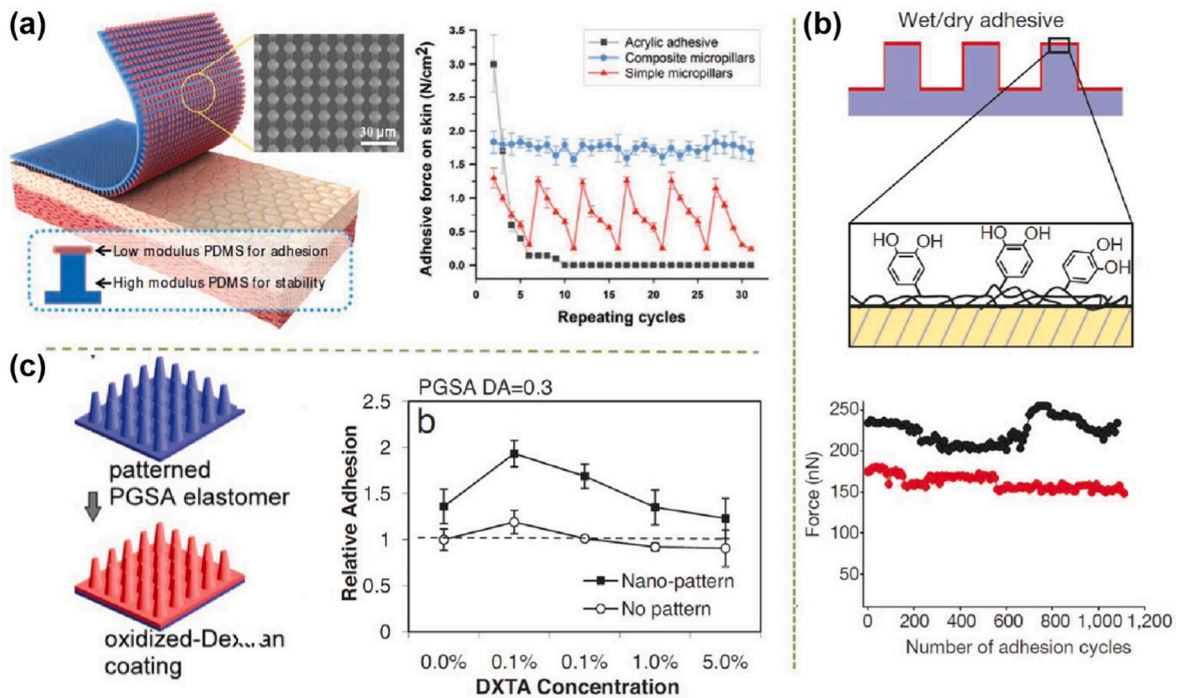


Fig. 4.4. Micropatterned tissue adhesives composed of composite microfibrils. (a) Micropatterned dry adhesive patch made of composite microfibrils combining stiff and soft PDMS. Schematic illustration and SEM image of the patch (left) and cyclic adhesion tests of composite microfibrils compared with homogeneous fibrils and acrylic-based adhesives (right). Reproduced with permission from [309], copyright (2013) Wiley. (b) Gecko and mussel inspired ‘geckel’ adhesive patch. Schematic illustration of the catechols-containing mussel-adhesive protein coated onto the fabricated microfibrils (upper). Cyclic adhesion performance tested by AFM in both water (red) and air (black) (lower). Reproduced with permission from [419], copyright (2007) Springer Nature. (c) Example of a biodegradable and biocompatible micropatterned tissue adhesive. PGSA-based microfibrils, with diameters between 100 nm and 1 μm , fabricated by molding and DXTA spin coating (left). Shear test results (erroneously called adhesion) for the micropatterned surface and a flat control (right). Reproduced with permission from [420], copyright (2008) National Academy of Sciences, U.S.A.

used in many of the adhesive gecko structures discussed in Section 3, are classic medical materials: for example, PDMS is widely used as implant material, for contact lenses, for cell cultures and in lab-on-chip applications, e.g. [416]. Its Young’s modulus can be tuned between several MPa and tens of kPa. Similar silicones were developed as wound dressings and band-aids because of their gentle adhesion to skin. The papers published to date are largely empirical as detailed models for adhesion to soft objects such as skin are not available. Direct transfer of fracture mechanics approaches, as described in Section 3.2, is not permissible due to the high compliance, large-scale deformation and possibly viscous response of the soft object. Adhesion of elastic fibrils to stiff objects is principally different from stiffer fibrils contacting a softer substrate, see also [258,259]. This situation opens up much room for future theoretical modeling.

4.3.1. Homogeneous microfibrils

Kwak et al. [399] pioneered a skin adhesive patch based on well-aligned homogenous mushroom-shaped microfibrils (Fig. 4.3a). Fabricated with PDMS (Sylgard 184) with an aspect ratio of 3, the patch provided a durable adhesion strength up to 13 kPa on skin. Adhesion strengths on skin are at least one to two orders of magnitude below those for stiff, smooth objects, but adhesion was found to be sufficient for ensuring electrocardiogram (ECG) function over two days. Compared with acrylic based PSA, the micropatterned patch maintained good adhesion up to 30 attachment/detachment cycles and was reported to leave no residues and to cause no visible damage (Fig. 4.3b). Moreover, the authors claim that the gaps between the fibrils allowed free air flow and therefore reduced the amount of enclosed moisture.

A simple mechanistic model was proposed by the authors to explain the adhesion performance of their patch on a surface with skin-like roughness at two levels (Fig. 4.3c). To ensure conformal contact with the macroscale roughness of curvature R^{-1} , the work to separate the adhesive contact, W_{sep} , has to overcome the bending energy per unit area generated in the curved backing layer. The resulting condition for conformal adhesion predicts the maximum thickness, t , of the backing layer as:

$$t^3 = 24 \frac{W_{sep} R^2}{E}, \quad (4.1)$$

where E is Young’s modulus of the backing layer. Similarly, a criterion was formulated for the minimum length of the microfibrils to form stable skin contact and to overcome microscale roughness. Optimum adhesion was reported for a fibril aspect ratio of 3.

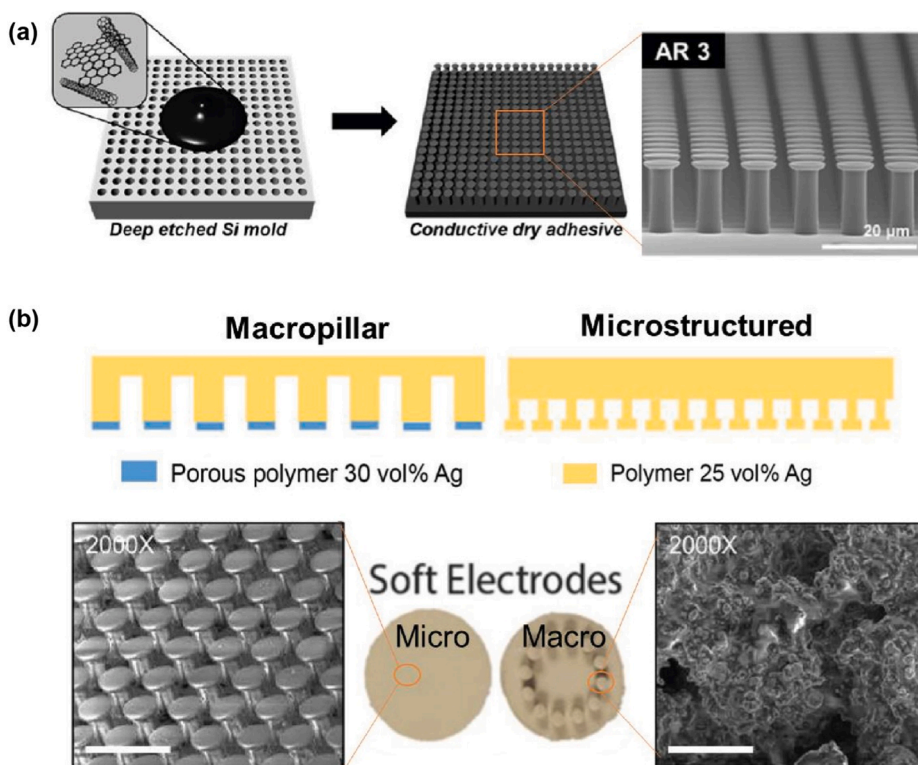


Fig. 4.5. Multifunctional microfibrillar structures used in healthcare devices. (a) Carbon-doped microstructured adhesives with built-in electrical conductivity. The inset SEM shows arrays of composite microfibrils with aspect ratio (AR) of 3. Reproduced with permission from [422], copyright (2016) American Chemical Society. (b) Ag-doped self-adhesive electrodes with fibrillar structure at different length scales. The surface of the mushroom-shaped microfibrils is smooth while that of the macrofibrils is porous. Reproduced with permission from [423], copyright (2018) Wiley.

The analytic model proposed by Kwak et al. indicates that using softer materials or designing a thinner backing layer with longer microfibrils can improve conformity with the contact surface, leading to improved adhesion. However, Fischer et al. [417] noted that soft polymeric microstructures often lack shear resistance, which is essential for a stable contact or when aiding the healing of wound tissues. To enhance shear resistance against wet tissue, PDMS microfibrils were reinforced by polyethylene to increase their stiffness. The reinforced microfibrils achieved a 6-fold increase in shear resistance compared with pure PDMS fibrils (Fig. 4.3d,e), showing a promising potential for future design of wound closure or stabilization of implants.

4.3.2. Composite microfibrils

Following Section 3.2.3.2 above, the conflict between softness for adhesion to a rough surface and stiffness for stability can be resolved by a composite fibril design. This strategy is particularly attractive for skin adhesives, as has been demonstrated by Bae et al. [309] (Fig. 4.4). By replica molding followed by inking, stiff PDMS ($E \sim 2.8$ MPa) in the stem region was combined with a soft PDMS (~ 0.8 MPa) in the tip layer. An adhesion strength of about 18 kPa was achieved on human skin in this way. Especially in repetitive adhesion cycles, composite fibrils significantly outperformed a conventional acrylic adhesive and homogeneous microfibrils (Fig. 4.4a, right). The authors reported that clear vital ECGs were recorded in real-time for 48 h, without any visible skin damage after removal. Adopting a similar strategy, Drotlef et al. [418] inked stiff PDMS microfibrils with partially crosslinked vinyl siloxane on the tip surface, followed by further crosslinking while in direct contact with the skin-like tissue. A similar adhesion strength of 18 kPa was obtained, with the limitation that the reusability degraded significantly after several cycles; this effect was attributed to the gradual destruction of the mushroom tips. Again, high-quality amplification of strain signals was reported.

Adhesive structures intended for biomedical application will have to cope with a humid or wet environment. To counter the loss of van der Waals interaction, chemical bonding in addition to the gecko effect was investigated. Inspired by the tenacious wet adhesion of mussel holdfasts, Lee et al. [419] dip-coated a thin layer of poly(dopamine methacrylamide-co-methoxyethyl acrylate) on nanoscale PDMS microfibrils (diameter ~ 400 nm) and created a flexible organic adhesive (Fig. 4.4b). Benefiting from various interactions, including metal coordination bonds, pi electron interactions and covalent bonds, between the catecholic amino acid 3,4-dihydroxy-L-phenylalanine and the other organic/inorganic surfaces, such fibrils attached firmly to both organic and inorganic surfaces. Compared

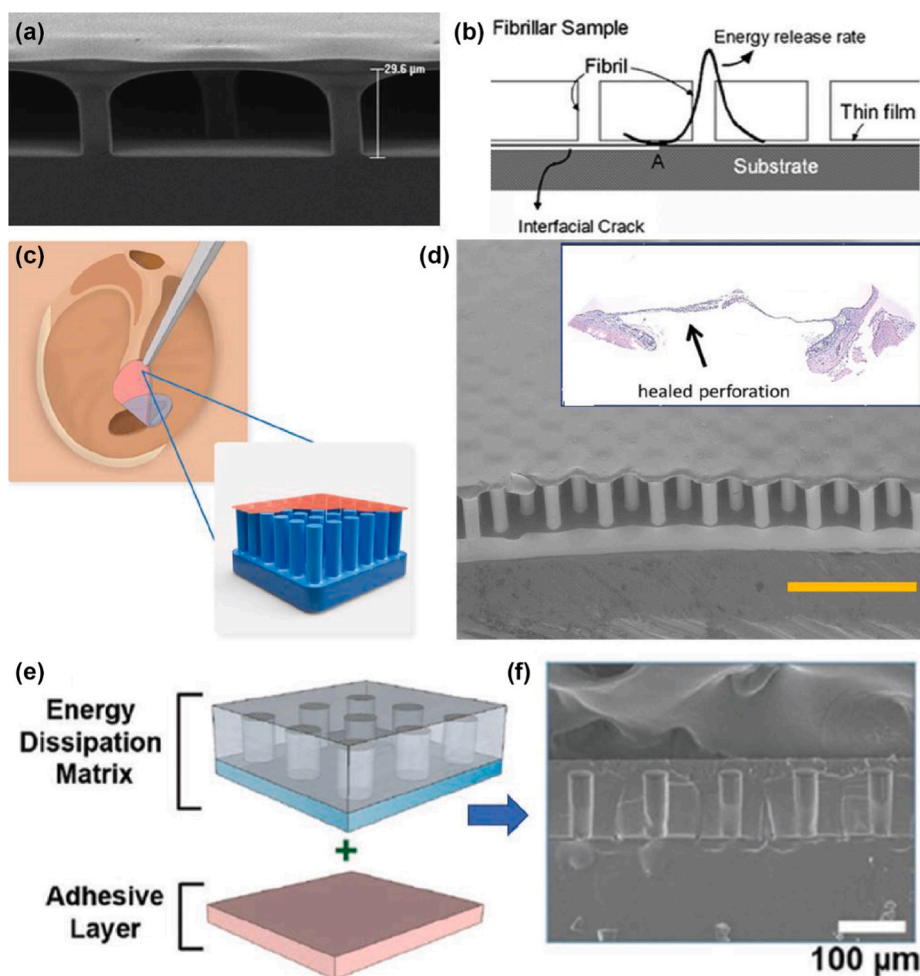


Fig. 4.6. Film-terminated and embedded fibrillar microstructures. (a) SEM image of a film-terminated patch made of PDMS. (b) Schematic illustration of the adhesion enhancement mechanism based on crack pinning effect. (c) Schematic diagram of the film-terminated microfibrillar adhesive patch developed for repair of perforated eardrums (INM research). (d) SEM image of the film-terminated product. The inset is the histological cross-section of a mouse eardrum whose healing was substantially improved by application of a micropatterned patch. (e) Conceptual illustration of the snail-inspired interlocking microstructure coupled with an adhesive layer. (f) SEM image of the cross-section of the interlocking architecture. (a,b) Reproduced with permission from [427], copyright (2008) Royal Society of Chemistry. (c,d) Pictures by courtesy of G. Moreira Lana, K. Kruttwig, G. Wenzel, B. Schick, INM and Saarland University Hospital. (e,f) Reproduced with permission from [438], copyright (2019) Wiley.

with uncoated controls, the adhesion was improved by a factor of three in dry condition and nearly 15 times under water. Moreover, in cyclic adhesion tests the adhesive strength diminished only slightly in both dry and wet conditions (Fig. 4.4b, lower). In spite of these advantages, this ‘geckel’ concept still has some potential challenges when used on internal organs. For instance, the material has to eventually be removed from the body and the strong chemical bond may cause secondary damage on delicate tissue. From a fundamental point of view, it is not fully clear that the contact splitting principle is compatible with strong chemical bonds.

Mahdavi et al. [420] designed a tissue-compliant synthetic adhesive consisting of biodegradable arrays of composite microfibrils (with diameters ranging from 1 μm down to 100 nm). Coating with a thin layer of tissue-reactive polymer, oxidized dextran, improved the interaction with wet porcine tissue by covalent crosslinking (Fig. 4.4c). With an optimized design, a maximum “separation force” of up to ~ 48 kPa was reported (regrettably, for most other mechanical results only relative values were given) (Fig. 4.4c, right). On close inspection, this study employed confusing terminology: all measurements were conducted in shear, hence were measurements of friction rather than adhesion; the microfibrils had a strong taper, with a tip up to ten times thinner than the base – the opposite of effective gecko structures; and the fact that friction increased for smaller tips and larger fibril spacings indicates that the mechanisms of (shear) resistance was related to tissue interlocking or even penetration, rather than a “gecko effect”. Nevertheless, the use of biocompatible and biodegradable materials will potentially avoid the tissue damage caused by implant removal and the pain and risk of a second surgery.

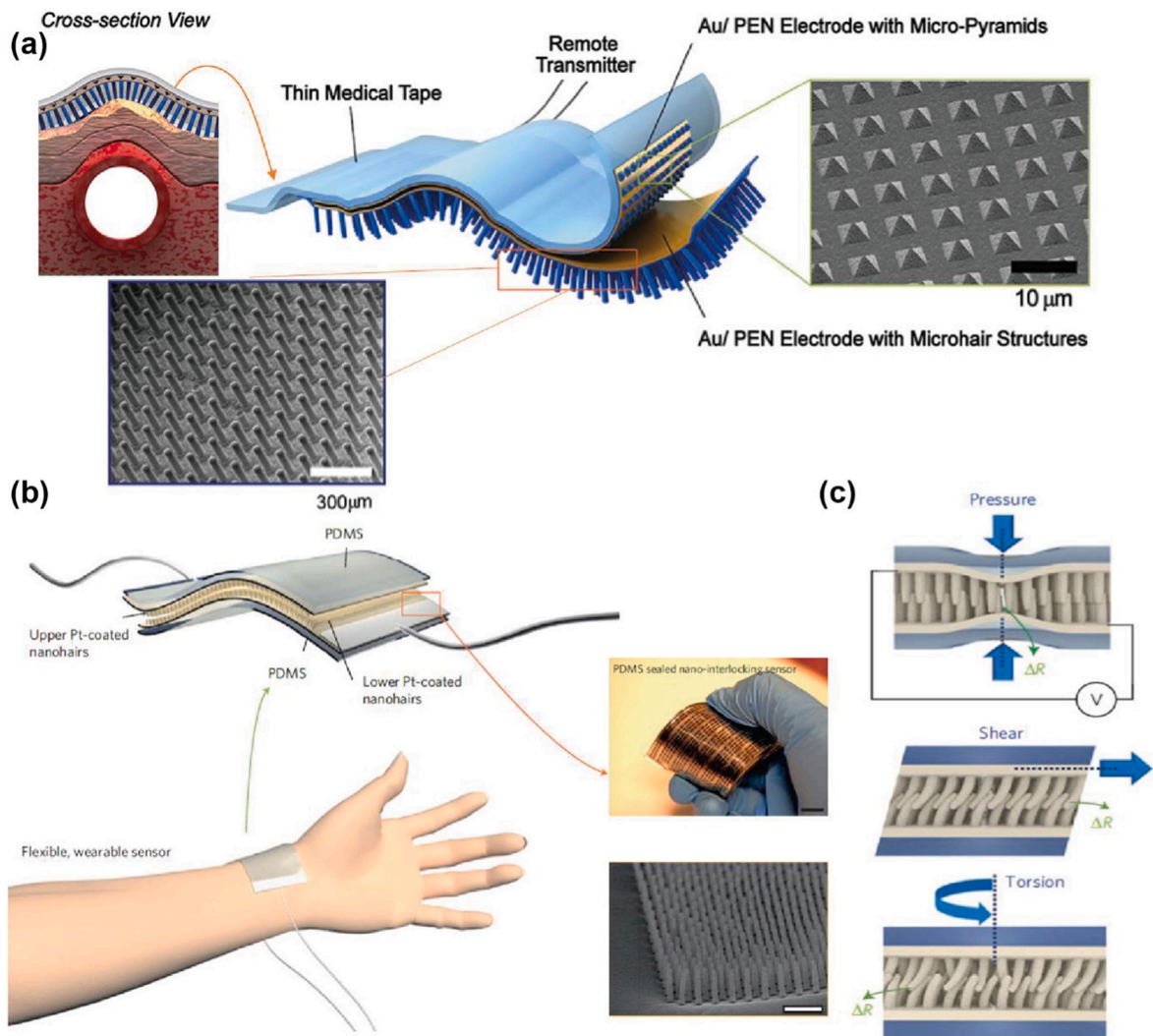


Fig. 4.7. Microfibril-aided skin sensor. (a) Cross-section of a microstructured pulse signal amplifier with fibrillar structures. Upper left inset illustrates the improved conformity between the signal sensor and the surface of human neck. Two inset SEM images are pyramid-shaped PDMS microstructures forming a dielectric layer (right) and the microfibril-structured contacting layer (lower left). Reproduced with permission from [444], copyright (2014) Wiley. (b) Concept of a sensitive strain sensor based on the interlocking of microfibrils, designed for application on the body. The inset shows the actual product and an SEM image of the microfibril morphology. (c) Schematic illustration of possible distortions of the interlocked fibrils corresponding to externally applied mechanical stimuli. (b,c) Reproduced with permission from [450], copyright (2012) Springer Nature.

In an alternative attempt [421] to increase adhesion to wet tissue, biocompatible and biodegradable chitosan films were patterned with comparatively flat nanostructures (length 70 nm, diameters from 100 to 600 nm). The patterned microstructures exhibited, under dry conditions, 10 times the adhesion of flat controls and retained these values under moist conditions. Contrary to the claims of the paper, the mechanism of interaction is not even remotely similar to a gecko effect and other processes must be responsible for the adhesion enhancement.

4.3.3. Conductive microfibrils

Portable soft digital devices that adhere to skin are on the verge of transforming diagnostic healthcare [396]. Real-time and long-term monitoring can help doctors diagnose medical problems earlier and more precisely, making health care more predictive, safer and more efficient. The next generation of the skin adhesive patch will very likely also integrate electrical conductivity. For this purpose, Kim et al. [422] mixed carbon nanotubes and graphene with PDMS (Fig. 4.5a). The resulting carbon-doped elastomeric microfibrils

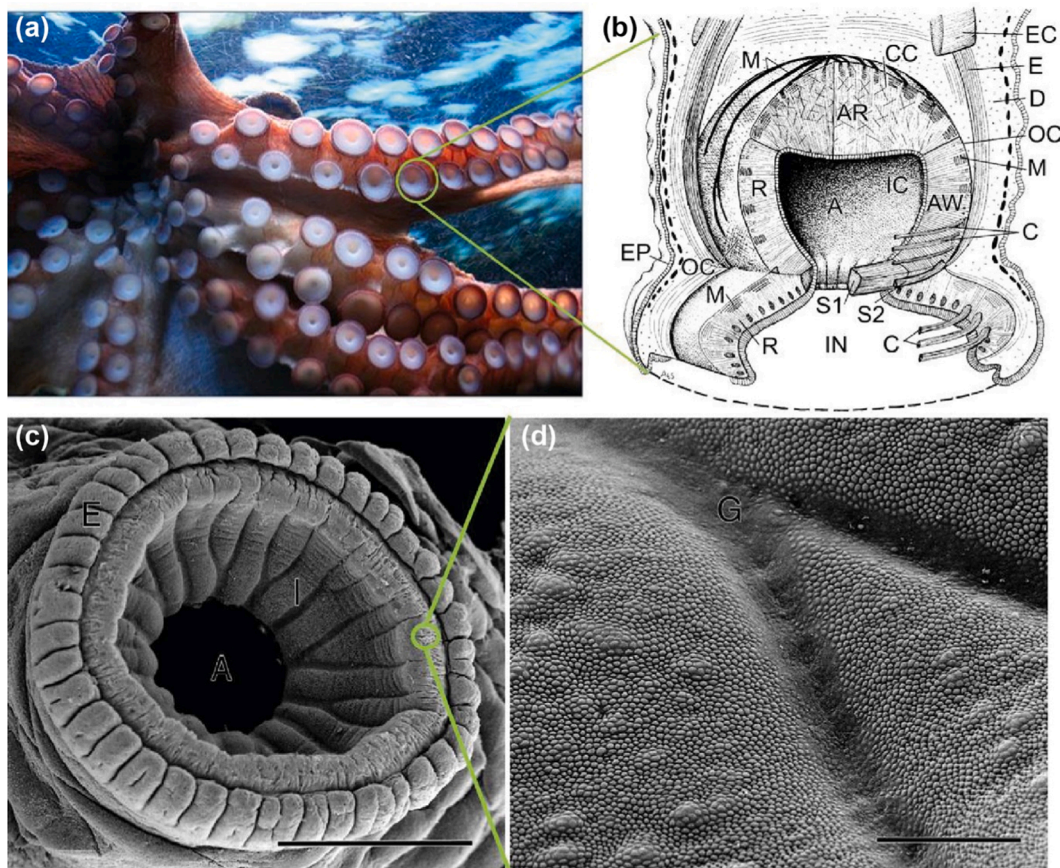


Fig. 4.8. The anatomy of an octopus sucker as an inspiration for micro suction cups. (a) Octopus arms equipped with suckers. The size of the suckers varies with location and species. Image from Pixabay (www.pixabay.com) under Creative Commons Zero License. (b) Schematic of an octopus sucker with a cavity and three sets of muscles for activation of the cavity and sealing of the rim. (c) SEM image of the sucker rim. Scale bar: 1 mm. (d) Close-up SEM image of the grooved rim surface showing numerous projections or denticles. Scale bar: 100 μm . (b–d) Reproduced with permission from [451], copyright (2002) Oxford University Press.

generated an adhesion strength of up to ~ 13 kPa, which is comparable to other values discussed previously. By optimization of the doping dose, the microstructured adhesive patch exhibited a specific resistance as low as $\sim 100 \Omega \cdot \text{cm}$, comparable to commercial electrodes. The authors claim that clear and more stable ECG signals were collected, especially in underwater conditions.

Employing a similar strategy, Stauffer et al. [423] incorporated silver microparticles (diameter 2–3.5 μm) in silicone rubber and fabricated self-adhesive electrodes with macro and microscale fibrils (Fig. 4.5b). However, the adhesion strength was still only ~ 1 kPa, significantly smaller than other reported values. It is unlikely that this amount of adhesion will survive physical activity by the wearer of the device. Therefore, it is surprising that high-quality ECG and electroencephalogram (EEG) signals could be recorded without additional fixation, even during vigorous movement like swimming. Furthermore, it was reported that the macrofibril-structured electrode detected EEG signals through dense hair on the head. If substantiated, these results underscore the potential of multi-functional microstructured adhesives for the development of innovative healthcare devices.

4.3.4. Film-terminated and embedded fibrillar microstructures

Although some of the reported microfibrillar structures exhibit promise for use in diagnostics, some of them suffered from loss of contact area, lateral collapse and undesirable buckling of fibrils [239,424]. Film-terminated structures are an alternative design that can be considered of as an extreme case of mushroom-shaped fibrils: the arrays of microfibrils are bridged at their terminal ends by a compliant thin film as shown in Fig. 4.6a [248,425,427]. The design resembles the embedded microchannels investigated by Ghatak et al., e.g. [428]. Such structures derive their improved adhesion from a crack trapping mechanism (Fig. 4.6b): the interfacial cracks “feels” the spatial modulation of the local compliance and is pinned in the space between the fibrils, where the energy release rate to drive crack propagation is reduced [426,427]. Following this strategy, numerous trials were made to develop PSAs with better performance [429–432] but only recently has the film-terminated microstructure been exploited for tissue engineering.

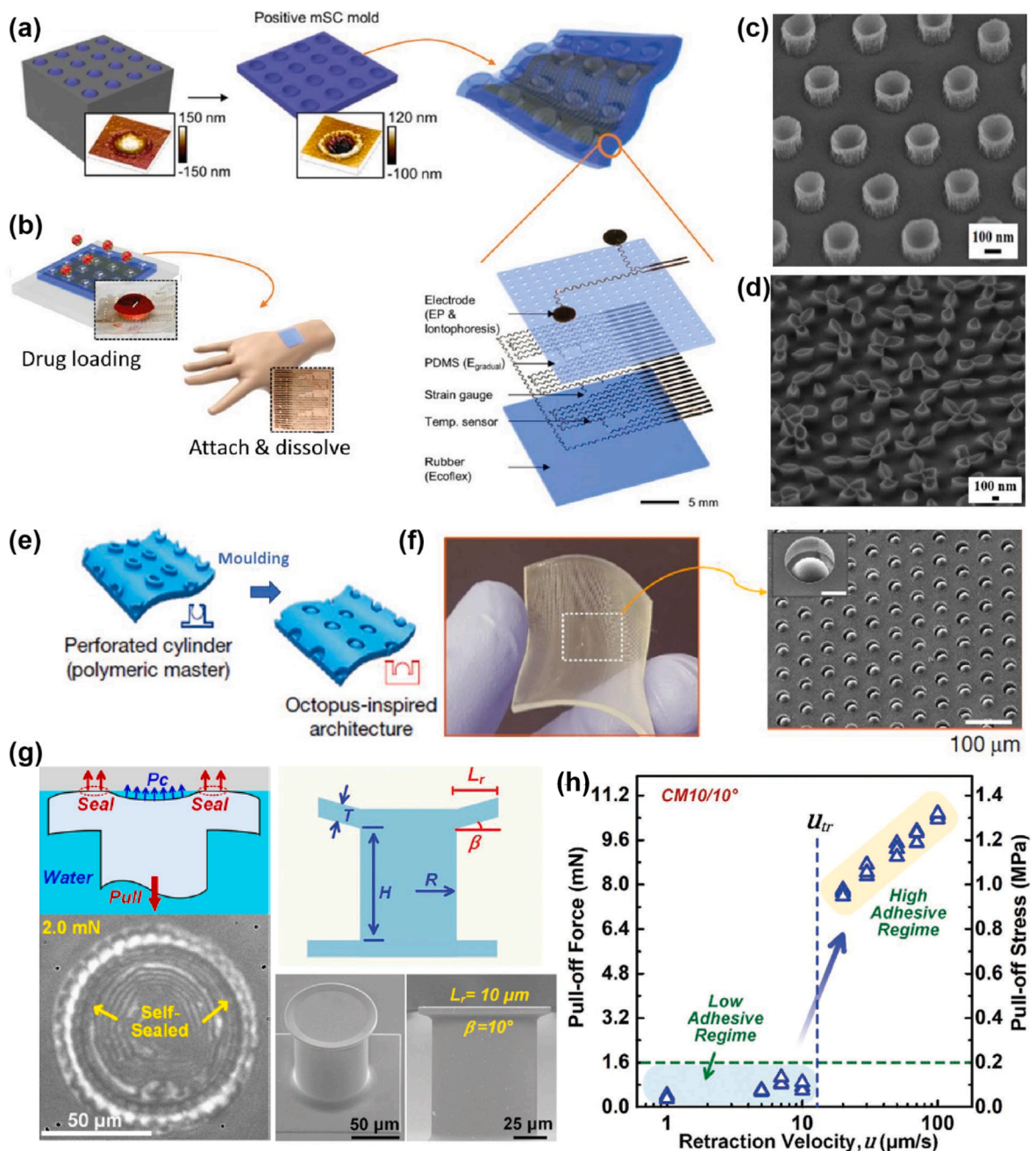


Fig. 4.9. Sucker-inspired skin adhesives and devices. (a,b) A multifunctional “smart medical skin” with miniaturized suction cups. (a) Illustration of the fabrication procedure for an electrode system with miniaturized suction cups of 1 μm diameter. (b) Schematic diagram of the proposed concept for controllable transdermal drug delivery. (c,d) A silicone adhesive with micro suction cups. (c) SEM of the PDMS suction cups. (d) SEM of collapsed micro suction cups after 30 cycles of adhesion. (e,f) Micro suction cups with dome-like protuberances. (e) Schematic diagram showing the fabrication of micro suction cups by moulding. (f) Photograph of the s-PUA patterned soft patch and close-up SEM of the interior protuberances. (g,h) Angled polyurethane microcups, 100 μm in diameter, with high and switchable wet adhesion. (g) Self-sealing behavior under water as observed *in situ* and schematic of the adhesion mechanism; optimum adhesion in wet and dry state was found for a cup angle of 15°. (h) Efficient switching of the adhesion strength underwater by selecting the retraction velocity. (a,b) Reproduced with permission from [455], copyright (2015) Wiley. (c,d) Reproduced with permission from [400], copyright (2017) American Chemical Society. (e,f) Reproduced with permission from [456], copyright (2017) Springer Nature. (g,h) Reproduced with permission from [292], copyright (2019) American Chemical Society and [293], copyright (2020) Wiley.

Such microstructures have been successfully developed at INM as gentle adhesives for the repair of injured eardrums, as proposed by Schick [433,434]. A soft skin adhesive (SSA) of typical thickness 100 μm was chosen, which demonstrated good adhesion on skin-like roughness [435,436] and explanted mouse ear drums [437]. This SSA layer was subsequently placed as a terminal layer on PDMS microstructures (Fig. 4.6c,d). The new microstructured patch with fibrils of 20 μm diameter and 60 μm length adhered more strongly than a flat reference sample to a rigid object of roughness similar to the ear drum (mean roughness $R_a = 0.28 \mu\text{m}$) and to rougher skin ($R_a = 13 \mu\text{m}$). Adhesion measurements on explanted perforated ear drums resulted in typical adhesion strengths of 12 kPa. The patch supported the wound healing process, which resulted in much reduced scar formation. Also, it was demonstrated that hearing ability could be improved over the injured state during the healing phase. Because of the sensitive adhesion, the microstructure was easier to handle by the surgeon and could be repositioned on the target surface. Another advantage is damping capacity, which protects delicate target tissue from overload during fixation. Clinical trials will have to validate this concept, which could substantially improve and accelerate patient care.

In a related design, the Pang group [438] fabricated a filled fibrillar microstructure to produce an “energy-dissipation layer” (Fig. 4.6e,f). For this complex structure, they measured an adhesion strength of about 70 kPa to a skin replica. The authors claim that their design was inspired by the pedal retractor muscle in snails.

4.3.5. Microfibril-aided haptic sensors

Highly sensitive skin-attachable strain sensors are vital to improve the precision of health monitors based on converting mechanical deformation, e.g. due to pulse, blood pressure, or heartbeat, into electrical signals [439,440]. The development of artificial skin also calls for strain-gauge sensors to confer on the robotic system human-like touch and haptic capability [441–443]. As fibrillar microstructures can adapt to rough surfaces more conformally, they have the potential to improve sensor sensitivity in these applications.

A high-performance pulse signal amplifier was designed by Pang et al. [444] (Fig. 4.7a). The upper half of the sensor followed a well-established protocol consisting of five conductive layers, combined with a pyramidally-microstructured PDMS layer, which enhanced sensitivity, stretchability and reduce hysteresis. The lower half of this device was a PDMS microfibrillar layer which was sealed against the upper half by a thin medical tape. Compared to the flat reference without microfibrils, the sensor exhibited an enhanced conformity to rough skin regions. Such conformal adhesion was able to double the sensitivity of electric signal detection, enabling the sensor to measure faint biomechanical signals such as the deep-lying venous pulse. Similar efforts were also made by other groups [445,446], again using surface micropatterns to increase conformity.

One of the major functions of skin is to sense the outer world through embedded sensors and neurons. Inspired by natural mechanotransduction systems [447–449], Pang et al. [450] developed a highly sensitive strain sensor based on reversible interlocking of nanofibers. Two arrays of Pt-coated PDMS microfibrillar patches, interlocked face to face (Fig. 4.7b), recorded various mechanical stimuli (illustrated in Fig. 4.7c). The variation of the degree of fibrillar interpenetration led to discernible electrical resistance changes. The authors claimed a highly sensitive and reversible response, for 10,000 on–off cycles, showing promise for application in artificial skin or haptic devices.

4.4. An alternative design: Micro suction cups

While microfibrillar adhesion structures used in locomotion and gripping are widely found in terrestrial animals, aquatic animals have evolved different mechanisms. The presence of water substantially weakens van der Waals interactions (see also Section 3.2.2.4) and can also provide lubrication, both of which substantially weakens the contact. An efficient solution for this challenge in aqueous environment is to exploit suction effects. The final section will be devoted to a brief overview of this alternative mechanism.

4.4.1. Suction-based attachment in nature: Another size effect?

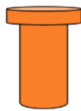
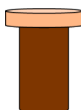
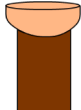
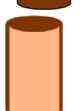
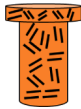
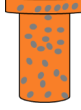
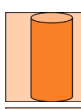







Suction cups are found in the cephalopod family, e.g. in the octopus (Fig. 4.8a). They enable the animal to walk on the bumpy seabed and to firmly grip prey or other objects [195,451]. Another example is the clingfish, a fairly small fish widespread in tropical and temperate areas. Its chest region is equipped with a robust suction disc. This intricate hierarchical microstructure [381] can generate an impressive attachment force from 80 to 250 times the fish’s body weight [452]. The remora, also called the suckerfish, has a suction pad evolving from dorsal fin spines. Remoras can attach to sharks, ships, and even occasionally to scuba divers, making them a “free-rider” in the ocean [453].

While suction devices in air are limited by the ambient air pressure (100 kPa), the incompressibility of water can produce much higher adhesion strengths underwater. The sealing function to the substrate will be essential for achieving high adhesion. Spolenak et al. [241] pointed out that, unlike van der Waals contacts, suction cups create an adhesion force proportional to the cup area; at a constant pressure difference, the adhesion strength should therefore not exhibit a size effect. This conclusion is in contrast to experiments by Smith [454], who found a negative correlation between sucker size and adhesion strength in European squid and common cuttlefish. The author speculated that smaller cavities would produce smaller hoop stresses and could therefore sustain larger pressure differences; this argument however would only hold for constant wall thickness, as the hoop stress scales with the ratio of cavity size to wall thickness. The source of a size effect for suction thus seems unclear.

Kier and Smith studied the detailed structure and mechanism of the octopus sucker [451]. The individual suction cup has a dome-like geometry with radial grooves on its surface and along the rim (Fig. 4.8b,c). The sucker is actuated by a muscle system which fulfills two functions: sealing the cavity and creating a pressure difference between the interior and the ambient environment by increasing

Table 4.1

Summary of the performance for various types of micropatterned skin adhesives with materials used and structural design. Diameters are designated by d , aspect ratio (=length/diameter) by AR , t is the cap thickness. PDMS stands for polydimethylsiloxane, VS for vinyl siloxane, p(DMA-co-MEA) for poly(dopamine methacrylamide-co-methoxyethyl acrylate), PUA for polyurethane-acrylate, CNT for carbon nanotubes and SSA for soft skin adhesive. ECG is the abbreviation of electrocardiogram and EEG of electroencephalogram.

Structure	Characteristic size	Material	Adhesion strength (kPa)	Application	Reference	
Fibril		$d \sim 5 \mu\text{m}$; AR:3 tip: $d \sim 9 \mu\text{m}$; $t \sim 0.6 \mu\text{m}$	PDMS $E \sim 2 \text{ MPa}$	13 (on shaved skin)	Electrode fixation	Kwak et al. [399]
		$d \sim 5 \mu\text{m}$; AR:3 tip: $d \sim 9 \mu\text{m}$; $t \sim 0.5 \mu\text{m}$	Hard PDMS (2.8 MPa)/ Soft PDMS (0.8 MPa)	18 (on shaved human skin)	Electrode fixation	Bae et al. [309]
		$d \sim 45 \mu\text{m}$; AR:2 tip: $d \sim 95 \mu\text{m}$; $t \sim 35\text{--}45 \mu\text{m}$	PDMS/VS (viscous)	18 (on shaved human skin)	Strain sensor fixation	Drotlef et al. [418]
		$d \sim 45 \mu\text{m}$; $h \sim 600 \text{ nm}$	PDMS/p(DMA-co-MEA)	90 (underwater on AFM tip)	Wet adhesive	Lee et al. [419]
		$d \sim 5 \mu\text{m}$; AR:3 tip: $d \sim 7 \mu\text{m}$	PDMS ($\sim 1.5 \text{ MPa}$)/ CNT + graphene	13 (on PUA skin replica)	ECG electrode	Kim et al. [422]
		Macro: $d \sim 1 \text{ mm}$, AR:2; Micro: $d \sim 5 \mu\text{m}$; AR:2 tip: $d \sim 7\text{--}8 \mu\text{m}$; $t \sim 2 \mu\text{m}$	PDMS ($\sim 1.5 \text{ MPa}$)/Ag particles	Macro ~ 0.16 ; Micro ~ 1 ; (on unshaved human skin)	ECG and EEG electrode	Stauffer et al. [423]
		$d \sim 30 \mu\text{m}$; AR:3	PDMS/PUA	130 (on silicon wafer)	Skin adhesive	Kim et al. [438]
Suction cup		$d \sim 20 \mu\text{m}$; AR:3 Film: $t \sim 15 \mu\text{m}$	PDMS (Sylgard/SSA)	12 (on mouse eardrum)	Eardrum wound healing	unpublished
		$d \sim 1 \mu\text{m}$	Hard PUA	1.5 (on PUA skin replica)	Sensor fixation and drug reservoir	Choi et al. [455]
		$d \sim 150 \text{ nm}$	PDMS	30 (dry); 28 (wet) (on glass)	Wet tissue adhesive	Chen et al. [400]
		$d \sim 50 \mu\text{m}$	Soft PUA	40 (underwater on silicon wafer)	Wound healing	Baik et al. [456]
		$d \sim 100 \mu\text{m}$	PU	1000 (underwater on glass)	Various applications	Wang et al. [292,293]
						
						

the cavity volume. Microscale denticles (of size $\sim 3 \mu\text{m}$) on the rim surface enhance the friction at the contact interface, presumably improving the shear resistance (Fig. 4.8d). In deep water, the octopus can reach adhesion strengths of hundreds of kPa, but attachment failure due to cavitation has also been observed [451].

4.4.2. Microsucker-inspired skin adhesives

Exploiting the size effect observed in animals, the Kim group pioneered miniaturized suction cups for medical applications [455]. With a molding technique, they integrated cups with a diameter of $\sim 1 \mu\text{m}$ in a soft electrode structure designed for the recording of biosignals (Fig. 4.9a). The rim of the cups was only tens of nanometers thick, creating sufficient compliance to ensure conformity on human skin. Another attractive feature of their design was the layer gradation, which progressively reduced the elastic modulus to about 100 kPa, comparable to the modulus of epidermis. In addition, the miniaturized suction cups were loaded with therapeutic drugs (Fig. 4.9b). However, given the complex architecture of the patch, its reported adhesion strength, as obtained from a tack test, was disappointingly low (around 1.5 kPa). But the authors claimed significantly improved durability over flat or microfibrillar references.

Even finer PDMS micro suction cups of size 200 nm were fabricated by Chen and Yang [400] using a templating method with self-assembled silica nanospheres (Fig. 4.9c). The normal adhesion and frictional shear strengths on a dry glass substrate reached 30 and 13 kPa, respectively, and on a wet substrate 28 and 12 kPa. These values are an order of magnitude above those reported in [455] but the underlying reasons are unclear. While the authors demonstrated attachment of the patch to a pig heart (Fig. 4.1b), reusability was limited as repeated attachment led to collapse of the suckers (Fig. 4.9d). For octopus cups, Tramacere et al. [457,458] reported that a round protrusion inside the cavity played an important role in adhesion by suction. Baik et al. [456] fabricated micro suction cups made from a polyurethane-acrylate based polymer with dome-like protuberances (Fig. 4.9 e,f). The authors developed an analytical equation describing the adhesion strength as a function of pressure difference and elastic deformation of the cup. The adhesion strength values reported are impressive: 41 kPa in water and 154 kPa in silicone oil, substantially exceeding other reported designs.

Mechanistic insight into wet adhesion was recently provided by Wang et al. [292], who designed single polyurethane microcups, of 100 μm diameter, with angled elastic flaps (Fig. 4.9g). In contrast to most previous studies, extremely high adhesion strength was measured both in air and in water (1.3 and 1 MPa, respectively). The detachment mechanisms, which were extensively studied by *in situ* observation, differed substantially: in air the cup, adhered by van der Waals interactions, separated from the substrate by rapid crack propagation, whereas under water the behavior was controlled by water leakage into the cavity. The high values under water were attributed to a self-sealing mechanism: higher tensile forces resulted in a better seal, leading to longer attachment times (as predicted e.g. by [349]). In a follow-up study [293], an interesting switching behavior was identified as a function of retraction velocity (Fig. 4.9h). The results were explained by theoretical estimates of water penetration into the contact zone. Such work, when extended to arrays, may pave the way for a more rational control of adhesion in the wet body environment.

In conclusion, it can be stated that micro or nanocups are a promising design idea; surprisingly, their understanding seems to lag behind that of gecko-inspired fibrillar microstructures. None of the previous studies provide a systematic variation of sizes and elastic parameters, which would be needed as a basis for a mechanism-based interpretation. Hence even the fundamental issue of a size effect in the deceptively simple suction mechanism appears unclear. It is surprising that a full theoretical model addressing the feedback loop between cavity stretching and the sealing at the rim does not appear to be available in the literature. Furthermore, to realize the potential of suction cups in biomedicine, essential questions of long-term stability, of fatigue behavior in a dynamically moving body environment, and finally of biocompatibility will need to be addressed.

4.5. Outlook – Microstructures for the biomedical environment

Surface micropatterning has proven to be an appealing strategy for creating materials intended for contact with the human body. Due to the higher complexity, the understanding of contact phenomena with skin is far less advanced than for inanimate stiff objects. Only a few studies have been reported in which design parameters were varied systematically over significant ranges. Additional theoretical modeling and simulation are indicated to guide future design and materials choice for more advanced microstructures. These models will need to capture the mechanisms of interaction in the presence of multiscale roughness, high elastic compliance of the underlying material, non-linear viscoelastic behavior and fluid–structure interactions.

An overview of the structural designs reviewed in this paper is presented in Table 4.1. It is apparent that the adhesion strength values reported for microfibrillar structures in contact with skin are of the order of 10 kPa; this value is a factor of 10 to 100 below those achievable with smooth stiff objects or with acrylic-based biomedical tapes. For many of the envisioned biomedical applications such a performance will be sufficient as the stresses exerted will be smaller than in other engineering applications. By contrast, micro and nanosuction devices exhibit higher adhesion strengths and work better on organs where they are immersed in body fluids. The particular design will have to be chosen with consideration of the target tissue whose properties vary considerably among tissue types [459].

Reliable and cost-effective fabrication will be essential for the success of biomedical microstructures (see also Appendix). While the adhesion strength can very likely be enhanced by downscaling the size of fibrils and suction cups, fabricating large-scale high-quality structures at sub-micron scale is still challenging. Further advances would be possible by manufacturing the microstructures with biodegradable materials (as in [433]) or by integrating active components; stimuli responsive materials such as shape-memory polymers [367,460] could add switchability triggered by body temperature.

Wearables and wound dressings can over time cause irritation and discomfort. The tactile softness and breathable architecture of microstructures will be an asset for the wearing comfort of sports or health monitoring devices. Challenges for such microstructures will lie in their long-term behavior (over days and weeks), their biocompatibility, and possible interference with wound healing.

Developments of drug eluting microstructures are currently underway to improve the healing process; here, advanced structures such as microneedles may provide an alternative solution [461,462]. More advanced testing protocols will be necessary in the future to allow comparison of data between laboratories and to provide a basis for quality control. If these problems can be solved, surface microstructures will have the potential to provide innovative solutions for a range of applications, from health monitoring and haptic sensing to wound management and drug delivery.

5. Perspectives and conclusions

The present review has discussed, from a mechanistic perspective, the developments, promises and present shortcomings of functional surface microstructures, with emphasis on studies from the last decade. A connection has been established between wetting, adhesion to solids and to soft skin and other organs, and manipulation and control of these phenomena by micropatterning. The parallelism lies in the effects of the architecture of microstructures: In wetting, micropatterns and their “gaps” prescribe the geometry of interaction with the liquid through capillarity; when in contact with solid objects, polymeric microstructures dictate interfacial stress distributions due to intermolecular forces, which control temporary adhesion to other objects; and innovative artificial surfaces designed for contact with the human body will exploit these fundamental mechanisms to pave the way to new therapies and to novel digital devices for diagnostics and health monitoring.

Microstructures have become a subtle, but powerful tool to alter and augment the functionality of surfaces without invoking or changing materials chemistry. Nature has frequently and repeatedly chosen the micropatterning solution, presumably as this evolutionary path was more likely and more versatile than modifications in surface chemistry. Exactly this fact implies that artificial microstructures are also particularly attractive because of their resource efficiency. They can replace environmentally harmful technologies by more sustainable solutions: examples are micropatterns that substitute for energy-consuming vacuum suction devices in handling or harmful chemical coatings to repel fluids. It can therefore be forecast that surface micropatterning will very likely increase in importance in future years.

The understanding of microstructure effects is, at the present state, advanced but far from complete. Manipulation of wetting behavior has become a rich branch of modern applied physics, with far reaching implications e.g. for water management, cooling systems, wind turbines, and oil exploration and extraction. Still, the wetting dynamics of deformable solids, the robustness of superhydrophobic microstructures or the prevention of biofilm formation are outstanding challenges. The fascination with gecko adhesion and its translation into the laboratory and novel applications has revived areas of both experimental and theoretical mechanics. Yet, systematic parameter variation in experiments and simulation are still needed to shed more light, e.g., on optimal designs for arbitrarily rough objects. This is particularly true for the interaction of surface microstructures with skin, soft tissue and internal organs, an area where reliable modeling approaches are lacking. Significant advances were made in demonstrating the potential of microstructures in a biomedical environment; here, however, the lack of systematic investigation is particularly striking: for example, the optimum feature size for fibrils or suction cups is far from definitive clarification.

Surface micropatterning, while intriguing as a basic concept, comes at a price. Discrete contacts invariably lead to detrimental stress concentrations or even singularities at their edges, which however can be attenuated by design (as was extensively discussed above). Another downside is the propensity for clogging and contamination of the “gaps” in the microstructures, compromising the intended function or inflicting irreparable damage on intricate fibrils. This limitation has been one of the show-stoppers for widespread use of superhydrophobic self-cleaning surfaces. The delicacy of fine surface structures will tend to destabilize the patterns, leading to detrimental clumping of fibrils. This and the generally severe irreversible changes due to wear and degradation can limit the long-term usability of surface micropatterns. A further challenge is the development of processing methods for hierarchical microstructures which include features at a very fine scale, comparable to those found in nature. Another drawback is the effort (and cost) expended in creating micropatterns; scalability to processes compatible with large-area fabrication, such as roll-to-roll patterning, is an essential practical and economic necessity. Future research will have to address these issues from an engineering point of view.

The reader will note that our review is not fully exhaustive as many additional phenomena exist that are affected by surface structures with micron and nanometer dimensions. On a continuum level, the manipulation of friction is an obvious omission which would require a separate review [233,234,463,464]. Fibrillar microstructures have also been developed that generate electricity by tribological effects, e.g. [465]. In the optical and photonic sciences, light is modulated and scattered by micro and nanopatterns [3], e.g. to create an iridescent structural coloration following the example of the butterfly [4,466]. In cell biology, researchers have demonstrated the guidance of molecular processes by suitable micropatterns: it is now well established that living cells react to surface features on several length scales, modulating intra- and intercellular communication and signaling, controlling cell morphogenesis and fate, and determining cell death or survival [467]. Perhaps most intriguing is the ability of surface microstructures to guide differentiation of stem cells [468–470] and hence to influence the formation of tissue, organs and - eventually - organisms.

Functional surface microstructures - *quo vaditis?* Obviously, inspiration by natural examples is far from being complete. Not only are we at a loss to match the clinging ability of real geckos to any surface with arbitrary roughness; but also our fabrication methods appear inefficient in comparison to genetically controlled natural growth of fibrils, bristles, and protrusions on plant and animal surfaces. Bioinspiration with regard to multi-scale synthesis could propel micropatterns into everyday use. Moreover, biological systems move, interact, heal by themselves or replace severed body parts. Here, artificial systems, which are so far mostly passive, still have a vast innovation space ahead of them, despite notable developments in various laboratories. Imagine actuated surface patterns that modify the wetting behavior on demand and simplify the cleaning of hygienic and medical surfaces. Or reliable stimuli-responsive materials that imitate muscular action in conjunction with gecko adhesion in innovative robotics concepts. And finally, nature teaches us how to replace worn gecko structures or suction cups in an elegant way - by shedding of the skin to expose pristine nanofibrillar

structures ready for engagement with its environment. The fascinating “art of leaving gaps” in modern materials and surfaces will very likely continue to occupy the imagination of generations to come.

Declaration of Competing Interest

Eduard Arzt is co-owner of a company commercializing new materials in this fields. This has not influenced the writing of this review paper.

Acknowledgments

Over many years, the authors have profited from numerous fruitful discussions and collaboration with colleagues all over the world. In particular, we acknowledge the input from, *inter alia*, A. Crosby (Amherst), J. Booth (Los Angeles), W. Federle (Cambridge), N. Fleck (Cambridge), H. Gao (Singapore), A. Ghatak (Kanpur), J. Israelachvili (Santa Barbara), A. Jagota (Lehigh), M. Meyers (San Diego), T. Saif (Urbana-Champaign), G. Wenzel and B. Schick (Saarland University Clinic). Enjoyable interaction is gratefully acknowledged, among others, with numerous former group members and the INM colleagues L. Barnefske, R. Bennewitz, G. Heppe, T. Kraus, K. Kruttwig, G. Moreira Lana, K. Moh, Y. Wang, and X. Zhang. The technical assistance by J. Blau, J. Dollmann, S. Selzer, L. Sold, A. Weyand over the years is appreciated.

EA acknowledges funding from the European Research Council (ERC) under the European Union’s Seventh Framework Program (FP/2007-2013)/ERC Advanced Grant Agreement No. 340929 and two subsequent ERC Proof-of-Concept Grants under the European Union’s Horizon 2020 research and innovation programme (Grant Agreement No. 842613 and Grant Agreement No. 790559). The Leibniz Association has provided funding, also within its competitive program through project MUSIGAND. RMM acknowledges funding from INM as Leibniz Chair holder and from the Humboldt Foundation as the recipient of a Humboldt Alumni Network grant.

Appendix A. Overview of micropatterning techniques

To create surface functionalities, surface patterning is key to design and realization. Such patterns typically consist of an array of fibrillar elements with sizes ranging from nano to millimeter scale (Fig. 1.2). The shape and arrangement of the elements can vary from regular to irregular and from two (2D) to three-dimensional (3D), which poses challenges for their fabrication. Recent advances in 3D patterning techniques enable customized hierarchical designs and their optimization for specific applications. Surface patterning methods can be classified into replication, lithography, micromachining and self-assembly techniques, as summarized in Table A.1.

The choice of technique will depend on the objective at hand: Model and feasibility experiments may only require micropatterns over small areas but with well-defined features and 3D contact geometries. For that, the preferred methods are optical and electron lithography, two-photon lithography as well as various micromachining and self-assembly techniques. For demonstration of practical viability and cost effectiveness, readily scalable processes need to be developed, where roll-to-roll, injection molding, interference lithography, and embossing are preferred. In this section, we briefly summarize the latest developments in these techniques and their potential for creating micropatterned surfaces.

A.1. Replication

Replicating micropatterned surfaces is attractive for biomimetic research, as it offers great variability of designs and materials that can be processed in combination with typically low cost. Examples are manifold ranging from direct replication of natural surfaces [49,471] to artificial designs with specific wetting, adhesion, or optical characteristics. Most replication techniques are not limited to 2D designs, but allow replicating 3D and even more complex hierarchical patterns. Examples include multi-patterned molds [472],

Table A.1
Classification of surface patterning techniques.

Replication	Micromachining
<ul style="list-style-type: none"> • Nanoimprint lithography • Embossing • Micro injection molding • Casting • Roll-to-roll processing 	<ul style="list-style-type: none"> • Mechanical (milling, drilling, cutting, ...) • Electrothermal (electric discharge, laser, ...) • Electrochemical (milling, drilling, plating, ...) • Abrasion and ablation
<p>Lithography</p> <ul style="list-style-type: none"> • Photo & EUV lithography • Laser & Electron beam lithography • Interference lithography • Two-photon lithography • Selective laser etching • LIGA 	<p>Self-assembly</p> <ul style="list-style-type: none"> • Colloidal lithography • Block copolymer lithography • Capillarity-assisted patterning • Dielectrophoresis • Field or temperature-induced instabilities • Self-folding or rolling • Epitaxial growth

multi-step imprints [473], sacrificial molds [474], or reverse imprint lithography [56]. Even three-dimensional microstructures with closed loops can be replicated by adding a supporting structure to the mold design [475]. To overcome mechanical interlocking of microstructures and the mold, one of them has to be deformable during demolding [296].

The main concept is to replicate surface patterns in the mold into the desired polymer. Techniques include casting, injection molding, forming, embossing and nanoimprint lithography; they are chosen in relation to target material, resolution, and throughput [476–478]. Thermoplastics can be patterned by hot embossing or thermal nanoimprint lithography, where the polymer is heated above its glass transition temperature to enable mechanical transfer of the mold into the polymer before it is cooled down. Liquid precursors of pre-polymers, elastomers, or thermosets are filled into molds where they are cured via UV exposure or thermal cross-linking reactions, known as casting or UV-nanoimprint lithography.

Although a high resolution of 5 nm was demonstrated [478], replication techniques face several challenges, which often limit defect-free, large-scale fabrication [479]. For example, patterns with large height to width aspect ratios require complete filling of the mold cavities, which must take process-dependent viscosity and wetting characteristics of the pre-polymer into account [480]. Residual layers between microstructural features have to be reduced by optimizing the pattern design and density to homogenize the interfacial compressive stress distribution between the mold and the pre-polymer [481]. Techniques for large-scale fabrication comprise step-and-repeat machines [478], roll-to-roll fabrication [296,379], and injection molding processes [476,482].

A.2. Optical and electron lithography

Lithography is the technique of producing patterns by adding or removing material in a writing or a mask-assisted process [483]. The design is realized by irradiating a radiation-sensitive material with light or electrons. Developed for semiconductor devices and integrated circuits, lithography is the most important top-down technique combining high resolution and high throughput. Progress has been driven mainly in the direction of increasing resolution, driven by miniaturization following Moore's law [484]. For bio-inspired micropatterns, resolution is at present not the main driver and therefore optical lithography, with nanometer resolution, is frequently suitable. Lithography enables patterning of multiple layers, and thus complex structures such as micro-electro-mechanical systems (MEMS), but is limited to planar substrates. In terms of surface microstructures, optical lithography has been extensively used to create artificial surfaces with defined dimensions [485]. Current state of the art photolithography utilizes 193 nm ArF light sources in combination with high-aperture, immersion lens systems to achieve a half-pitch resolution of 37 nm and, in advanced schemes, 19 nm [486]. Extreme ultraviolet (EUV) lithography can access the sub-10 nm regime [487], but remains the preserve of the semiconductor industry because of high cost and demanding technical requirements [488,489].

For research purposes, electron beam and laser lithography are alternative maskless techniques that offer much flexibility in generating two-dimensional, high-resolution surface patterns. Grayscale electron beam lithography in combination with polymer reflow of the patterned resist is a promising approach to enhance the complexity of structures and hierarchical patterns [490]. For large scale fabrication and high throughput, interference lithography has been established [491]. Here, the interference pattern of two or more coherent electromagnetic waves exposes the polymer resist and creates densely patterned arrays over large areas without the need for masks. Multiple exposures, or combination with pre-patterned substrates, offer opportunities for hierarchical patterns that mimic natural surfaces [232].

Three-dimensional capabilities have proven essential for the fabrication of bioinspired surface microstructures. Such surface patterns can be created with sub-micron resolution via two-photon lithography [492], selective laser-induced etching of fused silica or sapphire substrates [493], and focused ion beam chemical vapor deposition [494]. The latter is less suitable for patterning large areas, but offers a suitable technique for prototyping with a resolution below 100 nm [495]. Two-photon lithography exploits two- (or multiple-) photon absorption processes stimulated by pulsed laser beams that interact with a polymer resist. The focal point concentrates the probability of such multi-absorption events and initiates polymerization only locally [496,497]. The polymerization reaction is often terminated by oxygen quenching of radicals, which defines the size of the voxel, i.e. the smallest polymerization volume [498]. The lateral voxel size then depends on the diffraction limit of the optical system, the resist, and the applied laser power [499]. Interestingly, lower laser powers offer higher resolution down to 120 nm, but may require post-curing due to the mechanical fragility as a result of incomplete polymerization [500,501]. Selective laser-induced etching is a related technique: the non-linear absorption of the pulsed laser beam leads to local heating of fused silica, which in turn reduces the wet etch resistance. The ratio of the modified to the non-modified material etching rates can reach three orders of magnitude, which enables precise manufacturing of features with high aspect ratios and resolution down to 1 μm [502,503].

A.3. Micromachining

Micro or ultra-precision machining are non-MEMS technologies that have experienced large growth over the last 20 years [504]. The main advantage over lithography is that numerous materials of all materials classes can be processed. In particular, the electronics industry is driving new developments in the highly efficient machining of miniaturized components with tight tolerances, such as sensors, actuators, motors, valves and gears with applications in the automotive and aerospace industries [505].

While micromachining is mainly employed for the production of electrical components, these technologies can be easily implemented for the creation of surface patterns or for the development of tools and molds for forming and replication processes. As an example, ablation by ultra-short pulsed lasers has been established over the last few years for creating biomimetic surfaces; metallic, semiconductor and insulator surfaces can be patterned with similar quality [506]. For mechanical micromachining, considerable efforts have been made to improve the precision of machine tools by compensating for phenomena such as thermal distortion, tool

wear, kinematic error, machine-related error, etc. [507,508]. The resolution of micromechanical machining such as milling or drilling is around tens of micrometers, and is determined by the size of the toolings. Despite the poorer resolution in comparison to lithography and wet etching, these methods represent a cost-effective alternative for creating complex-shaped prototypes [509]. This tendency is reflected in a significant increase in published reports in this area [510].

A.4. Self-assembly

All functional surfaces in nature are the result of self-assembled organic matter. Such a bottom-up approach, in which building blocks organize themselves into microstructures, contrasts with the top-down methods discussed above. Typical building blocks for artificial surface patterns are DNA molecules [511], block copolymer chains [512], and colloidal particles [513]. The transfer of such self-assembled patterns onto the underlying substrate is, e.g., referred to as block copolymer lithography [514] or colloidal lithography [515,516]. Their resolution typically correlates with the size of building blocks.

To assemble building blocks into well-defined patterns, their physical properties, concentration and dispersity, and decoration with functional entities have to be considered, as these parameters control the self-assembly process in an unequilibrated energy landscape [517]. The mobility and kinetic energy of the building blocks originate mainly from random Brownian motion, which reduces with increasing size. For larger microscopic particles, convective flow [518], capillary forces [519], electric- or dielectrophoresis [520], etc. can induce or enhance mobility and direct motion. Successful assembly requires attractive interactions, and the binding energy has to exceed the kinetic energy of the building block. Rearrangement takes place when reversible bindings dissociate and re-associate, which can result in ordered crystalline microstructures. Self-assembled monolayers are an example. In contrast, diffusion-limited processes, in which the particles are slow and stick to the sites where they are first bound, lead to random dendritic microstructures [521]. Overall, prediction of self-assembly processes requires consideration of the energy landscape of the system and of the pathways to local minima, including particle concentrations, diffusion constants, chemical potentials, reaction kinetics, etc. Strategies to direct and guide self-assembly processes are based on templates with attractive sites [517] or confined reactors such as droplets [522] and fluid interfaces [523].

In conclusion, a vast arsenal of micropatterning methods has become available. The method chosen for a particular task will depend on the targeted design, the required resolution and the production rate. In addition, many sophisticated methods are available that can be used to tune functionalities. Micropatterning has become a creative way of abstracting design principles from nature, by emulating, re-building and testing of bioinspired concepts; this has led to an enhanced understanding of complex biological mechanisms.

References

- [1] Mittemeijer EJ. *Fundamentals of Materials Science*, vol. 11. Springer; 2011.
- [2] Arzt E. Size effects in materials due to microstructural and dimensional constraints: a comparative review. *Acta Mater* 1998;46:5611–26.
- [3] Gao H, Ji B, Jager IL, Arzt E, Fratzl P. Materials become insensitive to flaws at nanoscale: lessons from nature. *Proc Natl Acad Sci U S A* 2003;100:5597–600.
- [4] Sun J, Bhushan B, Tong J. Structural coloration in nature. *RSC Adv* 2013;3:14862–89.
- [5] Jacucci G, Schertel L, Zhang Y, Yang H, Vignolini S. Light management with natural materials. *Adv Mater* 2020;2001215.
- [6] Ashby M, Johnson K. *Materials and Design: The Art and Science of Material Selection in Product Design*, vol. 2. Butterworth-Heinemann; 2010.
- [7] Fratzl P, Weinkamer R. Nature's hierarchical materials. *Prog Mater Sci* 2007;52:1263–334.
- [8] Nachtigall W. *Vorbild Natur*. Springer; 1997.
- [9] Lee J-Y, Pechook S, Jeon D-J, Pokroy B, Yeo J-S. Three-dimensional triple hierarchy formed by self-assembly of wax crystals on CuO nanowires for nonwettability surfaces. *ACS Appl Mater Interfaces* 2014;6:4927–34.
- [10] Hensel R, Finn A, Helbig R, Killge S, Braun H-G, Werner C. In situ experiments to reveal the role of surface feature sidewalls in the Cassie-Wenzel transition. *Langmuir* 2014;30:15162–70.
- [11] Sethi S, Ge L, Ci L, Ajayan PM, Dhinojwala A. Gecko-inspired carbon nanotube-based self-cleaning adhesives. *Nano Lett* 2008;8:822–5.
- [12] Chu Z, Wang C, Hai X, Deng J, Cui J, Sun L. Analysis and measurement of adhesive behavior for gecko-inspired synthetic microwedge Structure. *Adv Mater Interfaces* 2019;6:100283.
- [13] Sameoto D, Menon C. Deep UV patterning of acrylic masters for molding biomimetic dry adhesives. *J Micromech Microeng* 2010;20:115037.
- [14] Luo Y, Shao J, Chen S, Chen X, Tian H, Li X, et al. Flexible capacitive pressure sensor enhanced by tilted micropillar arrays. *ACS Appl Mater Interfaces* 2019;11:17796–803.
- [15] Pokroy B, Kang SH, Mahadevan L, Aizenberg J. Self-organization of a mesoscale bristle into ordered, hierarchical helical assemblies. *Science* 2009;323:237–40.
- [16] Hensel R, Moh K, Arzt E. Engineering micropatterned dry adhesives: From contact theory to handling applications. *Adv Funct Mater* 2018;28:1800865. <https://doi.org/10.1002/adfm.201800865>.
- [17] Gorb SN. *Functional Surfaces in Biology: Little Structures with Big Effects*. Springer Science & Business Media; 2009.
- [18] Meyers MA, Chen P-Y. *Biological Materials Science*. Cambridge University Press; 2014.
- [19] Bhushan B. *Biomimetics: Bioinspired Hierarchical-Structured Surfaces for Green Science and Technology*. Springer; 2016.
- [20] Bhushan B. *Biomimetics*. Springer; 2012.
- [21] del Campo A, Arzt E. Fabrication approaches for generating complex micro- and nanopatterns on polymeric surfaces. *Chem Rev* 2008;108:911–45.
- [22] Ghasemlou M, Daver F, Ivanova EP, Adhikari B. Bio-inspired sustainable and durable superhydrophobic materials: from nature to market. *J Mater Chem A Mater Energy Sustain* 2019;7:16643–70.
- [23] Li S, Huang J, Chen Z, Chen G, Lai Y. A review on special wettability textiles: theoretical models, fabrication technologies and multifunctional applications. *J Mater Chem A Mater Energy Sustain* 2017;5:31–55.
- [24] Zhang M, Feng S, Wang L, Zheng Y. Lotus effect in wetting and self-cleaning. *Biotribology* 2016;5:31–43.
- [25] Wong T-S, Kang SH, Tang SKY, Smythe EJ, Hatton BD, Grinthal A, et al. Bioinspired self-repairing slippery surfaces with pressure-stable omniphobicity. *Nature* 2011;477:443–7.
- [26] Bormashenko E. Physics of pre-wetted, lubricated and impregnated surfaces: a review. *Philos Trans A Math Phys Eng Sci* 2019;377:20180264.
- [27] Chen Z, Zhang Z. Recent progress in beetle-inspired superhydrophilic-superhydrophobic micropatterned water-collection materials. *Water Sci Technol* 2020; 82:207–26.

- [28] Wang Q, Yu M, Chen G, Chen Q, Tai J. Facile fabrication of superhydrophobic/superoleophilic cotton for highly efficient oil/water separation. *BioResources* 2016;12.
- [29] Tian D, Zhang X, Tian Y, Wu Y, Wang X, Zhai J, et al. Photo-induced water–oil separation based on switchable superhydrophobicity–superhydrophilicity and underwater superoleophobicity of the aligned ZnO nanorod array-coated mesh films. *J Mater Chem* 2012;22:19652.
- [30] Guan Y, Cheng F, Pan Z. Superwetting polymeric three dimensional (3D) porous materials for oil/water separation: a review. *Polymers* 2019;11:806.
- [31] Latthe SS, Sutar RS, Bhosale AK, Nagappan S, Ha C-S, Sadasivuni KK, et al. Recent developments in air-trapped superhydrophobic and liquid-infused slippery surfaces for anti-icing application. *Prog Org Coat* 2019;137:105373.
- [32] Zhang Y, Klittich MR, Gao M, Dhinojwala A. Delaying frost formation by controlling surface chemistry of carbon nanotube-coated steel surfaces. *ACS Appl Mater Interfaces* 2017;9:6512–9.
- [33] Alizadeh A, Yamada M, Li R, Shang W, Otta S, Zhong S, et al. Dynamics of ice nucleation on water repellent surfaces. *Langmuir* 2012;28:3180–6.
- [34] Mishchenko L, Hatton B, Bahadur V, Taylor JA, Krupenkin T, Aizenberg J. Design of ice-free nanostructured surfaces based on repulsion of impacting water droplets. *ACS Nano* 2010;4:7699–707.
- [35] Bahadur V, Mishchenko L, Hatton B, Taylor JA, Aizenberg J, Krupenkin T. Predictive model for ice formation on superhydrophobic surfaces. *Langmuir* 2011;27:14143–50.
- [36] Kreder MJ, Alvarenga J, Kim P, Aizenberg J. Design of anti-icing surfaces: smooth, textured or slippery? *Nat Rev Mater* 2016;1. <https://doi.org/10.1038/natrevmats.2015.3>.
- [37] Barthlott W, Mail M, Neinhuis C. Superhydrophobic hierarchically structured surfaces in biology: evolution, structural principles and biomimetic applications. *Philos Trans A Math Phys. Eng Sci* 2016;374. <https://doi.org/10.1098/rsta.2016.0191>.
- [38] Mlot NJ, Tovey CA, Hu DL. Fire ants self-assemble into waterproof rafts to survive floods. *Proc Natl Acad Sci U S A* 2011;108:7669–73.
- [39] Marx MT, Messner B. A general definition of the term “plastron” in terrestrial and aquatic arthropods. *Org Divers Evol* 2012;12:403–8.
- [40] Flynn MR, Bush JWM. Underwater breathing: the mechanics of plastron respiration. *J Fluid Mech* 2008;608:275–96.
- [41] Brewer CA, Smith WK, Vogelmann TC. Functional interaction between leaf trichomes, leaf wettability and the optical properties of water droplets. *Plant, Cell Environ* 1991;14:955–62.
- [42] Hu DL, Chan B, Bush JWM. The hydrodynamics of water strider locomotion. *Nature* 2003;424:663–6.
- [43] Wei PJ, Shen YX, Lin JF. Characteristics of water strider legs in hydrodynamic situations. *Langmuir* 2009;25:7006–9.
- [44] Prakash M, Bush JWM. Interfacial propulsion by directional adhesion. *Int J Non Linear Mech* 2011;46:607–15.
- [45] Barthlott W, Neinhuis C. Purity of the sacred lotus, or escape from contamination in biological surfaces. *Planta* 1997;202:1–8.
- [46] Koch K, Barthlott W. Plant epicuticular waxes: chemistry, form, self-assembly and function. *Nat Prod Commun* 2006;1. 1934578X0600101.
- [47] Tuteja A, Choi W, Ma M, Mabry JM, Mazzella SA, Rutledge GC, et al. Designing superoleophobic surfaces. *Science* 2007;318:1618–22.
- [48] Helbig R, Nickler J, Neinhuis C, Werner C. Smart skin patterns protect springtails. *PLoS ONE* 2011;6:e25105.
- [49] Hensel R, Helbig R, Aland S, Voigt A, Neinhuis C, Werner C. Tunable nano-replication to explore the omniphobic characteristics of springtail skin. *NPG Asia Mater* 2013;5:e37. <https://doi.org/10.1038/am.2012.66>.
- [50] Nickler J, Tsurkan M, Hensel R, Neinhuis C, Werner C. The multi-layered protective cuticle of Collembola: a chemical analysis. *J R Soc Interface* 2014;11. <https://doi.org/10.1098/rsif.2014.0619>.
- [51] Richards C, Slaimi A, O'Connor NE, Barrett A, Kwiatkowska S, Regan F. Bio-inspired surface texture modification as a viable feature of future aquatic antifouling strategies: a review. *Int J Mol Sci* 2020;21. <https://doi.org/10.3390/ijms21145063>.
- [52] Feng DQ, Wang W, Wang X, Qiu Y, Ke CH. Low barnacle fouling on leaves of the mangrove plant *Sonneratia apetala* and possible anti-barnacle defense strategies. *Mar Ecol Prog Ser* 2016;544:169–82.
- [53] Ivanova EP, Hasan J, Webb HK, Truong VK, Watson GS, Watson JA, et al. Natural bactericidal surfaces: mechanical rupture of *Pseudomonas aeruginosa* cells by cicada wings. *Small* 2012;8:2489–94.
- [54] Barthlott W, Mail M, Bhushan B, Koch K. Plant surfaces: structures and functions for biomimetic innovations. *Nanomicro Lett* 2017;9:23.
- [55] Firlstner R, Barthlott W, Neinhuis C, Walzel P. Wetting and self-cleaning properties of artificial superhydrophobic surfaces. *Langmuir* 2005;21:956–61.
- [56] Hensel R, Finn A, Helbig R, Braun H-G, Neinhuis C, Fischer W-J, et al. Biologically inspired omniphobic surfaces by reverse imprint lithography. *Adv Mater* 2014;26:2029–33.
- [57] Hasan J, Crawford RJ, Ivanova EP. Antibacterial surfaces: the quest for a new generation of biomaterials. *Trends Biotechnol* 2013;31:295–304.
- [58] Hizal F, Rungraeng N, Lee J, Jun S, Busscher HJ, van der Mei HC, et al. Nanoengineered superhydrophobic surfaces of aluminum with extremely low bacterial adhesivity. *ACS Appl Mater Interfaces* 2017;9:12118–29.
- [59] Widyaratih DS, Hagedoorn P-L, Otten LG, Ganjian M, Tümer N, Apachitei I, et al. Towards osteogenic and bactericidal nanopatterns? *Nanotechnology* 2019;30:20LT01.
- [60] Starov VM, Velarde MG. *Wetting and Spreading Dynamics*. 2nd ed. CRC Press; 2019.
- [61] Pericet-Cámara R, Best A, Butt H-J, Bonaccorso E. Effect of capillary pressure and surface tension on the deformation of elastic surfaces by sessile liquid microdrops: an experimental investigation. *Langmuir* 2008;24:10565–8.
- [62] Park SJ, Weon BM, Lee JS, Lee J, Kim J, Je JH. Visualization of asymmetric wetting ridges on soft solids with X-ray microscopy. *Nat Commun* 2014;5:4369.
- [63] Bon D, Eggers J, Indekeu J, Meunier J, Rolley E. Wetting and spreading. *Rev Mod Phys* 2009;81:739–805.
- [64] Quéré D. Wetting and roughness. *Annual Rev Mater Res* 2008;38:71–99.
- [65] Derjaguin BV, Churaev NV, Muller VM. *Surface Forces*. New York: Springer Science+Business; 1987.
- [66] Brütin D, Starov V. Recent advances in droplet wetting and evaporation. *Chem Soc Rev* 2018;47:558–85.
- [67] Korhonen JT, Huhtamäki T, Ikkala O, Ras RHA. Reliable measurement of the receding contact angle. *Langmuir* 2013;29:3858–63.
- [68] Chen L, Bonaccorso E, Gambaryan-Roisman T, Starov V, Koursari N, Zhao Y. Static and dynamic wetting of soft substrates. *Curr Opin Colloid Interface Sci* 2018;36:46–57.
- [69] Ahmed G, Koursari N, Trybala A, Starov VM. Sessile droplets on deformable substrates. *Colloids and Interfaces* 2018;2:56.
- [70] Hui C-Y, Jagota A. Deformation near a liquid contact line on an elastic substrate. *Proc Roy Soc A: Math Phys Eng Sci* 2014;470:20140085.
- [71] Shuttleworth R. The surface tension of solids. *Proc Phys Soc London, Sect A* 1950;63:444–57.
- [72] Andreotti B, Snoeijer JH. Soft wetting and the Shuttleworth effect, at the crossroads between thermodynamics and mechanics. *EPL (Europhys Lett)* 2016;113:66001.
- [73] Das S, Marchand A, Andreotti B, Snoeijer JH. Elastic deformation due to tangential capillary forces. *Phys Fluids* 2011;23:072006.
- [74] Marchand A, Das S, Snoeijer JH, Andreotti B. Capillary pressure and contact line force on a soft solid. *Phys Rev Lett* 2012;108. <https://doi.org/10.1103/physrevlett.108.094301>.
- [75] Sokuler M, Auernhammer GK, Roth M, Liu C, Bonaccorso E, Butt H-J. The softer the better: fast condensation on soft surfaces. *Langmuir* 2010;26:1544–7.
- [76] Lopes MC, Bonaccorso E. Evaporation control of sessile water drops by soft viscoelastic surfaces. *Soft Matter* 2012;8:7875.
- [77] Petit J, Bonaccorso E. General frost growth mechanism on solid substrates with different stiffness. *Langmuir* 2014;30:1160–8.
- [78] Quéré D. Rough ideas on wetting. *Physica A* 2002;313:32–46.
- [79] Wenzel RN. Resistance of solid surfaces to wetting by water. *Ind Eng Chem* 1936;28:988–94.
- [80] Cassie ABD, Baxter S. Wettability of porous surfaces. *Trans Faraday Soc* 1944;40:546.
- [81] Lafuma A, Quéré D. Superhydrophobic states. *Nat Mater* 2003;2:457–60.
- [82] Herminghaus S. Roughness-induced non-wetting. *Europhys Lett (EPL)* 2000;52:165–70.
- [83] Singh N, Kakiuchida H, Sato T, Hönes R, Yagihashi M, Urata C, et al. Omniphobic metal surfaces with low contact angle hysteresis and tilt Angles. *Langmuir* 2018;34:11405–13.
- [84] Darmanin T, Guitard F. Wettability of conducting polymers: From superhydrophilicity to superoleophobicity. *Prog Polym Sci* 2014;39:656–82.

- [85] Yun G-T, Jung W-B, Oh MS, Jang GM, Baek J, Kim NI, et al. Springtail-inspired superomniphobic surface with extreme pressure resistance. *Sci Adv* 2018;4: eaat4978.
- [86] Cai R, De Smet D, Vanneste M, Nysten B, Glinel K, Jonas AM. One-step aqueous spraying process for the fabrication of omniphobic fabrics free of long perfluoroalkyl chains. *ACS Omega* 2019;4:16660–6.
- [87] Kota AK, Kwon G, Tuteja A. The design and applications of superomniphobic surfaces. *NPG Asia Mater* 2014;6:e109.
- [88] Hensel R, Neinhuis C, Werner C. The springtail cuticle as a blueprint for omniphobic surfaces. *Chem Soc Rev* 2016;45:323–41.
- [89] Callies M, Quéré D. On water repellency. *Soft Matter* 2005;1:55.
- [90] Hensel R, Helbig R, Aland S, Braun H-G, Voigt A, Neinhuis C, et al. Wetting resistance at its topographical limit: the benefit of mushroom and Serif T structures. *Langmuir* 2013;29:1100–12.
- [91] Liu T, Kim C-J. Turning a surface superrepellent even to completely wetting liquids. *Science* 2014;346:1096–100.
- [92] Verho T, Korhonen JT, Sainiemi L, Jokinen V, Bower C, Franze K, et al. Reversible switching between superhydrophobic states on a hierarchically structured surface. *Proc Natl Acad Sci* 2012;109:10210–3.
- [93] Rofman B, Dehe S, Frumkin V, Hardt S, Bercovici M. Intermediate states of wetting on hierarchical superhydrophobic surfaces. *Langmuir* 2020;36:5517–23.
- [94] Xue Y, Lv P, Lin H, Duan H. Underwater superhydrophobicity: stability, design and regulation, and applications. *Appl Mech Rev* 2016;68:1857.
- [95] Meloni S, Giacometto A, Casciola CM. Focus Article: Theoretical aspects of vapor/gas nucleation at structured surfaces. *J Chem Phys* 2016;145:211802.
- [96] Simovich T, Ritchie C, Belev G, Cooper DML, Lamb RN. Superhydrophobicity from the inside. *Langmuir* 2017;33:13990–5.
- [97] Xiang Y, Huang S, Huang T-Y, Dong A, Cao D, Li H, et al. Superrepellency of underwater hierarchical structures on leaf. *Proc Natl Acad Sci U S A* 2020;117: 2282–7.
- [98] Tobaldi DM, Graziani L, Seabra MP, Henriet L, Ferreira P, Quagliarini E, et al. Functionalised exposed building materials: Self-cleaning, photocatalytic and biofouling abilities. *Ceram Int* 2017;43:10316–25. <https://doi.org/10.1016/j.ceramint.2017.05.061>.
- [99] Mills A, Lepre A, Elliott N, Bhopal S, Parkin IP, O'Neill SA. Characterisation of the photocatalyst Pilkington Activ™: a reference film photocatalyst? *J Photochem Photobiol, A* 2003;160:213–24. [https://doi.org/10.1016/s1010-6030\(03\)00205-3](https://doi.org/10.1016/s1010-6030(03)00205-3).
- [100] Furnidge CGL. Studies at phase interfaces. I. The sliding of liquid drops on solid surfaces and a theory for spray retention. *J Colloid Sci* 1962;17:309–24.
- [101] Schellenberger F, Encinas N, Vollmer D, Butt H-J. How water advances on superhydrophobic surfaces. *Phys Rev Lett* 2016;116. <https://doi.org/10.1103/physrevlett.116.096101>.
- [102] Mahadevan L, Pomeau Y. Rolling droplets. *Phys Fluids* 1999;11:2449–53.
- [103] Richard D, Quéré D. Viscous drops rolling on a tilted non-wettable solid. *Europhys Lett (EPL)* 1999;48:286–91.
- [104] Hao P, Lv C, Yao Z, He F. Sliding behavior of water droplet on superhydrophobic surface. *EPL (Europhys Lett)* 2010;90:66003.
- [105] Aussillous P, Quéré D. Liquid marbles. *Nature* 2001;411:924–7.
- [106] Abolghasemibizaki M, Robertson CJ, Fergusson CP, McMasters RL, Mohammadi R. Rolling viscous drops on a non-wettable surface containing both micro- and macro-scale roughness. *Phys Fluids* 2018;30:023105.
- [107] Olin P, Lindström SB, Pettersson T, Wågberg L. Water drop friction on superhydrophobic surfaces. *Langmuir* 2013;29:9079–89.
- [108] Butt H-J, Gao N, Papadopoulos P, Steffen W, Kappl M, Berger R. Energy dissipation of moving drops on superhydrophobic and superoleophobic surfaces. *Langmuir* 2017;33:107–16.
- [109] Anachkov SE, Lesov I, Zanini M, Kralchevsky PA, Denkov ND, Isa L. Particle detachment from fluid interfaces: theory vs. experiments. *Soft Matter* 2016;12: 7632–43.
- [110] Mognetti BM, Yeomans JM. Modeling receding contact lines on superhydrophobic surfaces. *Langmuir* 2010;26:18162–8.
- [111] McHale G. Cassie and Wenzel: were they really so wrong? *Langmuir* 2007;23:8200–5.
- [112] Nosonovsky M. On the range of applicability of the Wenzel and Cassie equations. *Langmuir* 2007;23:9919–20.
- [113] Erbil HY. The debate on the dependence of apparent contact angles on drop contact area or three-phase contact line: A review. *Surf Sci Rep* 2014;69:325–65.
- [114] Gao N, Geyer F, Pilat DW, Wooh S, Vollmer D, Butt H-J, et al. How drops start sliding over solid surfaces. *Nat Phys* 2018;14:191–6.
- [115] Tang Y, Cheng S. Capillary forces on a small particle at a liquid-vapor interface: Theory and simulation. *Phys Rev E* 2018;98:517.
- [116] Israelachvili JN. *Intermolecular and Surface Forces*. Academic Press; 2011.
- [117] Geyer F, D'Acunzi M, Sharifi-Aghili A, Saal A, Gao N, Kaltbeitzel A, et al. When and how self-cleaning of superhydrophobic surfaces works. *Sci Adv* 2020;6: eaaw9727.
- [118] Wong WSY, Corrales TP, Naga A, Baumli P, Kaltbeitzel A, Kappl M, et al. Microdroplet contaminants: when and why superamphiphobic surfaces are not self-cleaning. *ACS Nano* 2020;14:3836–46.
- [119] Vuillers F, Peppou-Chapman S, Kavalenka MN, Hölscher H, Neto C. Effect of repeated immersions and contamination on plastron stability in superhydrophobic surfaces. *Phys Fluids* 2019;31:012102.
- [120] Chan J. Biofouling WS. Types, Impact, and Anti-fouling. Nova Science Pub Incorporated; 2010.
- [121] Mail M, Moosmann M, Häger P, Barthlott W. Air retaining grids—a novel technology to maintain stable air layers under water for drag reduction. *Philos Trans A Math Phys Eng Sci* 2019;377:20190126.
- [122] Renner LD, Weibel DB. Physicochemical regulation of biofilm formation. *MRS Bull* 2011;36:347–55.
- [123] Leslie DC, Waterhouse A, Berthet JB, Valentin TM, Watters AL, Jain A, et al. A bioinspired omniphobic surface coating on medical devices prevents thrombosis and biofouling. *Nat Biotechnol* 2014;32:1134–40.
- [124] Stoodley P, Sauer K, Davies DG, Costerton JW. Biofilms as complex differentiated communities. *Annu Rev Microbiol* 2002;56:187–209.
- [125] Chelmoswki R, Köster SD, Kerstan A, Prekelt A, Grunwald C, Winkler T, et al. Peptide-based SAMs that resist the adsorption of proteins. *J Am Chem Soc* 2008; 130:14952–3.
- [126] Leng C, Buss HG, Segalman RA, Chen Z. Surface structure and hydration of sequence-specific amphiphilic polypeptides for antifouling/fouling release applications. *Langmuir* 2015;31:9306–11.
- [127] Chen S, Li L, Zhao C, Zheng J. Surface hydration: Principles and applications toward low-fouling/nonfouling biomaterials. *Polymer* 2010;51:5283–93.
- [128] Cao Z, Jiang S. Super-hydrophilic zwitterionic poly(carboxybetaine) and amphiphilic non-ionic poly(ethylene glycol) for stealth nanoparticles. *Nano Today* 2012;7:404–13.
- [129] Wang W, Lu Y, Xie J, Zhu H, Cao Z. A zwitterionic macro-crosslinker for durable non-fouling coatings. *Chem Commun* 2016;52:4671–4.
- [130] Wei Q, Becherer T, Angioletti-Uberti S, Dzubiella J, Wischke C, Neffe AT, et al. Protein interactions with polymer coatings and biomaterials. *Angew Chem Int Ed Engl* 2014;53:8004–31.
- [131] Hannig C, Helbig R, Hilsenbeck J, Werner C, Hannig M. Impact of the springtail's cuticle nanotopography on bioadhesion and biofilm formation and in the oral cavity. *R Soc Open Sci* 2018;5:171742.
- [132] Zhao J, Song L, Yin J, Ming W. Anti-bioadhesion on hierarchically structured, superhydrophobic surfaces. *Chem Commun* 2013;49:9191–3.
- [133] Tuson HH, Weibel DB. Bacteria–surface interactions. *Soft Matter* 2013;9:4368.
- [134] Berne C, Ellison CK, Ducret A, Brun YV. Bacterial adhesion at the single-cell level. *Nat Rev Microbiol* 2018;16:616–27.
- [135] Kimkes TEP, Heinemann M. How bacteria recognise and respond to surface contact. *FEMS Microbiol Rev* 2020;44:106–22.
- [136] Dufrene YF, Persat A. Mechanomicrobiology: how bacteria sense and respond to forces. *Nat Rev Microbiol* 2020;18:227–40.
- [137] Wang Z, Scheres L, Xia H, Zuilhof H. Developments and challenges in self-healing antifouling materials. *Adv Funct Mater* 2020;30:1908098.
- [138] Damodaran VB, Sanjeeva MN. Bio-inspired strategies for designing antifouling biomaterials. *Biomater Res* 2016;20. <https://doi.org/10.1186/s40824-016-0064-4>.
- [139] Francolini I, Vuotto C, Piozzi A, Donelli G. Antifouling and antimicrobial biomaterials: an overview. *APMIS* 2017;125:392–417.
- [140] Helbig R, Günther D, Friedrichs J, Rößler F, Lasagni A, Werner C. The impact of structure dimensions on initial bacterial adhesion. *Biomater Sci* 2016;4: 1074–8.

- [141] Encinas N, Yang C-Y, Geyer F, Kaltbeitzel A, Baumli P, Reinholz J, et al. Submicrometer-sized roughness suppresses bacteria adhesion. *ACS Appl Mater Interfaces* 2020;12:21192–200.
- [142] Valle J, Burgui S, Langheinrich D, Gil C, Solano C, Toledo-Arana A, et al. Evaluation of surface microtopography engineered by direct laser interference for bacterial anti-biofouling. *Macromol Biosci* 2015;15:1060–9.
- [143] Hochbaum AI, Aizenberg J. Bacteria pattern spontaneously on periodic nanostructure arrays. *Nano Lett* 2010;10:3717–21.
- [144] Callow ME, Jennings AR, Brennan AB, Seeger CE, Gibson A, Wilson L, et al. Microtopographic cues for settlement of zoospores of the green fouling alga *Enteromorpha*. *Biofouling* 2002;18:229–36.
- [145] Scardino AJ, Guenther J, de Nys R. Attachment point theory revisited: the fouling response to a microtextured matrix. *Biofouling* 2008;24:45–53.
- [146] Long CJ, Schumacher JF, Robinson PAC, Finlay JA, Callow ME, Callow JA, et al. A model that predicts the attachment behavior of *Ulva linza* zoospores on surface topography. *Biofouling* 2010;26:411–9.
- [147] Decker JT, Kirschner CM, Long CJ, Finlay JA, Callow ME, Callow JA, et al. Engineered antifouling microtopographies: an energetic model that predicts cell attachment. *Langmuir* 2013;29:13023–30.
- [148] Fu J, Zhang H, Guo Z, Feng D-Q, Thiagarajan V, Yao H. Combat biofouling with microscopic ridge-like surface morphology: a bioinspired study. *J R Soc Interface* 2018;15. <https://doi.org/10.1098/rsif.2017.0823>.
- [149] Hasan J, Webb HK, Truong VK, Pogodin S, Baulin VA, Watson GS, et al. Selective bactericidal activity of nanopatterned superhydrophobic cicada *Psaltoda claripennis* wing surfaces. *Appl Microbiol Biotechnol* 2013;97:9257–62.
- [150] Pogodin S, Hasan J, Baulin VA, Webb HK, Truong VK, Phong Nguyen TH, et al. Biophysical model of bacterial cell interactions with nanopatterned cicada wing surfaces. *Biophys J* 2013;104:835–40.
- [151] Sun M, Watson GS, Zheng Y, Watson JA, Liang A. Wetting properties on nanostructured surfaces of cicada wings. *J Exp Biol* 2009;212:3148–55.
- [152] Kelleher SM, Habimana O, Lawler J, O' Reilly B, Daniels S, Casey E, et al. Cicada Wing Surface Topography: An Investigation into the Bactericidal Properties of Nanostructural Features. *ACS Appl Mater Interfaces* 2016;8:14966–74.
- [153] Wu S, Zuber F, Maniura-Weber K, Brugger J, Ren Q. Nanostructured surface topographies have an effect on bactericidal activity. *J Nanobiotechnol* 2018;16:20.
- [154] Elbourne A, Crawford RJ, Ivanova EP. Nano-structured antimicrobial surfaces: From nature to synthetic analogues. *J Colloid Interface Sci* 2017;508:603–16.
- [155] Elbourne A, Chapman J, Gelmi A, Cozzolino D, Crawford RJ, Truong VK. Bacterial-nanostructure interactions: The role of cell elasticity and adhesion forces. *J Colloid Interface Sci* 2019;546:192–210.
- [156] Chang Y-R, Weeks ER, Ducker WA. Surface topography hinders bacterial surface motility. *ACS Appl Mater Interfaces* 2018;10:9225–34.
- [157] Apsite I, Biswas A, Li Y, Ionov L. Microfabrication Using shape-transforming soft materials. *Adv Funct Mater* 2020;30:1908028.
- [158] Chudak M, Chopra V, Hensel R, Arzt E, Darhuber AA. Elastohydrodynamic dewetting of thin liquid films - elucidating underwater adhesion of topographically patterned surfaces. *Langmuir* 2020. <https://doi.org/10.1021/acs.langmuir.0c02005>.
- [159] Bayer IS. Superhydrophobic Coatings from ecofriendly materials and processes: A review. *Adv Mater Interfaces* 2020;7:2000095.
- [160] Jokinen V, Kankuri E, Hoshian S, Franssila S, Ras RHA. Superhydrophobic blood-repellent surfaces. *Adv Mater* 2018;30:e1705104.
- [161] Lee C, Choi C-H, Kim C-J. Superhydrophobic drag reduction in laminar flows: a critical review. *Exp Fluids* 2016;57. <https://doi.org/10.1007/s00348-016-2264-z>.
- [162] Feng W, Ueda E, Levkin PA. Droplet microarrays: from surface patterning to high-throughput applications. *Adv Mater* 2018;30:e1706111.
- [163] Lima AC, Mano JF. Micro/nano-structured superhydrophobic surfaces in the biomedical field: part II: applications overview. *Nanomedicine* 2015;10:271–97.
- [164] Groten J, Rühle J. Surfaces with combined microscale and nanoscale structures: a route to mechanically stable superhydrophobic surfaces? *Langmuir* 2013;29:3765–72.
- [165] Xiu Y, Liu Y, Hess DW, Wong CP. Mechanically robust superhydrophobicity on hierarchically structured Si surfaces. *Nanotechnology* 2010;21:155705.
- [166] Nicklerl J, Helbig R, Schulz H-J, Werner C, Neinhuis C. Diversity and potential correlations to the function of Collembola cuticle structures. *Zoomorphology* 2013;132:183–95.
- [167] Wang D, Sun Q, Hokkanen MJ, Zhang C, Lin F-Y, Liu Q, et al. Design of robust superhydrophobic surfaces. *Nature* 2020;582:55–9.
- [168] Scarratt LRJ, Steiner U, Neto C. A review on the mechanical and thermodynamic robustness of superhydrophobic surfaces. *Adv Colloid Interface Sci* 2017;246:133–52.
- [169] Barthelat F, Yin Z, Buehler MJ. Structure and mechanics of interfaces in biological materials. *Nat Rev Mater* 2016;1. <https://doi.org/10.1038/natrevmats.2016.7>.
- [170] Tsimbourni PM, Fisher L, Holloway N, Sjöstrom T, Nobbs AH, Meek RMD, et al. Osteogenic and bactericidal surfaces from hydrothermal titania nanowires on titanium substrates. *Sci Rep* 2016;6:36857.
- [171] Park S, Park H-H, Sun K, Gwon Y, Seong M, Kim S, et al. Hydrogel nanospine patch as a flexible anti-pathogenic scaffold for regulating stem cell behavior. *ACS Nano* 2019;13:11181–93.
- [172] Li J, Tan L, Liu X, Cui Z, Yang X, Yeung KWK, et al. Balancing bacteria-osteoblast competition through selective physical puncture and biofunctionalization of ZnO/polydopamine/arginine-glycine-aspartic acid-cysteine nanorods. *ACS Nano* 2017;11:11250–63.
- [173] Linklater DP, Juodkazis S, Crawford RJ, Ivanova EP. Mechanical inactivation of *Staphylococcus aureus* and *Pseudomonas aeruginosa* by titanium substrata with hierarchical surface structures. *Materialia* 2019;5:100197.
- [174] Mas-Moruno C, Su B, Dalby MJ. Multifunctional coatings and nanotopographies: toward cell instructive and antibacterial implants. *Adv Health Mater* 2019;8:e1801103.
- [175] Neto AI, Custódio CA, Song W, Mano JF. High-throughput evaluation of interactions between biomaterials, proteins and cells using patterned superhydrophobic substrates. *Soft Matter* 2011;7:4147.
- [176] Li L, Tian J, Li M, Shen W. Superhydrophobic surface supported bioassay – An application in blood typing. *Colloids Surf, B* 2013;106:176–80.
- [177] Xiong S, Zhong Z, Wang Y. Direct silanization of polyurethane foams for efficient selective absorption of oil from water. *AIChE J* 2017;63:2232–40. <https://doi.org/10.1002/aic.15629>.
- [178] Petersen DS, Gorb SN, Heepe L. The influence of material and roughness on the settlement and the adhesive strength of the barnacle *Balanus Improvisus* in the Baltic Sea. *Front Mar Sci* 2020;7. <https://doi.org/10.3389/fmars.2020.00664>.
- [179] Zanolto M, Boschetto F, Zhu W, Marin E, McEntire BJ, Bal BS, et al. 3D-additive deposition of an antibacterial and osteogenic silicon nitride coating on orthopaedic titanium substrate. *J Mech Behav Biomed Mater* 2020;103:103557.
- [180] Ruggeri ZM, Loredana Mendolicchio G. Adhesion mechanisms in platelet function. *Circ Res* 2007;100:1673–85.
- [181] Loskill P, Zeitz C, Grandthyll S, Thewes N, Müller F, Bischoff M, et al. Reduced adhesion of oral bacteria on hydroxyapatite by fluoride treatment. *Langmuir* 2013;29:5528–33.
- [182] Kendall K. *Molecular Adhesion and Its Applications: The Sticky Universe*. Springer Science & Business Media; 2007.
- [183] Butt H-J, Kappel M. *Surface and Interfacial Forces*. John Wiley & Sons; 2018.
- [184] Soto D, Parness A, Esparza N, Kenny TW, Autumn K, Cutkosky M. Microfabricated dry adhesive displaying frictional adhesion. 2008 Solid-State, Actuators, and Microsystems Workshop Technical Digest. 2008.
- [185] Khaleel WB, Sameoto D. Anisotropic dry adhesive via cap defects. *Bioinspir Biomim* 2013;8:044002.
- [186] Autumn K. Frictional adhesion: a new angle on gecko attachment. *J Exp Biol* 2006;209:3569–79.
- [187] Federle W, Labonte D. Dynamic biological adhesion: mechanisms for controlling attachment during locomotion. *Philos Trans R Soc Lond B Biol Sci* 2019;374:20190199.
- [188] Zeng H, Pesika N, Tian Y, Zhao B, Chen Y, Tirrell M, et al. Frictional adhesion of patterned surfaces and implications for gecko and biomimetic systems. *Langmuir* 2009;25:7486–95.
- [189] Mengüç Y, Yang SY, Kim S, Rogers JA, Sitti M. Gecko-inspired controllable adhesive structures applied to micromanipulation. *Adv Funct Mater* 2012;22:1246–54.

- [190] Zhou M, Tian Y, Sameoto D, Zhang X, Meng Y, Wen S. Controllable interfacial adhesion applied to transfer light and fragile objects by using gecko inspired mushroom-shaped pillar surface. *ACS Appl Mater Interfaces* 2013;5:10137–44.
- [191] Tinnemann V, Arzt E, Hensel R. Switchable double-sided micropatterned adhesives for selective fixation and detachment. *J Mech Phys Solids* 2019;123:20–7.
- [192] Cutkosky MR. Climbing with adhesion: from bioinspiration to biounderstanding. *Interface Focus* 2015;5:20150015.
- [193] Henrey M, Téllez JPD, Wormnes K, Pambaguian L, Menon C. Towards the use of mushroom-capped dry adhesives in outer space: Effects of low pressure and temperature on adhesion strength. *Aerosp Sci Technol* 2013;29:185–90.
- [194] Jiang H, Hawkes EW, Fuller C, Estrada MA, Suresh SA, Abcouwer N, et al. A robotic device using gecko-inspired adhesives can grasp and manipulate large objects in microgravity. *Sci Rob* 2017;2:eaa4545. <https://doi.org/10.1126/scirobotics.aan4545>.
- [195] Nachtigall W. Biological mechanisms of attachment: The comparative morphology and bioengineering of organs for linkage, suction, and adhesion. Springer Science & Business Media; 2013.
- [196] Gorb SSN. Attachment Devices of Insect Cuticle. Springer Science & Business Media; 2007.
- [197] Gorb S. Adhesion and Friction in Biological Systems. Springer; 2011.
- [198] Federle W. Why are so many adhesive pads hairy? *J Exp Biol* 2006;209:2611–21.
- [199] Stark AY, Subarajan S, Jain D, Niewiarowski PH, Dhinojwala A. Superhydrophobicity of the gecko toe pad: biological optimization versus laboratory maximization. *Philos Trans A Math Phys Eng Sci* 2016;374. <https://doi.org/10.1098/rsta.2016.0184>.
- [200] Higham TE, Russell AP, Niewiarowski PH, Wright A, Speck T. The ecomechanics of gecko adhesion: Natural surface topography, Evolution, and Biomimetics. *Integr Comp Biol* 2019;59:148–67.
- [201] Croll AB, Hosseini N, Bartlett MD. Switchable adhesives for multifunctional interfaces. *Adv Mater Technol* 2019;4:1900193.
- [202] Creton C, Ciccotti M. Fracture and adhesion of soft materials: a review. *Rep Prog Phys* 2016;79:046601.
- [203] King DR, Bartlett MD, Gilman CA, Irschick DJ, Crosby AJ. Creating gecko-like adhesives for “real world” surfaces. *Adv Mater* 2014;26:4345–51.
- [204] Gilman CA, Imburgia MJ, Bartlett MD, King DR, Crosby AJ, Irschick DJ. Geckos as springs: Mechanics explain across-species scaling of adhesion. *PLoS ONE* 2015;10:e0134604.
- [205] Imburgia MJ, Kuo C-Y, Briggs DR, Irschick DJ, Crosby AJ. Effects of digit orientation on gecko adhesive force capacity: Synthetic and behavioral Studies. *Integr Comp Biol* 2019;59:182–92.
- [206] Chan EP, Greiner C, Arzt E, Crosby AJ. Designing model systems for enhanced adhesion. *MRS Bull* 2007;32:496–503. <https://doi.org/10.1557/mrs2007.84>.
- [207] Niewiarowski PH, Stark AY, Dhinojwala A. Sticking to the story: outstanding challenges in gecko-inspired adhesives. *J Exp Biol* 2016;219:912–9.
- [208] Boesel LF, Greiner C, Arzt E, del Campo A. Gecko-inspired surfaces: a path to strong and reversible dry adhesives. *Adv Mater* 2010;22:2125–37.
- [209] Gorb SN, Koch K, Heepe L. Biological and biomimetic surfaces: adhesion, friction and wetting phenomena. *Beilstein J Nanotechnol* 2019;10:481–2.
- [210] Heepe L, Xue L, Gorb SN. Bio-inspired Structured Adhesives: Biological Prototypes, Fabrication. Tribological Properties: Contact Mechanics, and Novel Concepts. Springer; 2017.
- [211] Flammang P, Santos R, Aldred N, Gorb S. Biological and biomimetic adhesives: Challenges and opportunities. Royal Society of Chemistry; 2013.
- [212] Zhang C, Mcadams 2nd DA, Grunlan JC. Nano/micro-manufacturing of bioinspired materials: a review of methods to mimic natural structures. *Adv Mater* 2016;28:6292–321.
- [213] Zhou M, Pesika N, Zeng H, Tian Y, Israelachvili J. Recent advances in gecko adhesion and friction mechanisms and development of gecko-inspired dry adhesive surfaces. *Friction* 2013;1:114–29.
- [214] Eisenhaure J, Kim S. A review of the state of dry adhesives: Biomimetic structures and the alternative designs they inspire. *Micromachines* 2017;8:125.
- [215] Kwak J-S, Kim T-W. A review of adhesion and friction models for gecko feet. *Int J Precis Eng Manuf* 2010;11:171–86.
- [216] O’Rourke RD, Steele TWJ, Taylor HK. Bioinspired fibrillar adhesives: a review of analytical models and experimental evidence for adhesion enhancement by surface patterns. *J Adhes Sci Technol* 2016;30:362–91.
- [217] Sameoto D, Menon C. Recent advances in the fabrication and adhesion testing of biomimetic dry adhesives. *Smart Mater Struct* 2010;19:103001.
- [218] Kamperman M, Kroner E, del Campo A, McMeeking RM, Arzt E. Functional adhesive surfaces with “gecko” effect: The concept of contact splitting. *Adv Eng Mater* 2010;12:335–48.
- [219] Brodoceanu D, Bauer CT, Kroner E, Arzt E, Kraus T. Hierarchical bioinspired adhesive surfaces—a review. *Bioinspir Biomim* 2016;11:051001.
- [220] Sharma A, Swan KG, Franz Weitlaner: the great spreader of surgery. *J Trauma* 2009;67:1431–4.
- [221] Weitlaner F. Eine Untersuchung über den Haftfuss des Gecko. *Verhndl Zool Bot Ges Wien* 1902;52:328–32.
- [222] Kroner E, Davis CS. A study of the adhesive foot of the gecko: Translation of a publication by Franz Weitlaner. *The Journal of Adhesion* 2015;91:481–7.
- [223] Loskill P, Puthoff J, Wilkinson M, Mecke K, Jacobs K, Autumn K. Macroscale adhesion of gecko setae reflects nanoscale differences in subsurface composition. *J R Soc Interface* 2013;10:20120587.
- [224] Hiller U. Untersuchungen zum Feinbau und zur Funktion der Haftborsten von Reptilien. *Zeitschrift Für Morphologie Der Tiere* 1968;62:307–62.
- [225] Autumn K, Liang YA, Hsieh ST, Zesch W, Chan WP, Kenny TW, et al. Adhesive force of a single gecko foot-hair. *Nature* 2000;405:681–5.
- [226] Autumn K, Sitti M, Liang YA, Peattie AM, Hansen WR, Sponberg S, et al. Evidence for van der Waals adhesion in gecko setae. *Proc Natl Acad Sci U S A* 2002;99:12252–6.
- [227] Huber G, Mantz H, Spolenak R, Mecke K, Jacobs K, Gorb SN, et al. Evidence for capillarity contributions to gecko adhesion from single spatula nanomechanical measurements. *Proc Natl Acad Sci U S A* 2005;102:16293–6.
- [228] Brörmann K, Burger K, Jagota A, Bennewitz R. Discharge during detachment of micro-structured PDMS sheds light on the role of electrostatics in adhesion. *J Adhes* 2012;88:589–607.
- [229] Baumgartner W. Friction-reducing sandfish skin. In B B, editor. *Encyclopedia of Nanotechnolog*, Springer; 2015.
- [230] Staudt K, Saxe F, Schmied H, Böhme W, Baumgartner W. Sandfish inspires engineering. *Bioinspir Biomimet Biorepl* 2011. <https://doi.org/10.1117/12.888842>.
- [231] Knight K. Sandfish swim effortlessly to burrow. *J Experim Biol* 2013;216:i–ii.
- [232] Lasagni A, Alamri S, Aguilar-Morales A, Rößler F, Voisiat B, Kunze T. Biomimetic surface structuring using laser based interferometric methods. *Appl Sci* 2018; 8:1260.
- [233] Rosenkranz A, Grützmaker PG, Murzyn K, Mathieu C, Mücklich F. Multi-scale surface patterning to tune friction under mixed lubricated conditions. *Appl Nanosci* 2019. <https://doi.org/10.1007/s13204-019-01055-9>.
- [234] Greiner C, Schäfer M, Popp U, Gumbusch P. Contact splitting and the effect of dimple depth on static friction of textured surfaces. *ACS Appl Mater Interfaces* 2014;6:7986–90.
- [235] Schneider J, Djamiykov V, Greiner C. Friction reduction through biologically inspired scale-like laser surface textures. *Beilstein J Nanotechnol* 2018;9: 2561–72.
- [236] Yu D, Hensel R, Beckelmann D, Opsölder M, Schäfer B, Moh K, et al. Tailored polyurethane acrylate blend for large-scale and high-performance micropatterned dry adhesives. *J Mater Sci* 2019;54:12925–37.
- [237] Arzt E, Gorb S, Spolenak R. From micro to nano contacts in biological attachment devices. *Proc Natl Acad Sci U S A* 2003;100:10603–6.
- [238] Johnson KL, Kendall K, Roberts AD. Surface energy and the contact of elastic solids. *Proc R Soc Lond A Math Phys Sci* 1971;324:301–13.
- [239] Hui C-Y, Glassmaker NJ, Tang T, Jagota A. Design of biomimetic fibrillar interfaces: 2. Mechanics of enhanced adhesion. *J R Soc Interface* 2004;1:35–48.
- [240] Jagota A, Hui C-Y, Glassmaker NJ, Tang T. Mechanics of bioinspired and biomimetic fibrillar interfaces. *MRS Bull* 2007;32:492–5.
- [241] Spolenak R, Gorb S, Gao H, Arzt E. Effects of contact shape on the scaling of biological attachments. *Proc Roy Soc A: Math Phys Eng Sci* 2005;461:305–19.
- [242] Majumder A, Sharma A, Ghatak A. Controlling adhesion by micro-nano structuring of soft surfaces. *Microfluidics and Microfabrication. Bio-inspired Adhes* 2010:283–307.
- [243] McMeeking RM, Arzt E, Evans AG. Defect dependent adhesion of fibrillar surfaces. *J Adhes* 2008;84:675–81.
- [244] Booth JA, Tinnemann V, Hensel R, Arzt E, McMeeking RM, Foster KL. Statistical properties of defect-dependent detachment strength in bioinspired dry adhesives. *J R Soc Interface* 2019;16:20190239.

- [245] Gao H, Yao H. Shape insensitive optimal adhesion of nanoscale fibrillar structures. *Proc Natl Acad Sci U S A* 2004;101:7851–6.
- [246] Tang T, Hui C-Y, Glassmaker NJ. Can a fibrillar interface be stronger and tougher than a non-fibrillar one? *J R Soc Interface* 2005;2:505–16.
- [247] Chung JY, Chaudhury MK. Roles of discontinuities in bio-inspired adhesive pads. *J R Soc Interface* 2005;2:55–61.
- [248] Glassmaker NJ, Jagota A, Hui C-Y, Noderer WL, Chaudhury MK. Biologically inspired crack trapping for enhanced adhesion. *Proc Natl Acad Sci U S A* 2007;104:10786–91.
- [249] Jagota A, Bennisson SJ. Mechanics of adhesion through a fibrillar microstructure. *Integr Comp Biol* 2002;42:1140–5.
- [250] Persson BNJ, Gorb S. The effect of surface roughness on the adhesion of elastic plates with application to biological systems. *J Chem Phys* 2003;119:11437–44.
- [251] Gorb S, Varenberg M, Peressadko A, Tuma J. Biomimetic mushroom-shaped fibrillar adhesive microstructure. *J R Soc Interface* 2007;4:271–5.
- [252] Heepe L, Gorb SN. Biologically inspired mushroom-shaped adhesive microstructures. *Annu Rev Mater Res* 2014;44:173–203.
- [253] Yao H, Gao H. Optimal shapes for adhesive binding between two elastic bodies. *J Colloid Interface Sci* 2006;298:564–72.
- [254] Kendall K. The adhesion and surface energy of elastic solids. *J Phys D Appl Phys* 1971;4:1186–95.
- [255] Bartlett MD, Croll AB, King DR, Paret BM, Irschick DJ, Crosby AJ. Looking beyond fibrillar features to scale gecko-like adhesion. *Adv Mater* 2012;24:1078–83.
- [256] Bartlett MD, Crosby AJ. Scaling normal adhesion force capacity with a generalized parameter. *Langmuir* 2013;29:11022–7.
- [257] Carbone G, Pierro E. A review of adhesion mechanisms of mushroom-shaped microstructured adhesives. *Meccanica* 2013;48:1819–33.
- [258] Khaderi SN, Fleck NA, Arzt E, McMeeking RM. Detachment of an adhered micropillar from a dissimilar substrate. *J Mech Phys Solids* 2015;75:159–83.
- [259] Fleck NA, Khaderi SN, McMeeking RM, Arzt E. Cohesive detachment of an elastic pillar from a dissimilar substrate. *J Mech Phys Solids* 2017;101:30–43.
- [260] Balijepalli RG, Begley MR, Fleck NA, McMeeking RM, Arzt E. Numerical simulation of the edge stress singularity and the adhesion strength for compliant mushroom fibrils adhered to rigid substrates. *Int J Solids Struct* 2016;85–86:160–71.
- [261] Greiner C, Campo AD, Arzt E. Adhesion of bioinspired micropatterned surfaces: effects of pillar radius, aspect ratio, and preload. *Langmuir* 2007;23:3495–502.
- [262] Gao H, Wang X, Yao H, Gorb S, Arzt E. Mechanics of hierarchical adhesion structures of geckos. *Mech Mater* 2005;37:275–85.
- [263] Tang T, Jagota A, Chaudhury MK, Hui C-Y. Thermal fluctuations limit the adhesive strength of compliant solids. *J Adhes* 2006;82:671–96.
- [264] Aksak B, Hui C-Y, Sitti M. The effect of aspect ratio on adhesion and stiffness for soft elastic fibres. *J R Soc Interface* 2011;8:1166–75.
- [265] Hui C-Y, Jagota A, Shen L, Rajan A, Glassmaker N, Tang T. Design of bio-inspired fibrillar interfaces for contact and adhesion — theory and experiments. *J Adhes Sci Technol* 2007;21:1259–80.
- [266] Shahsavani H, Zhao B. Bioinspired functionally graded adhesive materials: Synergetic interplay of top viscous-elastic layers with base micropillars. *Macromolecules* 2014;47:353–64.
- [267] Castellanos G, Arzt E, Kamperman M. Effect of viscoelasticity on adhesion of bioinspired micropatterned epoxy surfaces. *Langmuir* 2011;27:7752–9.
- [268] Lorenz B, Krick BA, Mulakaluri N, Smolyakova M, Dieluwit S, Sawyer WG, et al. Adhesion: role of bulk viscoelasticity and surface roughness. *J Phys Condens Matter* 2013;25:225004.
- [269] Lakhera N, Graucob A, Schneider AS, Kroner E, Arzt E, Yakacki CM, et al. Effect of viscoelasticity on the spherical and flat adhesion characteristics of photopolymerizable acrylate polymer networks. *Int J Adhes Adhes* 2013;44:184–94.
- [270] Bullock JMR, Federle W. Beetle adhesive hairs differ in stiffness and stickiness: in vivo adhesion measurements on individual setae. *Naturwissenschaften* 2011;98:381–7.
- [271] del Campo A, Greiner C, Arzt E. Contact shape controls adhesion of bioinspired fibrillar surfaces. *Langmuir* 2007;23:10235–43.
- [272] Gorb SN, Varenberg M. Mushroom-shaped geometry of contact elements in biological adhesive systems. *J Adhes Sci Technol* 2007;21:1175–83.
- [273] Heepe L, Kovalev AE, Varenberg M, Tuma J, Gorb SN. First mushroom-shaped adhesive microstructure: A review. *Theor Appl Mech Lett* 2012;2:014008.
- [274] Varenberg M, Gorb S. Close-up of mushroom-shaped fibrillar adhesive microstructure: contact element behaviour. *J R Soc Interface* 2008;5:785–9.
- [275] Heepe L, Varenberg M, Itovich Y, Gorb SN. Suction component in adhesion of mushroom-shaped microstructure. *J R Soc Interface* 2011;8:585–9.
- [276] Heepe L, Carbone G, Pierro E, Kovalev AE, Gorb SN. Adhesion tilt-tolerance in bio-inspired mushroom-shaped adhesive microstructure. *Appl Phys Lett* 2014;104:011906.
- [277] Kroner E, Arzt E. Single macropillars as model systems for tilt angle dependent adhesion measurements. *Int J Adhes Adhes* 2012;36:32–8.
- [278] Varenberg M, Gorb S. A beetle-inspired solution for underwater adhesion. *J R Soc Interface* 2008;5:383–5.
- [279] Spuskanyuk AV, McMeeking RM, Deshpande VS, Arzt E. The effect of shape on the adhesion of fibrillar surfaces. *Acta Biomater* 2008;4:1669–76.
- [280] Carbone G, Pierro E, Gorb SN. Origin of the superior adhesive performance of mushroom-shaped microstructured surfaces. *Soft Matter* 2011;7:5545.
- [281] Carbone G, Pierro E. Sticky bio-inspired micropillars: finding the best shape. *Small* 2012;8:1449–54.
- [282] Zhang X, Hensel R, Arzt E. A design strategy for mushroom-shaped microfibrils with optimized dry adhesion: Experiments and finite element analyses. *J Appl Mech* n.d. [submitted for publication].
- [283] Aksak B, Sahin K, Sitti M. The optimal shape of elastomer mushroom-like fibers for high and robust adhesion. *Beilstein J Nanotechnol* 2014;5:630–8.
- [284] Marvi H, Song S, Sitti M. Experimental investigation of optimal adhesion of mushroomlike elastomer microfibrillar adhesives. *Langmuir* 2015;31:10119–24.
- [285] Varenberg M, Gorb S. Close-up of mushroom-shaped fibrillar adhesive microstructure: Contact element behavior. Volume 3: Design; Tribology. *Education* 2008. <https://doi.org/10.1115/esda2008-59095>.
- [286] Hossfeld CK, Schneider AS, Arzt E, Frick CP. Detachment behavior of mushroom-shaped fibrillar adhesive surfaces in peel testing. *Langmuir* 2013;29:15394–404.
- [287] Micciché M, Arzt E, Kroner E. Single macroscopic pillars as model system for bioinspired adhesives: influence of tip dimension, aspect ratio, and tilt angle. *ACS Appl Mater Interfaces* 2014;6:7076–83.
- [288] Neubauer JW, Xue L, Erath J, Drotlef D-M, Campo AD, Fery A. Monitoring the contact stress distribution of gecko-inspired adhesives using mechano-sensitive surface coatings. *ACS Appl Mater Interfaces* 2016;8:17870–7.
- [289] Peisker H, Michels J, Gorb SN. Evidence for a material gradient in the adhesive tarsal setae of the ladybird beetle *Coccinella septempunctata*. *Nat Commun* 2013;4:1661.
- [290] Balijepalli RG, Fischer SCL, Hensel R, McMeeking RM, Arzt E. Numerical study of adhesion enhancement by composite fibrils with soft tip layers. *J Mech Phys Solids* 2017;99:357–78.
- [291] Fischer SCL, Groß K, Abad OT, Becker MM, Park E, Hensel R, et al. Funnel-shaped microstructures for strong reversible adhesion. *Adv Mater Interfaces* 2017;4:1700292.
- [292] Wang Y, Kang V, Arzt E, Federle W, Hensel R. Strong wet and dry adhesion by cupped microstructures. *ACS Appl Mater Interfaces* 2019;11:26483–90.
- [293] Wang Y, Kang V, Federle W, Arzt E, Hensel R. Switchable underwater adhesion by deformable cupped microstructures. *Adv Mater Interfaces* 2020;4:2001269.
- [294] Heepe L, Kovalev AE, Gorb SN. Direct observation of microcavitation in underwater adhesion of mushroom-shaped adhesive microstructure. *Beilstein J Nanotechnol* 2014;5:903–9.
- [295] Gillies AG, Fearing RS. Shear adhesion strength of thermoplastic gecko-inspired synthetic adhesive exceeds material limits. *Langmuir* 2011;27:11278–81.
- [296] Yu D, Beckelmann D, Opsölder M, Schäfer B, Moh K, Hensel R, et al. Roll-to-roll manufacturing of micropatterned adhesives by template compression. *Materials* 2018;12. <https://doi.org/10.3390/ma12010097>.
- [297] Bin Khaled W, Sameoto D. Fabrication and characterization of thermoplastic elastomer dry adhesives with high strength and low contamination. *ACS Appl Mater Interfaces* 2014;6:6806–15.
- [298] Gösele U, Tong Q-Y, Schumacher A, Kräuter G, Reiche M, Plöbl A, et al. Wafer bonding for microsystems technologies. *Sens Actuators, A* 1999;74:161–8.
- [299] Persson BNJ. On the mechanism of adhesion in biological systems. *J Chem Phys* 2003;118:7614.
- [300] Barreau V, Hensel R, Guimard NK, Ghatak A, McMeeking RM, Arzt E. Fibrillar elastomeric micropatterns create tunable adhesion even to rough surfaces. *Adv Funct Mater* 2016;26:4687–94.
- [301] Hui C-Y, Glassmaker NJ, Jagota A. How compliance compensates for surface roughness in fibrillar adhesion. *The Journal of Adhesion* 2005;81:699–721.
- [302] Greiner C, Spolenak R, Arzt E. Adhesion design maps for fibrillar adhesives: the effect of shape. *Acta Biomater* 2009;5:597–606.

- [303] Gorb SN, Filippov AE. Fibrillar adhesion with no clusterisation: Functional significance of material gradient along adhesive setae of insects. *Beilstein J Nanotechnol* 2014;5:837–45.
- [304] Garcia-Gonzalez D, Snoeijer J, Kappl M, Butt H-J. Onset of elasto-capillary bundling of micropillar arrays: A direct visualization. *Langmuir* 2020. <https://doi.org/10.1021/acs.langmuir.0c02147>.
- [305] Spolenak R, Gorb S, Arzt E. Adhesion design maps for bio-inspired attachment systems. *Acta Biomater* 2005;1:5–13.
- [306] Scholz I, Baumgartner W, Federle W. Micromechanics of smooth adhesive organs in stick insects: pads are mechanically anisotropic and softer towards the adhesive surface. *J Comp Physiol A Neuroethol Sens Neural Behav Physiol* 2008;194:373–84.
- [307] Heepe L, Höft S, Michels J, Gorb SN. Material gradients in fibrillar insect attachment systems: the role of joint-like elements. *Soft Matter* 2018;14:7026–33.
- [308] Murphy MP, Aksak B, Sitti M. Adhesion and anisotropic friction enhancements of angled heterogeneous micro-fiber arrays with spherical and spatula tips. *J Adhes Sci Technol* 2007;21:1281–96.
- [309] Bae WG, Kim D, Kwak MK, Ha L, Kang SM, Suh KY. Enhanced skin adhesive patch with Modulus-Tunable composite micropillars. *Adv Healthc Mater* 2013;2:109–13.
- [310] Minsky HK, Turner KT. Achieving enhanced and tunable adhesion via composite posts. *Appl Phys Lett* 2015;106:201604.
- [311] Minsky HK, Turner KT. Composite microposts with high dry adhesion strength. *ACS Appl Mater Interfaces* 2017;9:18322–7.
- [312] Gorumlu S, Aksak B. Sticking to rough surfaces using functionally graded bio-inspired microfibres. *R Soc Open Sci* 2017;4:161105.
- [313] Fischer SCL, Arzt E, Hensel R. Composite pillars with a tunable interface for adhesion to rough substrates. *ACS Appl Mater Interfaces* 2017;9:1036–44.
- [314] Drotleff D-M, Dayan CB, Sitti M. Bio-inspired composite microfibers for strong and reversible adhesion on smooth surfaces. *Integr Comp Biol* 2019;9:227–35.
- [315] Hensel R, McMeeking RM, Kossa A. Adhesion of a rigid punch to a confined elastic layer revisited. *The Journal of Adhesion* 2019;95:44–63.
- [316] Webber RE, Shull KR, Roos A, Creton C. Effects of geometric confinement on the adhesive debonding of soft elastic solids. *Phys Rev E Stat Nonlin Soft Matter Phys* 2003;68:021805.
- [317] Yao H, Gao H. Multi-scale cohesive laws in hierarchical materials. *Int J Solids Struct* 2007;44:8177–93.
- [318] Gao H. Mechanical principles of a self-similar hierarchical structure. *MRS Online Proc Library* 2009;1188:23–34. <https://doi.org/10.1557/PROC-1188-LL01-01>.
- [319] Bauer CT, Kroner E, Fleck NA, Arzt E. Hierarchical macroscopic fibrillar adhesives: in situ study of buckling and adhesion mechanisms on wavy substrates. *Bioinspir Biomim* 2015;10:066002.
- [320] Yao H, Gao H. Mechanics of robust and releasable adhesion in biology: Bottom-up designed hierarchical structures of gecko. *J Mech Phys Solids* 2006;54:1120–46.
- [321] Kim S, Sitti M, Hui C-Y, Long R, Jagota A. Effect of backing layer thickness on adhesion of single-level elastomer fiber arrays. *Appl Phys Lett* 2007;91:161905.
- [322] Long R, Hui C-Y, Kim S, Sitti M. Modeling the soft backing layer thickness effect on adhesion of elastic microfiber arrays. *J Appl Phys* 2008;104:044301.
- [323] Chen S, Soh AK. Tuning the geometrical parameters of biomimetic fibrillar structures to enhance adhesion. *J R Soc Interface* 2008;5:373–83.
- [324] Bacca M, Booth JA, Turner KL, McMeeking RM. Load sharing in bioinspired fibrillar adhesives with backing layer interactions and interfacial misalignment. *J Mech Phys Solids* 2016;96:428–44.
- [325] Booth JA, Bacca M, McMeeking RM, Foster KL. Benefit of backing-layer compliance in fibrillar adhesive patches - resistance to peel propagation in the presence of interfacial misalignment. *Adv Mater Interfaces* 2018;5:1800272.
- [326] Tinnemann V, Hernández L, Fischer SCL, Arzt E, Bennewitz R, Hensel R. In situ observation reveals local detachment mechanisms and suction effects in micropatterned adhesives. *Adv Funct Mater* 2019;29:1807713.
- [327] Kroner E, Blau J, Arzt E. Note: An adhesion measurement setup for bioinspired fibrillar surfaces using flat probes. *Rev Sci Instrum* 2012;83:016101.
- [328] Paretkar D, Schneider AS, Kroner E, Arzt E. In situ observation of contact mechanisms in bioinspired adhesives at high magnification. *MRS Commun* 2011;1:53–6.
- [329] Eason EV, Hawkes EW, Windheim M, Christensen DL, Libby T, Cutkosky MR. Adhesive stress distribution measurement on a gecko. *Biomimetic Biohyb Syst* 2014;386–8.
- [330] Eason EV, Hawkes EW, Windheim M, Christensen DL, Libby T, Cutkosky MR. Stress distribution and contact area measurements of a gecko toe using a high-resolution tactile sensor. *Bioinspir Biomim* 2015;10:016013.
- [331] Porwal PK, Hui CY. Strength statistics of adhesive contact between a fibrillar structure and a rough substrate. *J R Soc Interface* 2008;5:441–8.
- [332] Barreau V, Yu D, Hensel R, Arzt E. Elevated temperature adhesion of bioinspired polymeric micropatterns to glass. *J Mech Behav Biomed Mater* 2017;76:110–8.
- [333] Gernay S, Federle W, Lambert P, Gilet T. Elasto-capillarity in insect fibrillar adhesion. *J R Soc Interface* 2016;13. <https://doi.org/10.1098/rsif.2016.0371>.
- [334] De Souza EJ, Brinkmann M, Mohrdieck C, Arzt E. Enhancement of capillary forces by multiple liquid bridges. *Langmuir* 2008;24:8813–20.
- [335] De Souza EJ, Brinkmann M, Mohrdieck C, Crosby A, Arzt E. Capillary forces between chemically different substrates. *Langmuir* 2008;24:10161–8.
- [336] De Souza EJ, Gao L, McCarthy TJ, Arzt E, Crosby AJ. Effect of contact angle hysteresis on the measurement of capillary forces. *Langmuir* 2008;24:1391–6.
- [337] Qian J, Gao H. Scaling effects of wet adhesion in biological attachment systems. *Acta Biomater* 2006;2:51–8.
- [338] Pesika NS, Zeng H, Kristiansen K, Zhao B, Tian Y, Autumn K, et al. Gecko adhesion pad: a smart surface? *J Phys Condens Matter* 2009;21:464132.
- [339] Puthoff JB, Prowse MS, Wilkinson M, Autumn K. Changes in materials properties explain the effects of humidity on gecko adhesion. *J Exp Biol* 2010;213:3699–704.
- [340] Buhl S, Greiner C, del Campo A, Arzt E. Humidity influence on the adhesion of biomimetic fibrillar surfaces. *Int J Mater Res* 2009;100:1119–26.
- [341] Cadirov N, Booth JA, Turner KL, Israelachvili JN. Influence of humidity on grip and release adhesion mechanisms for gecko-inspired microfibrillar surfaces. *ACS Appl Mater Interfaces* 2017;9:14497–505.
- [342] Meng F, Liu Q, Wang X, Tan D, Xue L, Barnes WJP. Tree frog adhesion biomimetics: opportunities for the development of new, smart adhesives that adhere under wet conditions. *Philos Trans A Math Phys Eng Sci* 2019;377:20190131.
- [343] Trentlage C, Stoll E. A Biomimetic docking mechanism for controlling uncooperative satellites on the ELISSA free-floating laboratory. In: 2018 3rd International Conference on Advanced Robotics and Mechatronics (ICARM); 2018. <https://doi.org/10.1109/icarm.2018.8610791>.
- [344] Stork NE. A scanning electron microscope study of tarsal adhesive setae in the Coleoptera. *Zool J Linn Soc* 1980;68:173–306.
- [345] Murphy MP, Aksak B, Sitti M. Gecko-inspired directional and controllable adhesion. *Small* 2009;5:170–5.
- [346] Sameoto D, Sharif H, Menon C. Investigation of low-pressure adhesion performance of mushroom shaped biomimetic dry adhesives. *J Adhes Sci Technol* 2012;26:2641–52.
- [347] Davies J, Haq S, Hawke T, Sargent JP. A practical approach to the development of a synthetic Gecko tape. *Int J Adhes Adhes* 2009;29:380–90.
- [348] Purto J, Frensemeier M, Kroner E. Switchable adhesion in vacuum using bio-inspired dry adhesives. *ACS Appl Mater Interfaces* 2015;7:24127–35.
- [349] Tiwari A, Persson BNJ. Physics of suction cups. *Soft Matter* 2019;15:9482–99.
- [350] Schargott M, Popov VL, Gorb S. Spring model of biological attachment pads. *J Theor Biol* 2006;243:48–53.
- [351] Bettscheider S, Yu D, Foster KL, McMeeking RM, Arzt E, Hensel R, et al. Breakdown of continuum models for spherical probe adhesion tests on micropatterned surfaces. *J Mech Phys Solids* 2021. under revision.
- [352] Thiemcke J, Hensel R. Contact aging enhances adhesion of micropatterned silicone adhesives to glass substrates. *Adv Funct Mater* 2020;2005826. <https://doi.org/10.1002/adfm.202005826>.
- [353] Dapp WB, Lücke A, Persson BNJ, Müser MH. Self-affine elastic contacts: percolation and leakage. *Phys Rev Lett* 2012;108:244301.
- [354] Pastewka L, Robbins MO. Contact between rough surfaces and a criterion for macroscopic adhesion. *Proc Natl Acad Sci U S A* 2014;111:3298–303.
- [355] Müser MH. On the contact area of nominally flat Hertzian contacts. *Tribol Lett* 2016;64. <https://doi.org/10.1007/s11249-016-0750-3>.
- [356] Persson BNJ. Contact mechanics for randomly rough surfaces. *Surf Sci Rep* 2006;61:201–27.
- [357] Jacobs TDB, Junge T, Pastewka L. Quantitative characterization of surface topography using spectral analysis. *Surf Topogr Metrol Prop* 2017;5:013001.
- [358] Kasem H, Varenberg M. Effect of counterface roughness on adhesion of mushroom-shaped microstructure. *J R Soc Interface* 2013;10:20130620.

- [359] Cañas N, Kamperman M, Völker B, Kroner E, McMeeking RM, Arzt E. Effect of nano- and micro-roughness on adhesion of bioinspired micropatterned surfaces. *Acta Biomater* 2012;8:282–8.
- [360] Bullock JMR, Federle W. The effect of surface roughness on claw and adhesive hair performance in the dock beetle *Gastrophysa viridula*. *Insect Science* 2011; 18:298–304.
- [361] Meiners F, Tracht K. Releasing principles for dry-adhesive handling of microobjects. *Procedia CIRP* 2020;91:503–7.
- [362] Paretkar D, Kamperman M, Martina D, Zhao J, Creton C, Lindner A, et al. Preload-responsive adhesion: effects of aspect ratio, tip shape and alignment. *J R Soc Interface* 2013;10:20130171.
- [363] Paretkar D, Kamperman M, Schneider AS, Martina D, Creton C, Arzt E. Bioinspired pressure actuated adhesive system. *Mater Sci Eng, C* 2011;31:1152–9.
- [364] Stark S, Begley MR, McMeeking RM. The buckling and postbuckling of fibrils adhering to a rigid surface. *J Appl Mech* 2013;80. <https://doi.org/10.1115/1.4023107>.
- [365] Peressadko A, Gorb SN. When less is more: experimental evidence for tenacity enhancement by division of contact area. *The Journal of Adhesion* 2004;80: 247–61.
- [366] Isla PY, Kroner E. A Novel Bioinspired Switchable Adhesive with Three Distinct Adhesive States. *Adv Funct Mater* 2015;25:2444–50.
- [367] Reddy S, Arzt E, del Campo A. Bioinspired surfaces with switchable adhesion. *Adv Mater* 2007;19:3833–7.
- [368] Eisenhaure JD, Xie T, Varghese S, Kim S. Microstructured shape memory polymer surfaces with reversible dry adhesion. *ACS Appl Mater Interfaces* 2013;5: 7714–7.
- [369] Frensemeier M, Kaiser JS, Frick CP, Schneider AS, Arzt E, Fertig RS, et al. Temperature-induced switchable adhesion using nickel-titanium-polydimethylsiloxane hybrid surfaces. *Adv Funct Mater* 2015;25:3013–21.
- [370] Cui J, Drotlef D-M, Larraza I, Fernández-Blázquez JP, Boesel LF, Ohm C, et al. Bioinspired actuated adhesive patterns of liquid crystalline elastomers. *Adv Mater Weinheim* 2012;24:4601–4.
- [371] Drotlef D-M, Blümler P, del Campo A. Magnetically actuated patterns for bioinspired reversible adhesion (dry and wet). *Adv Mater* 2014;26:775–9.
- [372] Kizilkcan E, Struoben J, Staubitz A, Gorb SN. Bioinspired photocontrollable microstructured transport device. *Sci Rob* 2017;2:eaak9454.
- [373] Wang Y, Tian H, Shao J, Sameoto D, Li X, Wang L, et al. Switchable dry adhesion with step-like micropillars and controllable interfacial contact. *ACS Appl Mater Interfaces* 2016;8:10029–37.
- [374] Wang Y, Lehmann S, Shao J, Sameoto D. Adhesion circle: A new approach to better characterize directional gecko-inspired dry adhesives. *ACS Appl Mater Interfaces* 2017;9:3060–7.
- [375] Rundel F. Neuartige adhäsive Mikrostrukturen mit kontrollierten Knickverhalten. Master Thesis, Universität des Saarlandes; 2020.
- [376] Geikowsky E, Aksak B. Bioinspired fibrillar adhesives with shape-controlled off-center caps for switchable and directional adhesion. *Bioinspir Biomim* 2020;15: 056007.
- [377] Bae W-G, Kim D, Suh K-Y. Instantly switchable adhesion of bridged fibrillar adhesive via gecko-inspired detachment mechanism and its application to a transportation system. *Nanoscale* 2013;5:11876–84.
- [378] Glick P, Suresh SA, Ruffatto D, Cutkosky M, Tolley MT, Parness A. A soft robotic gripper with gecko-inspired adhesive. *IEEE Robot Autom Lett* 2018;3:903–10.
- [379] Lee S, Yi H, Park C, Jeong H, Kwak M. Continuous tip widening technique for roll-to-roll fabrication of dry adhesives. *Coatings* 2018;8:349.
- [380] Shintake J, Cacucciolo V, Floreano D, Shea H. Soft robotic grippers. *Adv Mater* 2018;30:1707035. <https://doi.org/10.1002/adma.201707035>.
- [381] Sandoval JA, Jadhav S, Quan H, Deheyn DD, Tolley MT. Reversible adhesion to rough surfaces both in and out of water, inspired by the clingfish suction disc. *Bioinspir Biomim* 2019;14:066016.
- [382] Ditsche P, Summers A. Learning from Northern clingfish (*Gobiesox maeandricus*): bioinspired suction cups attach to rough surfaces. *Philos Trans R Soc Lond B Biol Sci* 2019;374:20190204.
- [383] Song S, Drotlef D-M, Majidi C, Sitti M. Controllable load sharing for soft adhesive interfaces on three-dimensional surfaces. *Proc Natl Acad Sci U S A* 2017;114: E4344–53.
- [384] Hawkes EW, Jiang H, Christensen DL, Han AK, Cutkosky MR. Grasping without squeezing: Design and modeling of shear-activated grippers. *IEEE Trans Rob* 2018;34:303–16. <https://doi.org/10.1109/tro.2017.2776312>.
- [385] Ge L, Ci L, Goyal A, Shi R, Mahadevan L, Ajayan PM, et al. Cooperative adhesion and friction of compliant nanohairs. *Nano Lett* 2010;10:4509–13.
- [386] Ge L, Sethi S, Ci L, Ajayan PM, Dhinojwala A. Carbon nanotube-based synthetic gecko tapes. *Proc Natl Acad Sci U S A* 2007;104:10792–5.
- [387] Chopra V, Chudak M, Hensel R, Darhuber AA, Arzt E. Enhancing dry adhesion of polymeric micropatterns by electric fields. *ACS Appl Mater Interfaces* 2020; 12:27708–16.
- [388] Krahn J, Menon C. Electro-dry-adhesion. *Langmuir* 2012;28:5438–43.
- [389] Ruffatto D, Parness A, Spenko M. Improving controllable adhesion on both rough and smooth surfaces with a hybrid electrostatic/gecko-like adhesive. *J R Soc Interface* 2014;11:20131089. <https://doi.org/10.1098/rsif.2013.1089>.
- [390] Tian H, Liu H, Shao J, Li S, Li X, Chen X. An electrically active gecko-effect soft gripper under a low voltage by mimicking gecko's adhesive structures and toe muscles. *Soft Matter* 2020;16:5599–608.
- [391] Kroner E, Arzt E. Gecko adhesion. In B B, editor. *Encyclopedia of Nanotechnology*, Springer; 2014.
- [392] Kroner E, Maboudian R, Arzt E. Adhesion characteristics of PDMS surfaces during repeated pull-Off force measurements. *Adv Eng Mater* 2010;12:398–404.
- [393] Hench LL, Thompson I. Twenty-first century challenges for biomaterials. *J R Soc Interface* 2010;7(Suppl 4):S379–91.
- [394] Honig F, Vermeulen S, Zadpoor AA, de Boer J, Fratila-Apachitei LE. Natural architectures for tissue engineering and regenerative medicine. *J Funct Biomater* 2020;11. <https://doi.org/10.3390/jfb11030047>.
- [395] Meyers MA, McKittrick J, Chen P-Y. Structural biological materials: critical mechanics-materials connections. *Science* 2013;339:773–9.
- [396] Xu S, Jayaraman A, Rogers JA. Skin sensors are the future of health care. *Nature* 2019;571:319–21.
- [397] Hwang L, Kim HN, Seong M, Lee S-H, Kang M, Yi H, et al. Multifunctional smart skin adhesive patches for advanced health care. *Adv Healthc Mater* 2018;7: e1800275.
- [398] Baik S, Lee HJ, Kim DW, Kim JW, Lee Y, Pang C. Bioinspired adhesive architectures: From skin patch to integrated bioelectronics. *Adv Mater* 2019;31: e1803309.
- [399] Kwak MK, Jeong H-E, Suh KY. Rational design and enhanced biocompatibility of a dry adhesive medical skin patch. *Adv Mater* 2011;23:3949–53.
- [400] Chen Y-C, Yang H. Octopus-inspired assembly of nanosucker arrays for dry/wet adhesion. *ACS Nano* 2017;11:5332–8.
- [401] Agache P, Humbert P. *Measuring the Skin*. Springer Science & Business Media; 2004.
- [402] Pissarenko A, Meyers MA. The materials science of skin: Analysis, characterization, and modeling. *Prog Mater Sci* 2020;110:100634.
- [403] Jor JWY, Parker MD, Taberner AJ, Nash MP, Nielsen PMF. Computational and experimental characterization of skin mechanics: identifying current challenges and future directions. *Wiley Interdiscip Rev Syst Biol Med* 2013;5:539–56.
- [404] Hussain SH, Limthongkul B, Humphreys TR. The biomechanical properties of the skin. *Dermatol Surg* 2013;39:193–203.
- [405] Hendriks FM, Brokken D, Oomens CWJ, Bader DL, Baaijens FPT. The relative contributions of different skin layers to the mechanical behavior of human skin in vivo using suction experiments. *Med Eng Phys* 2006;28:259–66.
- [406] Leyva-Mendivil MF, Page A, Bressloff NW, Limbert G. A mechanistic insight into the mechanical role of the stratum corneum during stretching and compression of the skin. *J Mech Behav Biomed Mater* 2015;49:197–219.
- [407] Corcuff P, De Rigo J, Leveque JL, Makki S, Agache P. Skin relief and aging. *J Soc Cosmet Chem* 1983;34:177–90.
- [408] Highley KR, Coomey M, DenBeste M, Wolfram LJ. Frictional properties of skin. *J Invest Dermatol* 1977;69:303–5.
- [409] Kovalev AE, Dening K, Persson BNJ, Gorb SN. Surface topography and contact mechanics of dry and wet human skin. *Beilstein J Nanotechnol* 2014;5:1341–8.
- [410] Silver FH, Freeman JW, DeVore D. Viscoelastic properties of human skin and processed dermis. *Skin Res Technol* 2001;7:18–23.
- [411] Maibach HI, Aly R. *Skin Microbiology: Relevance to Clinical Infection*. Springer Science & Business Media; 2012.
- [412] Vector stock. url: <https://www.vectorstock.com/royalty-free-vector/3d-structure-of-the-hair-skin-scalp-anatomical-vector-23933201>.

- [413] de Jr Almeida HL, Isaacsson H, Guarenti IM, Marques e Silva R, Castro LASde. Scanning electron microscopy of the collodion membrane from a self-healing collodion baby. *An Bras Dermatol* 2015;90:581–4.
- [414] Karp JM, Langer R. Dry solution to a sticky problem. *Nature* 2011.
- [415] Lailicht B, Langer R, Karp JM. Quick-release medical tape. *Proc Natl Acad Sci U S A* 2012;109:18803–8.
- [416] Lloyd AW, Faragher RG, Denyer SP. Ocular biomaterials and implants. *Biomaterials* 2001;22:769–85.
- [417] Fischer SCL, Levy O, Kroner E, Hensel R, Karp JM, Arzt E. Bioinspired polydimethylsiloxane-based composites with high shear resistance against wet tissue. *J Mech Behav Biomed Mater* 2016;61:87–95.
- [418] Drotlef D-M, Amjadi M, Yunusa M, Sitti M. Bioinspired composite microfibers for skin adhesion and signal amplification of wearable sensors. *Adv Mater* 2017;29. <https://doi.org/10.1002/adma.201701353>.
- [419] Lee H, Lee BP, Messersmith PB. A reversible wet/dry adhesive inspired by mussels and geckos. *Nature* 2007;448:338–41.
- [420] Mahdavi A, Ferreira L, Sundback C, Nichol JW, Chan EP, Carter DJD, et al. A biodegradable and biocompatible gecko-inspired tissue adhesive. *Proc Natl Acad Sci U S A* 2008;105:2307–12.
- [421] Frost SJ, Mawad D, Higgins MJ, Ruprai H, Kuchel R, Tilley RD, et al. Gecko-inspired chitosan adhesive for tissue repair. *NPG Asia Mater* 2016;8:e280. <https://doi.org/10.1038/am.2016.73>.
- [422] Kim T, Park J, Sohn J, Cho D, Jeon S. Bioinspired, highly stretchable, and conductive dry adhesives based on 1D–2D hybrid carbon nanocomposites for all-in-one ECG electrodes. *ACS Nano* 2016;10:4770–8.
- [423] Stauffer F, Thielen M, Sauter C, Chardonnens S, Bachmann S, Tybrandt K, et al. Skin conformal polymer electrodes for clinical ECG and EEG recordings. *Adv Healthc Mater* 2018;7:e1700994.
- [424] Glassmaker NJ, Himeno T, Hui C-Y, Kim J. Design of biomimetic fibrillar interfaces: 1. Making contact. *J R Soc Interface* 2004;1:23–33.
- [425] Glassmaker NJ, Jagota A, Chaudhury MK, Hui CY. Contact and adhesion mechanics of biomimetic fibrillar interfaces. *Proc Adhes Soc* 2006;93–5.
- [426] Noderer WL, Shen L, Vajpayee S, Glassmaker NJ, Jagota A, Hui C-Y. Enhanced adhesion and compliance of film-terminated fibrillar surfaces. *Proc Roy Soc A: Math Phys Eng Sci* 2007;463:2631–54.
- [427] Shen L, Glassmaker NJ, Jagota A, Hui C-Y. Strongly enhanced static friction using a film-terminated fibrillar interface. *Soft Matter* 2008;4:618–25.
- [428] Arul EP, Ghatak A. Control of adhesion via internally pressurized subsurface microchannels. *Langmuir* 2012;28:4339–45.
- [429] Shahsavan H, Zhao B. Biologically inspired enhancement of pressure-sensitive adhesives using a thin film-terminated fibrillar interface. *Soft Matter* 2012;8:8281–4.
- [430] He Z, Hui C-Y, Levrard B, Bai Y, Jagota A. Strongly modulated friction of a film-terminated ridge-channel structure. *Sci Rep* 2016;6:26867.
- [431] Liew K, Shahsavan H, Zhao B. Functionally graded dry adhesives based on film-terminated silicone foam. *Int J Adhes Adhes* 2017;76:47–53.
- [432] He Z, Moyle NM, Hui C-Y, Levrard B, Jagota A. Adhesion and friction enhancement of film-terminated structures against rough surfaces. *Tribol Lett* 2017;65. <https://doi.org/10.1007/s11249-017-0935-4>.
- [433] Kaiser JS, Kamperman M, De Souza EJ, Schick B, Arzt E. Adhesion of biocompatible and biodegradable micropatterned surfaces. *Int J Artif Organs* 2011;34:180–4.
- [434] De Souza EJ, Kamperman M, Castellanos G, Kroner E, Armbruster V, Romann MS, et al. In vitro adhesion measurements between skin and micropatterned poly(dimethylsiloxane) surfaces. *Conf Proc IEEE Eng Med Biol Soc* 2009;2009:6018–21.
- [435] Fischer SCL, Kruttwig K, Bandmann V, Hensel R, Arzt E. Adhesion and cellular compatibility of silicone-based skin adhesives. *Macromol Mater Eng* 2017;302:1600526. <https://doi.org/10.1002/mame.201600526>.
- [436] Fischer SCL, Boyadzheva S, Hensel R, Kruttwig K, Arzt E. Adhesion and relaxation of a soft elastomer on surfaces with skin like roughness. *J Mech Behav Biomed Mater* 2018;80:303–10.
- [437] Boyadzheva S, Sorg K, Danner M, Fischer SCL, Hensel R, Schick B, et al. A self-adhesive elastomeric wound scaffold for sensitive adhesion to tissue. *Polymers* 2019;11. <https://doi.org/10.3390/polym11060942>.
- [438] Kim J, Kim DW, Baik S, Hwang GW, Kim T, Pang C. Snail-inspired dry adhesive with embedded microstructures for enhancement of energy dissipation. *Adv Mater Technol* 2019;4:1900316.
- [439] Amjadi M, Kyung K-U, Park I, Sitti M. Stretchable, skin-mountable, and wearable strain sensors and their potential applications: A review. *Adv Funct Mater* 2016;26:1678–98.
- [440] Kim D-H, Lu N, Ma R, Kim Y-S, Kim R-H, Wang S, et al. Epidermal electronics. *Science* 2011;333:838–43.
- [441] Chortos A, Liu J, Bao Z. Pursuing prosthetic electronic skin. *Nat Mater* 2016;15:937–50.
- [442] Benight SJ, Wang C, Tok JBH, Bao Z. Stretchable and self-healing polymers and devices for electronic skin. *Prog Polym Sci* 2013;38:1961–77.
- [443] Shih B, Shah D, Li J, Thuruthel TG, Park Y-L, Iida F, et al. Electronic skins and machine learning for intelligent soft robots. *Sci Rob* 2020;5. <https://doi.org/10.1126/scirobotics.aaz9239>.
- [444] Pang C, Koo JH, Nguyen A, Caves JM, Kim M-G, Chortos A, et al. Highly skin-conformal microhairy sensor for pulse signal amplification. *Adv Mater* 2015;27:634–40.
- [445] Park H, Jeong YR, Yun J, Hong SY, Jin S, Lee S-J, et al. Stretchable array of highly sensitive pressure sensors consisting of polyaniline nanofibers and Au-coated polydimethylsiloxane micropillars. *ACS Nano* 2015;9:9974–85.
- [446] Park Y, Shim J, Jeong S, Yi GR, Chae H, Bae J, et al. Microtopography-guided conductive patterns of liquid-driven graphene nanoplatelet networks for stretchable and skin-conformal sensor array. *Advanced* 2017.
- [447] Ashmore J. Cochlear outer hair cell motility. *Physiol Rev* 2008;88:173–210.
- [448] Akhmanova A, Yap AS. Organizing junctions at the cell-cell interface. *Cell* 2008;135:791–3.
- [449] Kawaguchi S, Ng DTW. Sensing ER stress. *Science* 2011;333:1830–1.
- [450] Pang C, Lee G-Y, Kim T-I, Kim SM, Kim HN, Ahn S-H, et al. A flexible and highly sensitive strain-gauge sensor using reversible interlocking of nanofibres. *Nat Mater* 2012;11:795–801.
- [451] Kier WM, Smith AM. The structure and adhesive mechanism of octopus suckers. *Integr Comp Biol* 2002;42:1146–53.
- [452] Wainwright DK, Kleinteich T, Kleinteich A, Gorb SN, Summers AP. Stick tight: suction adhesion on irregular surfaces in the northern clingfish. *Biol Lett* 2013;9:20130234.
- [453] Gamel KM, Garner AM, Flammang BE. Bioinspired remora adhesive disc offers insight into evolution. *Bioinspir Biomim* 2019;14:056014.
- [454] Smith A. Cephalopod sucker design and the physical limits to negative pressure. *J Exp Biol* 1996;199:949–58.
- [455] Choi MK, Park OK, Choi C, Qiao S, Ghaffari R, Kim J, et al. Cephalopod-inspired miniaturized suction cups for smart medical skin. *Adv Healthc Mater* 2016;5:80–7.
- [456] Baik S, Kim DW, Park Y, Lee T-J, Ho Bhang S, Pang C. A wet-tolerant adhesive patch inspired by protuberances in suction cups of octopi. *Nature* 2017;546:396–400.
- [457] Tramacere F, Beccai L, Kuba M, Gozzi A, Bifone A, Mazzolai B. The morphology and adhesion mechanism of Octopus vulgaris suckers. *PLoS ONE* 2013;8:e65074.
- [458] Tramacere F, Pugno NM, Kuba MJ, Mazzolai B. Unveiling the morphology of the acetabulum in octopus suckers and its role in attachment. *Interface Focus* 2015;5:20140050.
- [459] Taboada GM, Yang K, Pereira MJN, Liu SS, Hu Y, Karp JM, et al. Overcoming the translational barriers of tissue adhesives. *Nat Rev Mater* 2020;5:310–29.
- [460] Seppälä J, van Bochove B, Lendlein A. Developing advanced functional polymers for biomedical applications. *Biomacromolecules* 2020;21:273–5.
- [461] Lee H, Choi TK, Lee YB, Cho HR, Ghaffari R, Wang L, et al. A graphene-based electrochemical device with thermoresponsive microneedles for diabetes monitoring and therapy. *Nat Nanotechnol* 2016;11:566–72.
- [462] Yang SY, O' Cearbhaill ED, Sisk GC, Park KM, Cho WK, Villiger M, et al. A bio-inspired swellable microneedle adhesive for mechanical interlocking with tissue. *Nat Commun* 2013;4:1702.

- [463] Etsion I. Improving tribological performance of mechanical components by laser surface texturing. *Tribol Lett* 2004;17:733–7. <https://doi.org/10.1007/s11249-004-8081-1>.
- [464] Braun D, Greiner C, Schneider J, Gumbsch P. Efficiency of laser surface texturing in the reduction of friction under mixed lubrication. *Tribol Int* 2014;77:142–7. <https://doi.org/10.1016/j.triboint.2014.04.012>.
- [465] Wang ZL, Lin L, Chen J, Niu S, Zi Y. *Triboelectric Nanogenerators*. Springer; 2016.
- [466] Li Q, Zeng Q, Shi L, Zhang X, Zhang K-Q. Bio-inspired sensors based on photonic structures of Morpho butterfly wings: a review. *J Mater Chem C* 2016;4:1752–63. <https://doi.org/10.1039/c5tc04029a>.
- [467] Chen CS. Geometric control of cell life and death. *Science* 1997;276:1425–8. <https://doi.org/10.1126/science.276.5317.1425>.
- [468] Choi YS, Vincent LG, Lee AR, Kretschmer KC, Chirasatitsin S, Dobke MK, et al. The alignment and fusion assembly of adipose-derived stem cells on mechanically patterned matrices. *Biomaterials* 2012;33:6943–51.
- [469] Kim C, Young JL, Holle AW, Jeong K, Major LG, Jeong JH, et al. Stem cell mechanosensation on gelatin methacryloyl (GelMA) stiffness gradient hydrogels. *Ann Biomed Eng* 2020;48:893–902.
- [470] Huehorst E, Cutiungco MF, Campbell FA, Saeed A, Love R, Reynolds PM, et al. Customizable, engineered substrates for rapid screening of cellular cues. *Biofabrication* 2020;12:025009.
- [471] Kumar C, Palacios A, Surapaneni VA, Bold G, Thielm M, Licht E, et al. Replicating the complexity of natural surfaces: technique validation and applications for biomimetics, ecology and evolution. *Philos Trans A Math Phys Eng Sci* 2019;377:20180265.
- [472] Finn A, Hensel R, Hagemann F, Kirchner R, Jahn A, Fischer W-J. Geometrical properties of multilayer nano-imprint-lithography molds for optical applications. *Microelectron Eng* 2012;98:284–7. <https://doi.org/10.1016/j.mee.2012.04.022>.
- [473] Hensel R, Braun H-G. Free-floating hydrogel-based rafts supporting a microarray of functional entities at fluid interfaces. *Soft Matter* 2012;8:5293.
- [474] Steinberg C, Ruml M, Runkel M, Papenheim M, Wang S, Mayer A, et al. Complex 3D structures via double imprint of hybrid structures and sacrificial mould techniques. *Microelectron Eng* 2017;176:22–7. <https://doi.org/10.1016/j.mee.2017.01.009>.
- [475] LaFratta CN, Li L, Fourkas JT. Soft-lithographic replication of 3D microstructures with closed loops. *Proc Natl Acad Sci U S A* 2006;103:8589–94.
- [476] Caloon M, Quagliotti D, Tosello G. Surface replication in micro injection molding. *Micro Injection Molding* 2018:83–112. <https://doi.org/10.3139/9781569906545.004>.
- [477] Peng L, Deng Y, Yi P, Lai X. Micro hot embossing of thermoplastic polymers: a review. *J Micromech Microeng* 2014;24:013001. <https://doi.org/10.1088/0960-1317/24/1/013001>.
- [478] Schift H, Kristensen A. Nanoimprint lithography – patterning of resists using molding. *Springer Handbook of Nanotechnology* 2010:271–312. https://doi.org/10.1007/978-3-642-02525-9_9.
- [479] Iwamoto K. Lithography today: challenges and solutions across a diverse market. *Novel Patterning Technologies for Semiconductors, MEMS/NEMS and MOEMS 2020* 2020. <https://doi.org/10.1117/12.2551815>.
- [480] Taylor H. Simulation and mitigation of pattern and process dependencies in nanoimprint lithography. *J Photopolym Sci Technol* 2011;24:47–55. <https://doi.org/10.2494/photopolymer.24.47>.
- [481] Yin M, Sun H, Wang H. Effect of stamp design on residual layer thickness and contact pressure in UV nanoimprint lithography. *Micro Nano Lett* 2018;13:887–91.
- [482] Jakubowsky M, Werder J, Rytka C, Kristiansen PM, Neyer A. Design, manufacturing and experimental validation of a bonded dual-component microstructured surface for vertical light emission. *Microsyst Technol* 2020;26:2087–93. <https://doi.org/10.1007/s00542-020-04767-z>.
- [483] Smith BW, Suzuki K. *Microlithography: Science and Technology*. 2nd ed. CRC Press; 2018.
- [484] Moore GE. Cramming more components onto integrated circuits. *Proc IEEE* 1998;86:82–5. <https://doi.org/10.1109/jproc.1998.658762>.
- [485] Yan YY, Gao N, Barthlott W. Mimicking natural superhydrophobic surfaces and grasping the wetting process: a review on recent progress in preparing superhydrophobic surfaces. *Adv Colloid Interface Sci* 2011;169:80–105.
- [486] Lin BJ. Optical lithography—present and future challenges. *CR Phys* 2006;7:858–74. <https://doi.org/10.1016/j.crrhy.2006.10.005>.
- [487] Fan D, Ekinci Y. Photolithography reaches 6 nm half-pitch using EUV light. In: *Extreme Ultraviolet (EUV) Lithography VII*; 2016. <https://doi.org/10.1117/12.2219737>.
- [488] Fomenkov IV, Schafgans AA, Tao Y, Rafac RJ, Purvis M, Rokitski SI, et al. Industrialization of a robust EUV source for high-volume manufacturing and power scaling beyond 250W. In: *Extreme Ultraviolet (EUV) Lithography IX*; 2018. <https://doi.org/10.1117/12.2305955>.
- [489] Preil ME. Patterning challenges in the sub-10 nm era. In *Proceedings, Optical Microlithography XXIX*, vol. 9780; 2016, p. 978002.
- [490] Kirchner R, Schift H. Thermal reflow of polymers for innovative and smart 3D structures: A review. *Mater Sci Semicond Process* 2019;92:58–72. <https://doi.org/10.1016/j.mssp.2018.07.032>.
- [491] Wolf AJ, Hauser H, Kübler V, Walk C, Höhn O, Bläsi B. Origination of nano- and microstructures on large areas by interference lithography. *Microelectron Eng* 2012;98:293–6. <https://doi.org/10.1016/j.mee.2012.05.018>.
- [492] Sun H-B, Kawata S. Two-Photon Photopolymerization and 3D Lithographic Microfabrication. In *NMR 3D Analysis Photopolymerization*, vol. 170. Berlin, Heidelberg: Springer Berlin Heidelberg; 2004, p. 169–273.
- [493] Marcinkevičius A, Juodkaziš S, Watanabe M, Miwa M, Matsuo S, Misawa H, et al. Femtosecond laser-assisted three-dimensional microfabrication in silica. *Opt Lett* 2001;26:277. <https://doi.org/10.1364/ol.26.000277>.
- [494] Matsui S, Kaito T, Fujita J-I, Komuro M, Kanda K, Haruyama Y. Three-dimensional nanostructure fabrication by focused-ion-beam chemical vapor deposition. *J Vac Sci Technol B* 2000;18:3181.
- [495] Hoshino T, Watanabe K, Kometani R, Morita T, Kanda K, Haruyama Y, et al. Development of three-dimensional pattern-generating system for focused-ion-beam chemical-vapor deposition. *J Vac Sci Technol B* 2003;21:2732.
- [496] Kawata S, Sun HB, Tanaka T, Takada K. Finer features for functional microdevices. *Nature* 2001;412:697–8.
- [497] Zhou X, Hou Y, Lin J. A review on the processing accuracy of two-photon polymerization. *AIP Adv* 2015;5:030701. <https://doi.org/10.1063/1.4916886>.
- [498] Mueller JB, Fischer J, Mayer F, Kadic M, Wegener M. Polymerization kinetics in three-dimensional direct laser writing. *Adv Mater* 2014;26:6566–71. <https://doi.org/10.1002/adma.201402366>.
- [499] Sun H-B, Suwa T, Takada K, Zaccaria RP, Kim M-S, Lee K-S, et al. Shape precompensation in two-photon laser nanowriting of photonic lattices. *Appl Phys Lett* 2004;85:3708–10. <https://doi.org/10.1063/1.1807019>.
- [500] Purto J, Rogin P, Verch A, Johansen VE, Hensel R. Nanopillar diffraction gratings by two-photon lithography. *Nanomaterials* 2019;9:1495. <https://doi.org/10.3390/nano9101495>.
- [501] Purto J, Verch A, Rogin P, Hensel R. Improved development procedure to enhance the stability of microstructures created by two-photon polymerization. *Microelectron Eng* 2018;194:45–50. <https://doi.org/10.1016/j.mee.2018.03.009>.
- [502] Hermans M. Selective, Laser-induced etching of fused silica at high scan-speeds using KOH. *J Laser Micro/Nanoeng* 2014;9:126–31. <https://doi.org/10.2961/jlmn.2014.02.0009>.
- [503] Kim S, Kim J, Joung Y-H, Ahn S, Choi J, Koo C. Optimization of selective laser-induced etching (SLE) for fabrication of 3D glass microfluidic device with multi-layer micro channels. *Micro Nano Syst Lett* 2019;7:15.
- [504] Qin Y. Integrated, multidisciplinary approaches for micro-manufacturing research, and new opportunities and challenges to micro-manufacturing. *Proc IMechE* 2018;232:5–21.
- [505] Qin Y. *Micromanufacturing Engineering and Technology*. William Andrew; 2015.
- [506] Müller FA, Kunz C, Gräf S. Bio-inspired functional surfaces based on laser-induced periodic surface structures. *Materials* 2016;9. <https://doi.org/10.3390/ma9060476>.
- [507] Ramesh R, Mannan MA, Poo AN. Error compensation in machine tools — a review: Part II: thermal errors. *Int J Mach Tools Manuf* 2000;40:1257–84.
- [508] Ramesh R, Mannan MA, Poo AN. Error compensation in machine tools — a review. *Int J Mach Tools Manuf* 2000;40:1235–56.

- [509] Ku X, Zhang Z, Liu X, Chen L, Li G. Low-cost rapid prototyping of glass microfluidic devices using a micromilling technique. *Microfluid Nanofluid* 2018;22. <https://doi.org/10.1007/s10404-018-2104-y>.
- [510] Boswell B, Islam MN, Davies LJ. A review of micro-mechanical cutting. *Int J Adv Manuf Technol* 2018;94:789–806.
- [511] Hong F, Zhang F, Liu Y, Yan H. DNA Origami: Scaffolds for creating higher order structures. *Chem Rev* 2017;117:12584–640.
- [512] Song D-P, Jacucci G, Dunder F, Naik A, Fei H-F, Vignolini S, et al. Photonic Resins: Designing optical appearance via block copolymer self-assembly. *Macromolecules* 2018;51:2395–400.
- [513] Kinge S, Crego-Calama M, Reinhoudt DN. Self-assembling nanoparticles at surfaces and interfaces. *ChemPhysChem* 2008;9:20–42.
- [514] Nunns A, Gwyther J, Manners I. Inorganic block copolymer lithography. *Polymer* 2013;54:1269–84. <https://doi.org/10.1016/j.polymer.2012.11.057>.
- [515] Ai B, Möhwald H, Wang D, Zhang G. Colloidal Lithography: Advanced Colloidal Lithography Beyond Surface Patterning. *Adv Mater Interfaces* 2017;4:1600271.
- [516] Hughes RA, Menumerov E, Neretina S. When lithography meets self-assembly: a review of recent advances in the directed assembly of complex metal nanostructures on planar and textured surfaces. *Nanotechnology* 2017;28:282002.
- [517] Kraus T, Wolf H. Templated Self-Assembly of Particles. *Springer Handbook of Nanotechnology* 2010:187–210. https://doi.org/10.1007/978-3-642-02525-9_6.
- [518] Bisker G. Dissipate your way to self-assembly. *Nat Phys* 2020. <https://doi.org/10.1038/s41567-020-0888-7>.
- [519] Malaquin L, Kraus T, Schmid H, Delamarche E, Wolf H. Controlled particle placement through convective and capillary assembly. *Langmuir* 2007;23:11513–21.
- [520] Li M, Li WH, Zhang J, Alici G, Wen W. A review of microfabrication techniques and dielectrophoretic microdevices for particle manipulation and separation. *J Phys D Appl Phys* 2014;47:063001. <https://doi.org/10.1088/0022-3727/47/6/063001>.
- [521] Sander LM. Diffusion-limited aggregation: A kinetic critical phenomenon? *Contemp Phys* 2000;41:203–18.
- [522] Wintzheimer S, Granath T, Oppmann M, Kister T, Thai T, Kraus T, et al. Supraparticles: Functionality from uniform structural motifs. *ACS Nano* 2018;12:5093–120.
- [523] Ariga K, Yamauchi Y, Mori T, Hill JP. 25th Anniversary Article: What can be done with the Langmuir-Blodgett method? Recent developments and its critical role in materials science. *Adv Mater* 2013;25:6477–512. <https://doi.org/10.1002/adma.201302283>.